3-11-2011

Improving the Efficiency of Photon Collection by Compton Rescue

Alexander W. Stevenson

Improving the Efficiency of Photon Collection By Compton Rescue

THESIS

Alexander W. Stevenson, 2nd Lieutenant, USAF

AFIT/GAP/ENP/11-M10

DEPARTMENT OF THE AIR FORCE
AIR UNIVERSITY

AIR FORCE INSTITUTE OF TECHNOLOGY

Wright-Patterson Air Force Base, Ohio

AFIT/GAP/ENP/11-M10

Improving the Efficiency of Photon Collection By Compton Rescue

THESIS

Presented to the Faculty

Department Engineering Physics

Graduate School of Engineering and Management

Air Force Institute of Technology

Air University

Air Education and Training Command

in Partial Fulfillment of the Requirements for the

Degree of Master of Science in Nuclear Physics

Alexander W. Stevenson, BS

2nd Lieutenant, USAF

March 2011

AFIT/GAP/ENP/11-M10

Improving the Efficiency of Photon Collection

By Compton Rescue

Alexander W. Stevenson, BS
2nd Lieutenant, USAF

Approved:

Lt Col Christopher S. Williams (Chairman)	Date
Larry W. Burggraf, PhD (Member)	Date
Maj Benjamin R. Kowash (Member)	Date

Abstract

A method to improve the efficiency of photon collection in thin planar HPGe detectors was investigated. The method involved implementing a second HPGe detector to collect Compton scattered photons from the primary detector and incorporating coincident interactions in the two detectors that sum to the full energy event into the energy spectrum. This method is termed "Compton rescue" because the Compton scattered photons make a partial energy deposition in the primary detector and are added back to the spectrum after being detected by the second detector. This research has implications on improving the efficiency of positron annihilation spectroscopy (PAS) techniques including the use of the method in angular correlation of annihilation radiation (ACAR) and Doppler-broadening of annihilation radiation (DBAR) applications. The effect of using Compton rescue on the energy and spatial resolution on these two PAS techniques was investigated. The research was conducted in two phases: simulation, in which a Monte-Carlo program was used to predict the effectiveness of the Compton rescue method based on photon interaction simulations, and experiment, in which a position-sensitive HPGe detector and a large coaxial HPGe detector were used to implement Compton rescue. A two-detector DBAR experiment on single-crystal Ni was conducted using the Compton rescue setup to illustrate its utility.

Acknowledgements

I would like to thank my advisor Christopher Williams for his insightful guidance in conducting this research, Eric Taylor for his reliable assistance in the lab, and Josh Hess for his invaluable help in using LaTeX. I would also like to thank my classmates for their support and comraderie during the thesis process.

It is the glory of God to conceal things, but the glory of kings is to seek things out.

Alexander W. Stevenson

Table of Contents

Page

Page

List of Figures

List of Abbreviations

Improving the Efficiency of Photon Collection
By Compton Rescue

I. Introduction and Theory

1.1 Background

The Engineering Physics Department at the Air Force Institute of Technology (AFIT) has been pursuing research in the area of positron physics. Research has focused on both positron physics and materials science based on positron annihilation characteristics. Experiments in the area of positron annihilation spectroscopy (PAS) require the detection of photons in the energy range of hundreds of kiloelectron-Volts (keV). The community standard for these experiments requires the use of high-resolution detectors since many experiments examine fine details in energy spectra from a source. Often, however, the cost of using detector systems that provide highly resolved data is the detection efficiency, and many experiments require long periods of time for good data collection. By developing techniques to improve detector efficiency, the pace of research in this and other areas may be accelerated.

1.1.1 The Compton Rescue Technique

The subject of this research is the investigation of a method of improving the efficiency of a particular type of experiment used in positron annihilation research. These experiments require the use of detectors that can determine, to a certain precision, the location of photons when they interact within the detector. This requirement is often met by the use of thin planar detectors that are position-sensitive. The small thickness of these detectors is a handicap to their efficiency in the energy range of

interest since the photons are more likely to fly through the detector unobserved than be fully detected. However, another possibility is that photons incident on the detector will be partially observed interacting by a process known as Compton scattering before continuing through the detector. These partially detected photons may be observed by a secondary detector and the energy of the secondary detection may be summed with the energy of the partial primary detection to reconstruct the energy of the initial photon. The scattering interaction in the primary detector will still register location information in the detector and the position-sensitivity of the detection system may be maintained. Since this technique involves restoring photons to the data set that would have otherwise not contributed to the experimental data, the technique is known as Compton rescue, in reference to the phenomenon known as Compton scattering discussed in section 1.9.

1.1.2 Applications

The use of PAS techniques has applications in the area of materials science for characterizing solid state samples at the level of atomic structure [1]. By measuring the radiation emitted by the annihilation of positrons in a material sample, information may be determined about characteristics of the sample material such as defect concentration and plasticity. Positron techniques can even be used to make fatigue failure predictions in material samples [2:1827], and are therefore useful for non-destructive testing the health of solid material components, such as airplane wings, that are regularly subjected to high amounts of stress and strain [3].

While this research is focused on improving detection efficiency for position-sensitive detectors used in positron annihilation experiments, the technique may be useful for a number of other applications. For example, Compton rescue could be used to improve the efficiency of Compton imagers used for radioactive materials interrogation in Homeland Security [4]. Position sensitive detectors similar to those

used in this research are also used for applications in astrophysics [5] and medical imaging [6].

1.1.3 Semiconductor Detector Technology

The use of semiconductors for highly resolved photon detection has been critical to numerous research projects and studies for the past fifty years [7:353]. The development of semiconductor technology has led to materials able to detect photons with exceptional resolution and the data gathered from the use of these materials have expanded research capabilities. High-Purity Germanium (HPGe) has been used to produce remarkably well-resolved spectra and provide a critical tool for researchers to gain a clear picture of the phenomena they intend to observe. While the resolution of the spectra produced by HPGe detectors is impressively sharp, the choice to use these detectors comes at the cost of efficiency in detecting photons relative to other detectors such as sodium iodide scintillator crystals [7:359]. Engineering advances to improve the efficiency of these detectors would expand their usefulness in research and could accelerate radiation studies.

1.2 Thesis Goal

The intent of this research is to increase the efficiency of photon detection for eventual use in positron experiments by implementing engineering improvements in the detection apparatus. This research investigates the use of a secondary detector in coincidence with a primary detector to capture single-scattered photons partially absorbed by the primary detector. The aim of this investigation is increasing overall efficiency by adding partial energy deposition events in the primary detector back to the experiment data set. This add-back process is termed "Compton rescue" to suggest the salvaging of partial energy depositions that would otherwise not contribute to the spectrum. This research consists of two components; simulation, in which

a Monte-Carlo code is used to predict the efficiency characteristics of the detector scheme, and experiment, in which the engineering improvements to the detection apparatus is tested in a laboratory environment. After the Compton rescue system is characterized, it is used in a standard positron annihilation experiment that tests material properties of a sample of single-crystal nickel.

1.3 Positron Theory

The positron is the antiparticle of the electron; thus its mass is equivalent to that of an electron and its charge is equal to but opposite of an electron [8:31]. The theory of the positron was proposed by Dirac in 1928 [9] through quantum mechanics and their existence was experimentally verified by Carl Anderson in 1932 when particle tracks were observed in a Wilson cloud chamber with a curvature that would be expected from an electron but in the opposite direction [10:491]. Positrons are Coulombically attracted to electrons and when the two particles are brought together they form a hydrogen-like quasi-bound state known as positronium (Ps) with an intrinsic life time on the order of 10^{-10} seconds (for the most probable case in which the spins of the two particles are anti-parallel) [11:455]. The decay of Ps occurs when the two particles come together and annihilate. In the process of annihilation, the rest mass of each particle is converted into energy in the form of two 511 keV photons. Positrons are produced in the β^+ decay of radioactive isotopes such as ^{22}Na.

^{22}Na is the most commonly used source of positrons for several reasons, including ease of production and laboratory safety [12:7]. The isotope is an ingredient in various salts which makes it easy to handle and simple to produce as a laboratory source. The isotope has a half-life of 2.6 years. The branching ratio for β^+ decay in this isotope is 90.4%, which results in a relatively high yield of positrons. For this decay mode, shown in figure 1.1, a gamma-ray with an energy of 1.247 MeV is emitted approximately in coincidence (3 ps later). Positrons produced by this source have a

broad energy distribution (0-540 keV [12:28]) with an average energy of 215.54 keV [13].

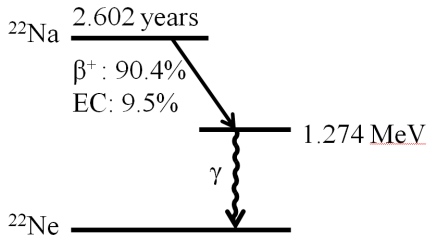

Figure 1.1. ^{22}Na decay scheme

The properties of positron interactions with matter are useful in the area of material science. Positrons incident on a material sample, such as a metal or semiconductor, may penetrate a depth on the order of 100 microns [12:28] into the sample before thermalizing by interacting with the lattice in the interrogated material. When the positron thermalizes, it slows down to lower energies at which they are more likely to interact with an electron. Thermalized positrons diffusing through the material will tend to be attracted to negatively-charged vacancy defects in the lattice of the material [ibid]. Vacancy defects are locations in the solid structure where an atomic nucleus is absent resulting in a region of relative negative potential to which the positrons are attracted and can be trapped (figure 1.2). Positrons in vacancy traps will eventually interact with valence electrons bound to the surrounding atoms. The density and size of these vacancies are manifested in characteristics of the annihilation photon spectrum [8, 14, 15]. The effect of vacancies on the spectrum is discussed in section 1.6.

1.4 Positron Experimentation

PAS techniques require the detection of the coincident pairs of annihilation photons that result from the annihilation of a positron and an electron. These 511 keV

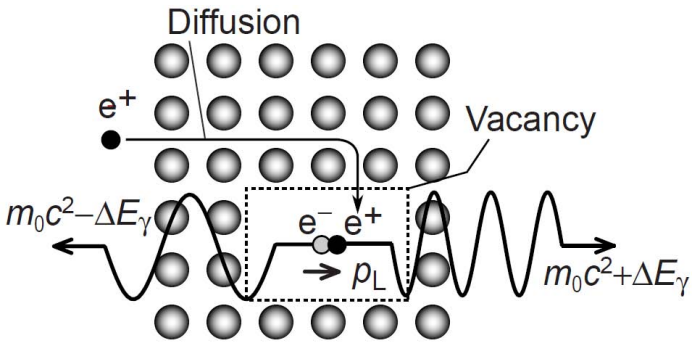

Figure 1.2. Representation of a positron thermalizing and being trapped in a vacancy-type defect. Note the deviation of the energy of the annihilation photons from the electron rest mass energy by $\pm\Delta E$, due to the momentum of the annihilating pair, p_L [15].

photons are emitted exactly collinear to each other in the center-of-mass reference frame. However, the momentum of the positron-electron pair prior to annihilation leads to angular deviation from collinearity, θ, and energy deviation from 511 keV, $\pm\Delta E$, in the laboratory reference frame due to the conservation of energy and momentum [12:4-7]. These momentum variations can occur in three dimensions and may be measured using two different PAS techniques. For the momentum component perpendicular to the annihilation photon emission direction ($p^{\perp}$), a small angular variation, on the order of milliradians (mrad), will result that can be detected with a position-sensitive detector. The angular variations are governed by

$$\theta = \frac{p^{x,y}}{mc} = \frac{p^{\perp}}{mc} \tag{1.1}$$

where θ is the angular deviation from collinearity [16:27]. Measurement of this angular deviation is a PAS technique known as angular correlation of annihilation radiation (ACAR). For the momentum component parallel to the direction of photon emission, a difference in energy between the two emitted annihilation photons is measured such that each photon will differ from 511 keV by an equal and opposite amount [12:16]. This phenomenon is known as Doppler-broadening of annihilation radiation (DBAR)

and may be detected by placing detectors on opposite sides of the radiation origin. These momentum variations over a statistically large number of annihilation events are best detected by high-resolution detectors, such as those that use HPGe.

1.5 Angular Correlation of Annihilation Radiation

ACAR measures the momentum density of electron-positron pairs in the plane parallel to the direction of photon propagation prior to annihilation. As discussed in section 1.4, photons produced by electron-positron annihilation propagate away from each other at an angle that differs from collinearity by θ from equation 1.1. The first ACAR experiments were one-dimensional measurements carried out by Beringer and Montgomery using two Geiger counters [17]. One Geiger counter was rotated around the positron-interrogated sample and angular variations of annihilation radiation levels in the plane of rotation were observed (figure 1.3). These early observations of the variation in the annihilation radiation in one dimension revealed characteristics of the momentum density of the electrons in the substance.

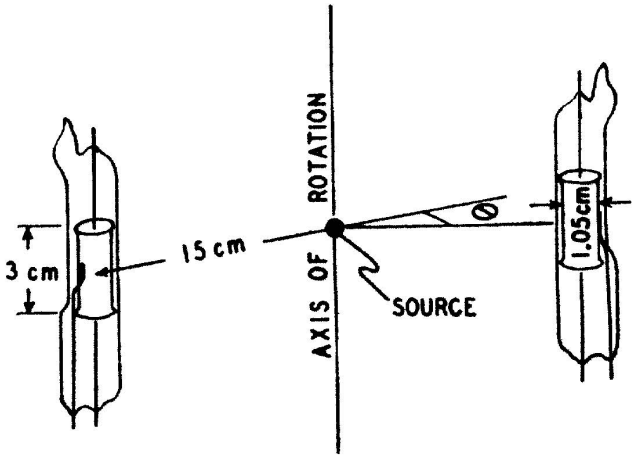

Figure 1.3. Layout of 1D ACAR experiment [17:222]

Two-dimensional ACAR (2D ACAR) measurements are carried out using two

position-sensitive detectors where the interrogated material is centered collinear with the detector axis (figure 1.4) and oriented relative to crystallographic axes. The

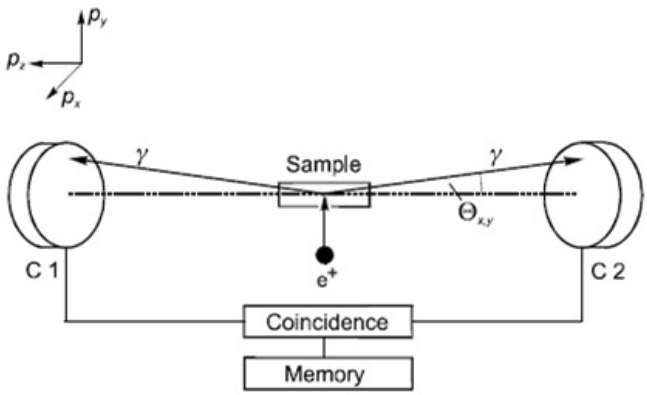

Figure 1.4. Diagram of ACAR measurement layout [12:26]

angular deviation θ can be determined from the difference in the position-sensitive data relative to the alignment axis of the two detectors (the dashed line in figure 1.4). The collection of a statistically large number of coincident photons leads to two-dimensional ACAR spectra, such as the one shown in figure 1.5. These spectra reveal information about the two-dimensional momentum distribution of the electrons in the x-y plane of the target substance.

1.6 Doppler Broadening of Annihilation Radiation

The two-dimensional ACAR technique collects information about the momentum component of an annihilating pair in the plane perpendicular to the emission direction. In contrast, the DBAR technique measures the momentum component in the parallel direction. Electron-positron momentum in the parallel direction are seen in the energy difference between annihilation photons (figure 1.6). This is the phenomenon known as Doppler broadening, in which the annihilation photons carry an energy of 511

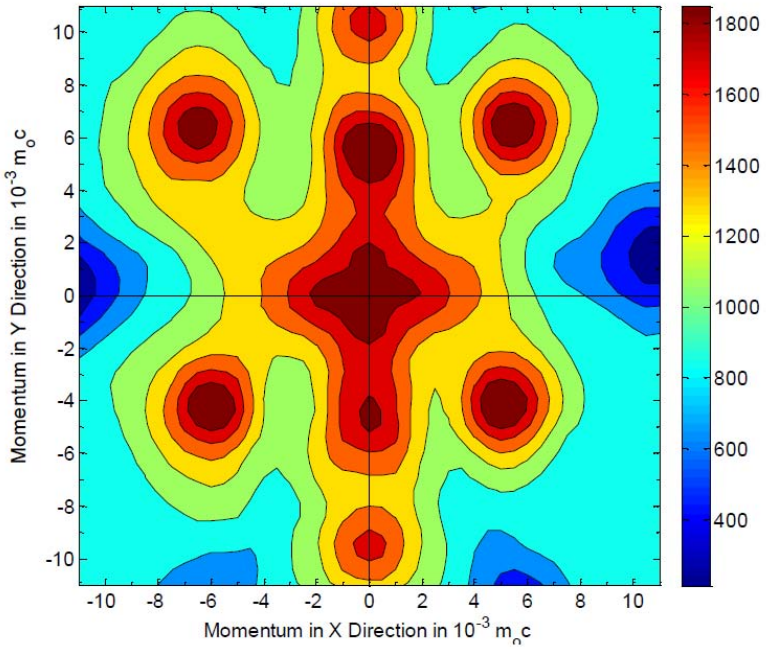

Figure 1.5. Example of a typical ACAR spectrum, taken on a sample of virgin, unannealed silicon carbide [16:125]. This spectrum shows the 2-dimensional distribution of bound electrons in the plane perpendicular to the detector axis in momentum space. The momentum peaks in the figure ("hot spots") reveal electron bonding directions and a time-averaged picture of the crystal bond structure in the interrogated sample

$keV \pm \Delta E_\gamma$ (the Doppler shift) such that

$$\Delta E_\gamma = mc\nu_{cm}Cos\phi = \frac{cp_\parallel}{2} \tag{1.2}$$

where ν_{cm} is the velocity of the center-of-mass of the Ps pair, c is the speed of light, ϕ is the angular deviation between the Ps pair momentum and one of the photon emission directions, and $p_\parallel$ is the component of the photon direction parallel to the Ps pair momentum [16:18]. In the energy spectrum, this effect is observed as a broadening of the 511 keV full energy peak (FEP). Because bound electrons are far more energetic than thermalized positrons, the features of the broadened peak are a result of trends in the momentum of the bound electrons in the target substance [12, 15, 18]. These trends reveal characteristics of the substance's electron bonding structure.

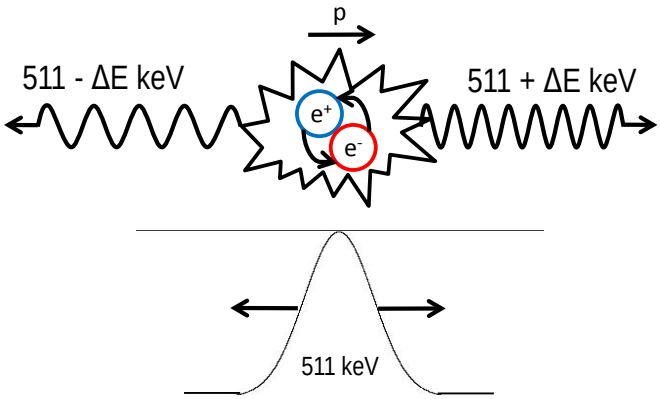

Figure 1.6. The momentum of the positron-electron pair causes Doppler broadening of annihilation radiation

DBAR is measured by exposing a material sample to a positron source and collecting the energy from the coincident annihilation photons resulting from interaction in the sample. A one-detector DBAR measurement can be made simply by observing the broadening of the 511 keV peak from annihilation photons, however, the background radiation and measurements resulting from incomplete charge collection may interfere significantly with the spectrum. This background may be significantly reduced by collecting both photons from each annihilation which requires two detectors operating in coincidence [12:19]. They are oriented opposite to each other with the sample in between and are operated in coincidence as shown in figure 1.7. Coincident photons are detected and added to the DBAR spectrum. Since the Doppler shift is typically on the order of 1.2 keV [19:14], a detector with very good resolution, such as an HPGe detector, is required to measure the Doppler broadening. Ideally the measurement would be carried out with two coincident HPGe detectors so that both photons in each annihilation pair can be added to the spectrum. This can reduce the noise in the measurement by four orders of magnitude [20:424]. However, the measurement can be done with a single HPGe detector in coincidence with a different type of detector for coincidence, and only the photon energy detected by the HPGe detector will contribute to the spectrum. Since the annihilation photons are emitted

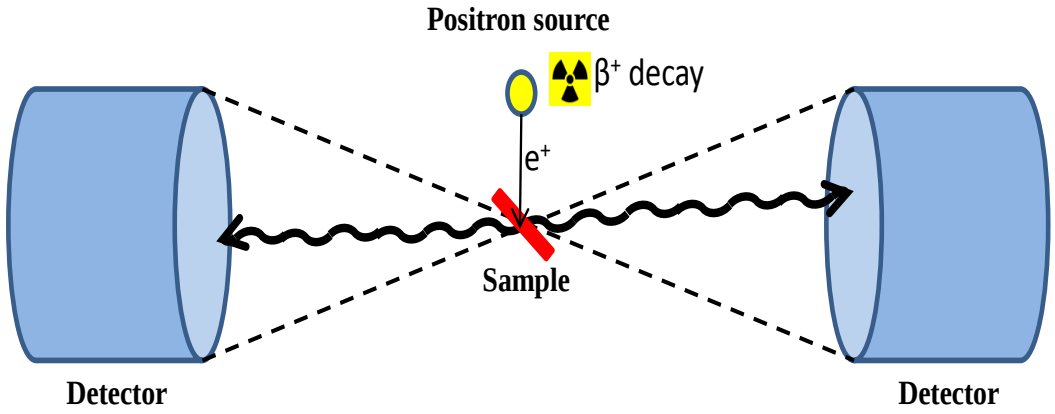

Figure 1.7. Layout of a standard 2-detector DBAR experiment. The region between the dashed lines represents the region for which annihilation photons can be detected.

isotropically, there is no preferential direction of emission and the HPGe detector will detect approximately the same number of photons of energy greater than 511 keV as below 511 keV according to stochastic principles of a large population of events.

1.6.1 DBAR Data Analysis

Doppler broadened FEPs are generally analyzed by determining two parameters: the S-parameter ("sharpness") and the W-parameter ("wing") [12:21]. DBAR is a relative measurement and the S- and W-parameters must be benchmarked against spectra taken from defect-free (virgin or annealed) samples using the identical detection system and identification. The S- and W-parameters are determined by grouping the channels of the broadened FEP into five regions as shown in figure 1.8. The bounds of the central region, which defines the S-parameter (S), are then set such that

$$S = \frac{C}{T} \approx 0.5 \tag{1.3}$$

where C is the number of counts in the C region of figure 1.8 and T is the total number of counts in all five regions. Similarly, the bounds of the A and E regions,

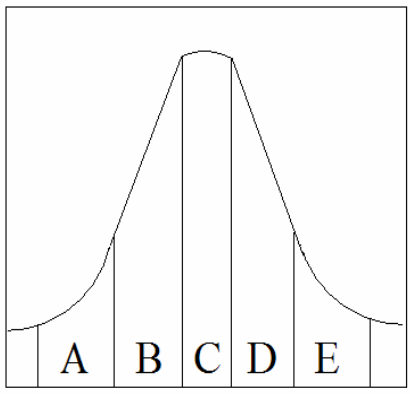

Figure 1.8. S- and W- parameter regions

which determine the W-parameter (W), are set such that

$$W = \left(\frac{A+E}{T}\right) \approx 0.25 \tag{1.4}$$

and the number of counts in the A and E regions are approximately equal. When these bounds have been set with a measurement of the virgin sample, the S and W parameters may be measured for defect bulk samples. Typical values for the bounds on the C region are $\Delta E_\gamma = \pm .5keV$ and $\Delta E_\gamma = \pm 4keV$ for the inner bounds on the A and E regions. S_{bulk} and W_{bulk} may then be compared to the virgin S- and W-parameters for defect analysis as exemplified in [18]. An example of DBAR data which has been analyzed for S- and W-parameters is seen in figure 1.9.

The S- and W-parameters can be generally defined as measures of positron interactions with valence electrons and core electrons, respectively. Valence electrons are much less energetic than core electrons, thus the effects of Doppler broadening will be a smaller ΔE_γ for positron interactions with valence electrons than for core electrons. The ratio of valence to core interactions will depend generally on the number of vacancy-type defects in the target sample, because the less tightly bound valence electrons are more likely to be found in the vacancy region. Increasing vacancy type

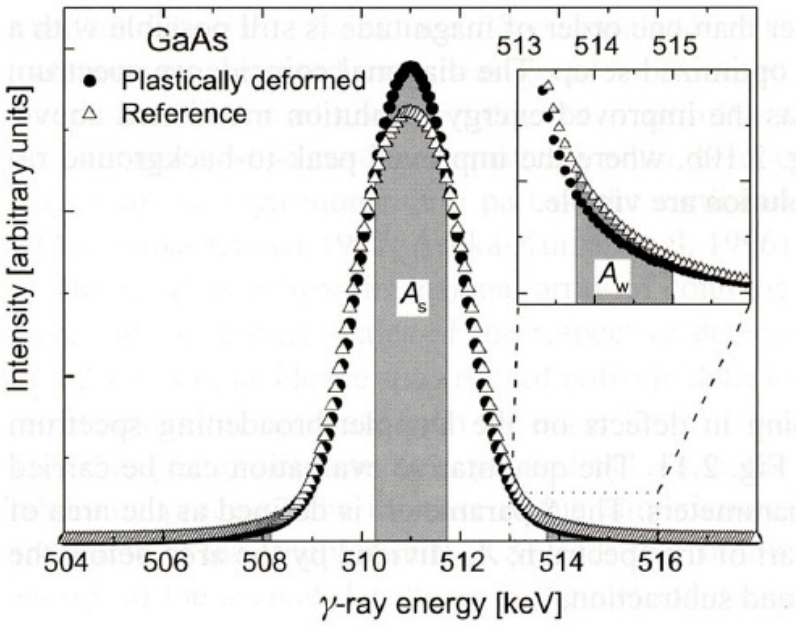

Figure 1.9. Example of DBAR analysis using S and W parameters [12:22]

defects, for example, will have the effect of increasing the S-parameter because the lower potential of the defect will tend to trap positrons. Because vacancy defects are farther from the nuclei of the lattice atoms, trapped positrons will be more likely to interact with valence electrons (figure 1.10). The effects of other types of material defects and features on DBAR spectra are discussed in [12:84-110]. The data for a DBAR spectrum must be referenced to a control spectrum from a defect-free sample taken by the same detector because the broadening is influenced by resolution which varies with the detector.

Ideally, a DBAR measurement is taken with the use of two HPGe detectors in coincidence in order to maximize background interference reduction. The effects of the core electron-positron interactions seen in the tails are especially susceptible to background interference. The superior resolution of the energy data can be analyzed and the Doppler shift (equation 1.2) of each photon in an annihilation pair can be compared. Since the Doppler shift of either photon should be equal and opposite of the

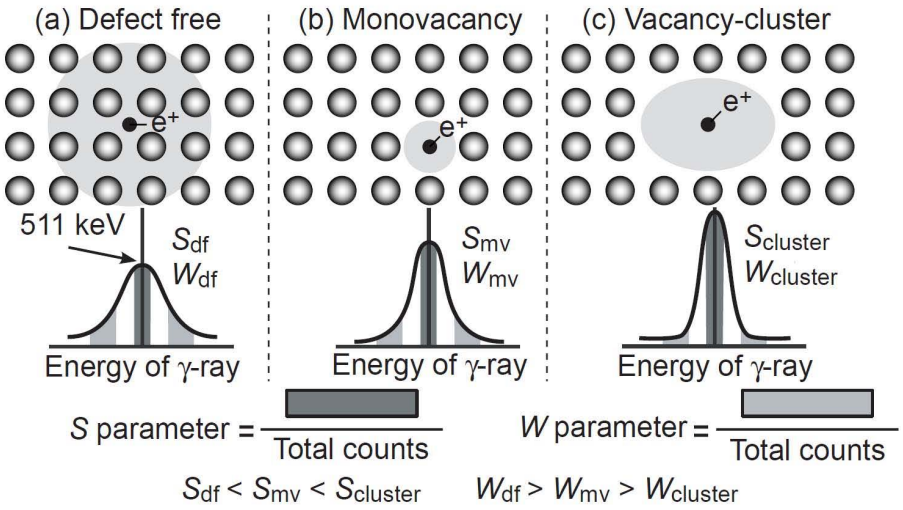

Figure 1.10. As the number and size of defects in a sample of positron interrogated material increases, the S-Parameter will also increase relatively and the FEP will be narrower and taller [15]

other the coincident energy can be plotted as a two-dimensional energy distribution as in figure 1.11 [20, 21]. However, the DBAR measurement can be carried out with a single HPGe detector in coincidence with another type of detector, even if it does not have the high-quality energy resolution necessary for the DBAR data. The second detector may be used only for coincidence identification for annihilation events. The DBAR analysis can then be carried out for the coincidence events in the 511 keV peak of the HPGe data.

1.6.2 Ratio Plots

Ratio plot are an effective way to examine DBAR data for trends in the annihilation spectrum. In a ratio plot, the annihilation peak spectrum of an interrogated material sample is plotted relative to a benchmark spectrum, usually a virgin or annealed sample of the same material. By plotting data in this way, features in the annihilation peak from defects can be examined and defect implantation can be qualitatively analyzed. An example of a ratio plot is shown in figure 1.12. This figure

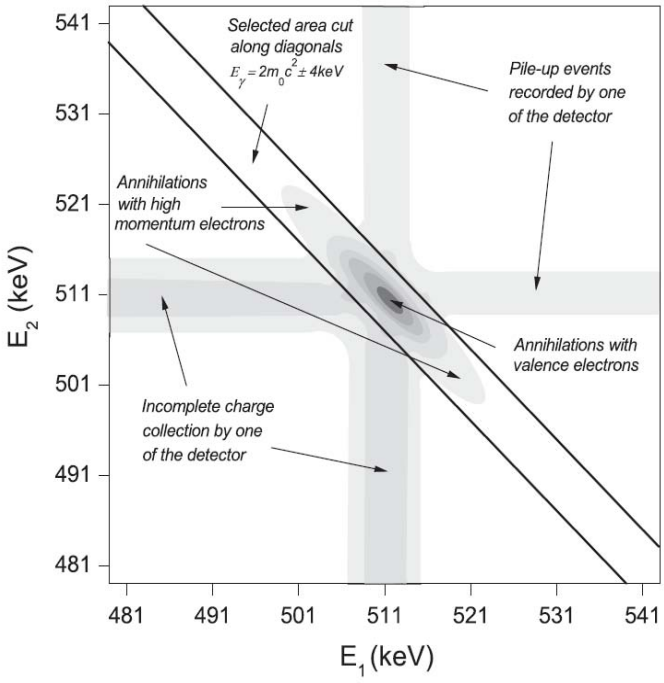

Figure 1.11. Two-dimensional energy distribution of coincidence data [20]

shows the relative difference in momentum density distribution from different material samples.

1.7 Semiconductor Detector Principles

The use of semiconductor detectors is what makes high-quality ACAR and DBAR measurements possible. The superior resolution of the energy spectra gained by the use of semiconductors allows the location of an interaction to be be determined more accurately in a position-sensitive detector and the S- and W- parameters to be determined precisely in Doppler broadening applications. Photons are best detected with solid-state materials rather than liquid or gas because the material density can be up to three orders of magnitude greater [7:353]. While scintillator detectors are generally more efficient than semiconductors in detecting photons, the processes that generate the electric signals are much less efficient and lead to much poorer energy

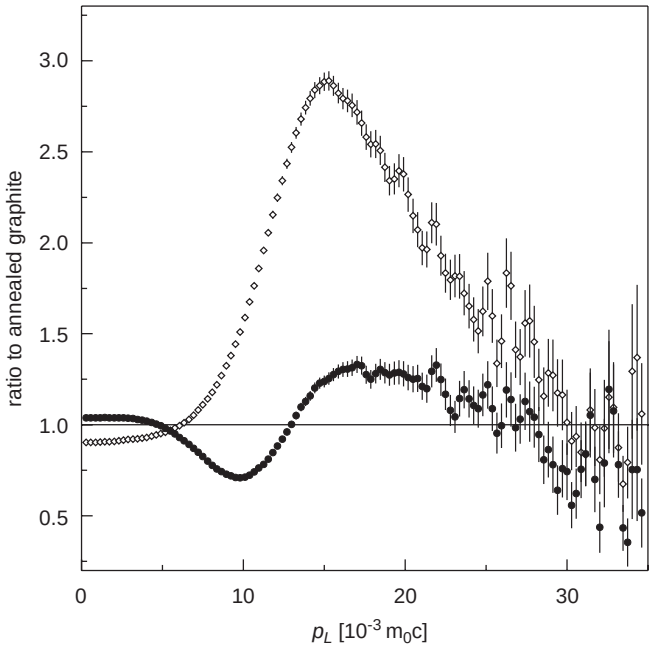

Figure 1.12. Example of DBAR ratio plot. Note that the x-axis is in units of momentum beginning at zero. This means that ΔE has been converted to momentum (eqn. 1.2). In this figure, the ratio of well-annealed carbon steel (full circles) is shown relative to annealled graphite (solid line at y=1). The ratio curve of pure Fe (open rhombs) is provided for comparison [22:835].

resolution [ibid]. In the category of semiconductor detectors, germanium has become the material of choice because of the high levels of purity attainable by modern industrial techniques [ibid].

1.7.1 Physical Mechanism

The advantages of using semiconductor detectors follow from the high efficiency of the process by which a photon interaction in the detector crystal produces an electronic output signal. For the energy regime of interest to this research, photons cause ionization of crystal atoms when they interact by one of two main processes: photoelectric absorption and Compton scattering, detailed in [7:48-52]. When this ionization occurs in a semiconductor crystal, an electron transitions from the valence band to the conduction band and becomes a free charge in the crystal (figure 1.13).

For most semiconductors, the energy band gap is only a few electron-volts (eV).

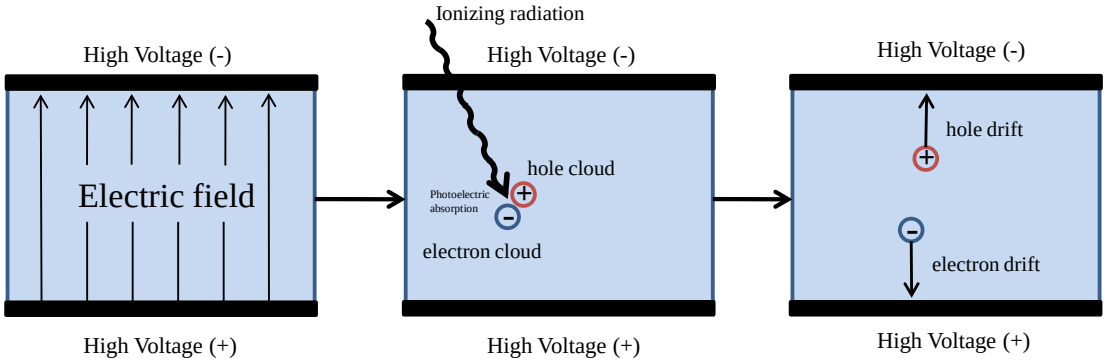

Figure 1.13. A photon is detected in a semiconductor crystal when free charge is created by photon interaction and drifts to collection points, motivated by high-voltage bias

Excess ionization energy is carried by the electron and can be transferred to other bound electrons, resulting in the formation of a number of charge carriers directly proportional to the energy deposited by the photon in the interaction. High-energy photons, on the order of hundreds of keV, may produce a "charge cloud" of tens of thousands of free charge carriers [ibid]. Because of the low energy necessary for ionization in semiconductors, the number of charge carriers that make up the signal from a semiconductor detector is many times that of scintillator or gas detectors, and is the statistical reason for superior energy resolution. If a bias voltage is applied high enough to fully deplete the semiconductor of intrinsic free charges, the free charge clouds created by ionization will drift across the crystal to the collection points and the detector will output a signal pulse [23:93-99].

1.7.2 Segmentation

Segmentation is a technique that can be used to give a semiconductor crystal position-sensitivity. The principle behind segmentation is that the positive and negative charge collection nodes (represented in figure 1.13) may be split into several nodes. Since the voltage required to fully deplete a semiconductor crystal is very

high (∼ 100 V to several kV), the charges created by photon interaction with the crystal are drawn in a nearly straight line from the point of interaction to the nearest collection node. The drift velocity of the charge carriers is related to the electric

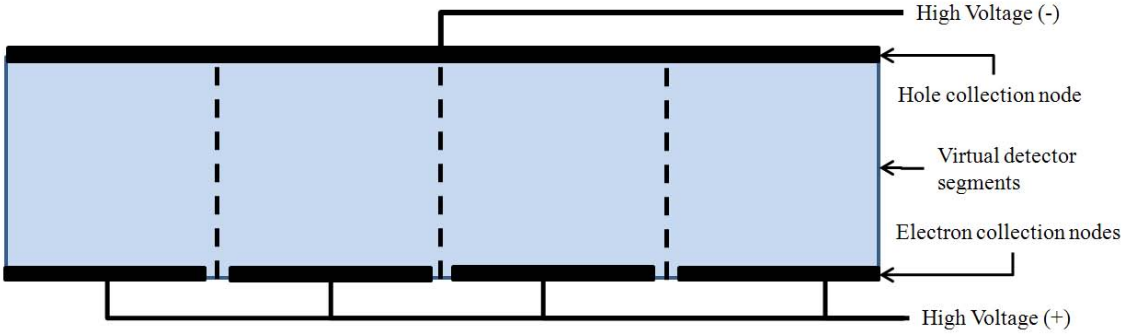

Figure 1.14. The use of multiple charge collection nodes segments a single semiconductor crystal into multiple detector volumes

field produced by the bias voltage by a factor know as the *mobility*, μ, a function of the semiconductor material, impurity concentration, and temperature [23:48-51]. For the high voltage necessary for full depletion, the drift velocity is much higher than the diffusion rate and the spreading of the free charge cloud is marginal. By creating a charge collection array with many nodes that each cover a small area of a planar crystal surface, the location of interaction can be determined to within a smaller volume within the detector crystal. By this method, a single detector crystal can be virtually segmented into smaller detector volumes, each with its own output signal channel.

1.7.3 Transient Charge

Segmentation of a semiconductor detector allows photon interactions to be located to within a physical volume of the crystal, however, the precision of the location can be improved even within the segmented volume by utilizing the phenomenon of transient charge [24:34-38]. As the charge carriers drift from the point of ionization

to the collection node, current is drawn through the collection node defined by

$$I\left(t\right) = \frac{dQ}{dt}[ibid], \tag{1.5}$$

where dQ is the differential charge created by the photon interaction ($dQ = dQ_e + dQ_h$, where the e and h subscripts denote negative electron and positive hole charge) [24:28-31]. The differential charge produced by the motion of the ionization charges from location $r_{e,h}$ to $(r_{e,h} + dr_{e,h})$ can be determined from the equation

$$dQ_{e,h} = \frac{qE(r_{e,h})dr_{e,h}}{V_0}[ibid], \tag{1.6}$$

where V_0 is the applied bias voltage, E is the electric field, and q is the total free charge (holes and electrons) created by the ionization. Drift velocity is expressed as $v_{e,h} = dr_{e,h}dt$ which allows equation 1.6 to be expressed as

$$dQ = \frac{q}{V_0}\left(E(r_e)v_e + E(r_h)v_h\right)dt[ibid]. \tag{1.7}$$

As the free charge approaches the collection node, the differential charge in the main collection node rises until it meets a maximum when the charges are collected. However, charge will also be induced on the surrounding nodes by the motion of the free charge. Since no actual charge is collected on the surrounding nodes, the induced charge will fall back to zero instantly after collection in the main node. This is termed "transient charge". An example of transient charge measurement is provided in figure 1.15. This transient charge is often large enough to be measured by the detector electronics and can be used to interpolate the location of the photon interaction more precisely within the segmented volume where it was detected. This interpolation introduces a subarea resolution to the detector. This subarea resolution is only in the two dimensions perpendicular to the normal of the charge collection surface. For segmented planar detectors, this is the plane of the detector face, and

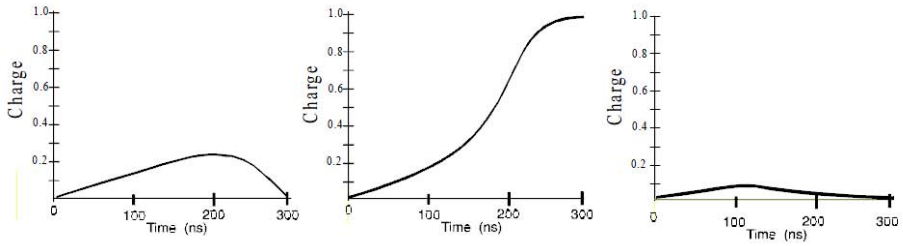

Figure 1.15. Typical signal pulse from a photon absorption in the central collection node of a segmented HPGe detector (center) and the transient charge pulses seen in the adjacent segments [24:37]

for segmented coaxial detectors, such as the one described in [24], this is the axial-azimuthal plane. Processing transient charge data can increase the spatial precision of a position-sensitive detector and can significantly enhance ACAR measurements.

1.7.4 Charge Sharing

Because the free charge created by a photon interaction is not an infinitesimal point but a charge cloud, it can be expected that some events will occur for which the free charge will be collected on more than one node. This effect will be amplified by the diffusion phenomenon which will cause the charge cloud to spread as it approaches the collection nodes [25]. Amman and Luke identified charge sharing as a source of degradation in segmented detector performance because it can lead to incomplete charge collection [26]. The weak electric field in the region between the charge collection strips can lead to some free charge carriers being caught in the intervening space and not contributing to the signal. This loss of charge carriers could lead to degraded energy resolution and photopeak efficiency [26:165].

1.8 Double-Sided Strip Detector

The double-sided strip detector (DSSD) is a design that takes advantage of the characteristics of semiconductors to make a detector that has very good position and

energy resolution. The design consists of sandwiching a planar crystal of HPGe between two banks of charge collection strips oriented orthogonally to each other [27]. The orientation of the strips effectively segments the detector in two dimensions creating a matrix of small detector pixels. Each pixel can be indexed by the intersection of the front and rear collection strips it touches. Because of the close proximity of the strips, the transient charge can be easily measured and used to pinpoint the location each interaction to within its subvolume resolution. Each pixel can therefore be broken down into even smaller "subpixels," virtual area segments that subdivide the detector pixels for increased precision in the spatial measurement (figure 1.16).

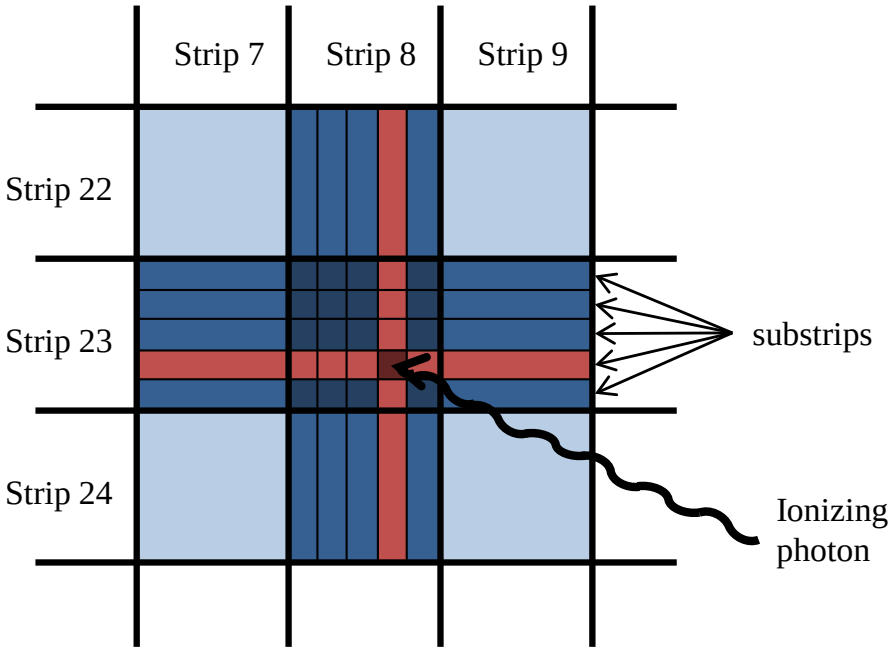

Figure 1.16. Illustration of substrips principle. The photon interacts in the crystal and the charge is collected in strips 8 and 23. The transient charge seen in strips 7 and 8 determines the horizontal substrip location of the interaction, likewise for the vertical substrip location by transient charge in strips 22 and 24.

1.8.1 Subpixel Interpolation

Each interaction detected by the DSSD is indexed according to which strip collects the free charge from the interaction on both the front and rear faces of the crystal. In addition, a substrip number is also assigned by calculating a fine correction (FC) value and scaling it to the number of substrips in each strip The method used to determine the substrip for a given interaction was calculated by using the transient charge figures of merit (FOM) for each recorded interaction. The FOM is a measure of the time integral of the transient charge seen by an adjacent strip. While the generation method for the FOM is proprietary, the FOM for the predecessor and successor strips is included with each hit in a coincidence event by the digital electronics used for this research discussed in section 2.2. By balancing the predecessor and successor FOM, the location of the interaction can be placed in a substrip. While the substrips are an arbitrary division of the charge collection strips, for this research they were made to be uniform divisions according to work done in [16:83], and were set to a width of .10 mm or one-fifth of a collection strip. Thus, there are 5 substrips on a strip and 25 subpixels in a pixel. The transient charge FOMs were used to calculate the FC used to place the location of an event left or right of the center substrip according to the equation

$$FC = \left[\left[\left[\left(\frac{FOM_{successor}}{FOM_{predecessor} + FOM_{successor}}\right) - .5\right] \times 2\right] \times \frac{5(\#\text{ of substrips})}{2}\right] \tag{1.8}$$

The result of calculating the FC, when scaled to the number of substrips and rounded, is a number from -1 to 1 indicating the number of substrips to the left or right (predecessor side or successor side) in which the interaction took place. A certain amount of error may be introduced in spatial measurements due to degradation of subpixel efficiency for edge subpixels. This degradation is induced by the charge sharing effects (discussed in section 1.7.4) which are more prominent for interactions

in edge subpixels. It may be possible to improve the edge subpixel efficiency by implementing a spatially dependent function into the FC equation or the parsing algorithm to compensate for the loss of charge from charge sharing events.

1.8.2 Germanium Limitations

As with nearly all engineered designs, the high-quality of the spatial and energy resolution comes at a cost to other characteristics. The size of the germanium crystal is limited by a number of factors. The production of germanium at the high levels of purity necessary for the detector is a complicated process [28] that limits the diameter of the crystals produced. Furthermore, the planar crystal must be kept thin for two reasons. The first is that the high voltage required to fully deplete the semiconductor increases with the crystal thickness. The maximum crystal thickness d that can be depleted with a bias voltage V is

$$d \simeq \sqrt{\frac{2\epsilon V}{eN_D}} \tag{1.9}$$

where ϵ is the dielectric of the semiconductor (for germanium, $16\epsilon_0$) and N_D is the concentration of dopants in the semiconductor [7:383]. The highest-purity germanium available for detectors has an impurity concentration below $10^9 cm^{-3}$, and the dopant concentration must be higher than the impurity level for diode characteristics in the semiconductor. Using equation 1.9 and considering a high voltage practical for laboratory application on the order of kV, the maximum crystal thickness possible is on the order of $\sim$1 cm. Secondly, the spreading of the free charge cloud will increase with the distance to the collection node, reducing the spatial resolution. Because of the requirement that the crystal be thin, the probability of a high-energy photon interacting in the crystal is reduced and the detector efficiency is very low.

1.9 Photon Interaction in Germanium

The inefficiency of HPGe in collecting annihilation photons is the impetus for this research. According to the exponential attenuation law [29], the fraction of incident photons, ξ, that interact with a material with a thickness t may be expressed as

$$\xi = 1 - e^{-\frac{\mu}{\rho}\cdot\rho\cdot t} \tag{1.10}$$

where ρ is the density of the material and $\frac{\mu}{\rho}$ is the mass attenuation coefficient. For photons in the 511 keV energy range, $\frac{\mu}{\rho}$ for pure germanium is $.08212\frac{cm^2}{g}$ [29], and ρ is $5.323\frac{g}{cm^3}$. For the 1 cm thickness of the DSSD crystal, equation 1.10 dictates that only 35.41% of incident photons will interact with the detector. This figure represents the total interaction probability. The FEPs in energy spectra collected using HPGe detectors are a result of photoelectric (PE) absorption of photons. The free charge carriers generated by a PE interaction in turn produce a signal pulse from the detector proportional to the amount of free charge. However, the PE cross section in germanium decreases with increasing photon energy and is very small for 511 keV photons (figure 1.17). Compton scattering in HPGe is significantly more likely in this energy regime as shown in figure 1.18. Note that there is nearly an order of magnitude difference between the PE cross section for 511 keV gamma-rays and that for 200 keV gamma-rays. In the process of Compton scattering, a photon imparts a portion of its energy into a bound electron that results in a signal pulse just as in PE absorption. The scattered photon will carry on with its remaining energy in an altered direction. The relationship between the photon scattering angle and the energy deposited in the crystal is governed by the Klein-Nishina formula [32:128],

$$\begin{aligned}\frac{d\sigma}{d\Omega} = Zr_0 &\left(\frac{1}{1+\alpha(1-cos\theta)}\right)^3 \left(\frac{1+cos^2\theta}{2}\right) \\ &\times \left(1 + \frac{\alpha^2(1-cos\theta)^2}{(1+cos^2\theta)[(1+\alpha(1-cos\theta)]}\right)\end{aligned} \tag{1.11}$$

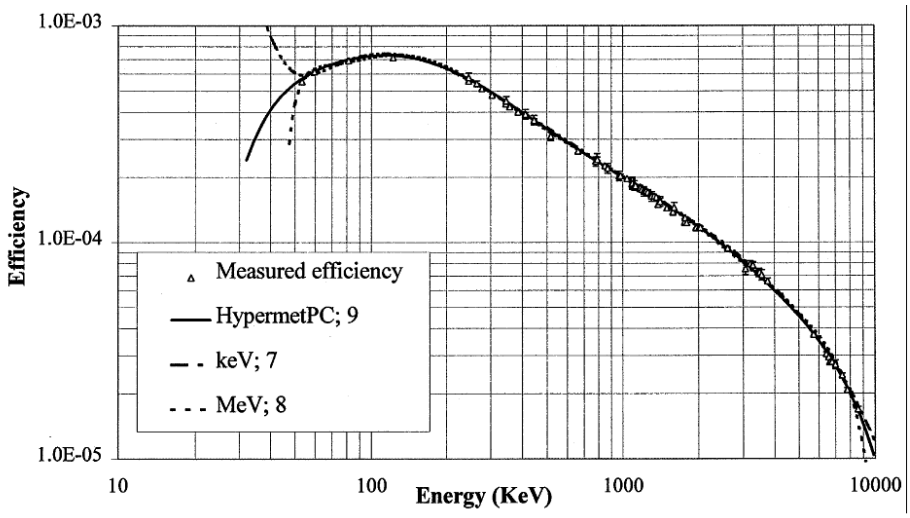

Figure 1.17. Intrinsic efficiency of a typical HPGe detector [30]

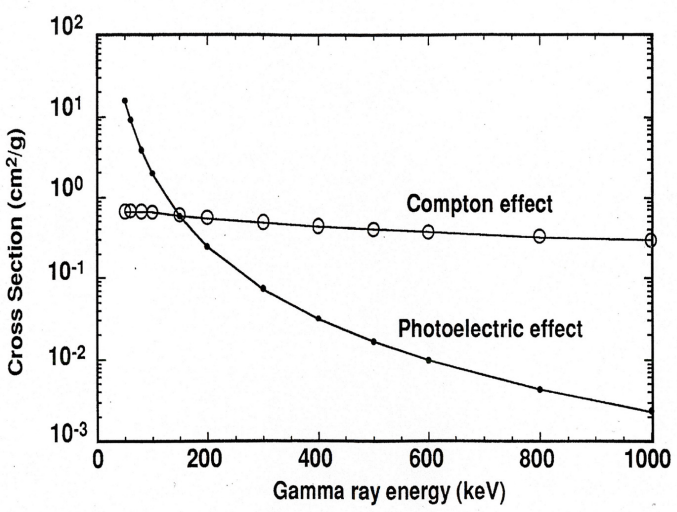

Figure 1.18. Compton Scatter and PE cross sections for germanium [31]

where Z is the atomic number, α is the gamma-ray energy divided by the electron rest mass, r_0 is the classical electron radius, and θ is the scattering angle. Because the Compton scattered photon has a lower energy, it is more likely to be absorbed in a secondary reaction by PE. If a second detector is used, it is possible to improve efficiency of full energy deposition by capturing these scattered photons and correlating

them to the original Compton event in the primary detector. This effectively adds some Compton events back to the full energy peak (or "rescues" them) as if they had been absorbed by PE.

This technique has been modeled using simulation software on a similar experiment by Decman and Namboodiri [31] who modeled a detector setup designed to catch all photons from a source by surrounding the source with detectors and creating a 4π solid angle detector. Their work took into account multiple Compton scatters and energy deposition in multiple crystals. Their simulation predicted a nearly two-fold increase in full energy efficiency when coincidence summing was implemented as Compton rescue.

1.10 Solid Angle Considerations

The geometry of the source and primary detector is an important consideration for Compton rescue because it is a critical factor in determining the intrinsic efficiency of the primary detector. Calculation of intrinsic efficiency requires knowledge of the solid angle of the source radiation field that is observed by the primary detector. The radiation sources used in this research were planchette sources which can be described geometrically as a thin disc. At a large distance from the source, it is assumed that the source will resemble a point source, but for the sake of academic rigor, the precise solid angle for a disc source must be modeled according to the formula given in [33]:

$$\Omega_{disc}(c,d) = \frac{4\pi}{c^2}[(1+c^2)^{\frac{1}{2}} + (1+d^2)^{\frac{1}{2}} - 1 - (1+c^2+d^2)^{\frac{1}{2}}] \tag{1.12}$$

where c and d are the radii of a disc source and detector (both oriented on-axis), divided by distance D, the separation between them. The solid angle is important in efficiency calculations for detectors because it allows the intrinsic efficiency to be determined from the absolute efficiency. The absolute efficiency of a measurement

is calculated as the ratio of the total number of photons detected to the number emitted by the source. The absolute efficiency can be useful for making comparisons of detectors used for similar measurements, however it does not provide a "fair" measure of the efficiency of a detector with respect to incident photons. The intrinsic efficiency uses the solid angle of radiation from the source covered by the detector to restrict the absolute efficiency figure to determine the ratio of photons detected to photons incident on the detector. This figure is more useful in making comparisons between detectors when efficiency data only exists for disparate measurements. See appendix A.1 for intrinsic efficiency calculations.

1.11 Evaluation of Data

The results of the experiment are an evaluation of the utility of Compton rescue. The Compton rescue technique is intended to capture more photons than a lone detector would by itself, however, the effects of adding rescue events to primary detector data must be considered. The energy distribution of rescue events will differ from the distribution of full energy events from the primary detector. This could decrease the quality of energy resolution for DBAR measurements. Additionally, the spatial response of the position-sensitive detector could be degraded by including rescue data, which would have an impact on ACAR measurements. The effects of Compton rescue on energy and spatial resolution will need to be characterized to evaluate the utility of the technique.

II. Equipment

2.1 Detectors

High-purity germanium (HPGe) detectors were used for the experimental portion of this research because of their superior energy resolution properties. A DSSD was used for position-sensitive measurements and a coaxial detector with a much larger active volume was used for Compton rescue. Initial characterization data of the HPGe detectors can be found in appendix A. The energy resolution and efficiency data for the HPGe detectors are summarized in appendix A.2.

2.1.1 Double Sided Strip Detector

The position-sensitive detector is a single-crystal, planar, high-purity germanium (HPGe) double-sided strip detector (DSSD) manufactured by PHDs Co. The crystal is circular, 9 cm in diameter, 1 cm in thickness, and sandwiched between two orthogonal sets of sixteen parallel charge collection strips (figure 2.1). Since the crystal is circular, the outside strips are shorter than the center strips and the pixelation is not completely square (figure 2.2). The strips on the front side of the detector are designated the "DC side" and the strips on the back side are designated the "AC side." The naming scheme is simply a designation and should not be confused with AC- or DC-coupled currents. The high-voltage bias is applied across the crystal through the collection strips to deplete the semiconductor. Normal bias voltage is +600 V, but full depletion occurs around +250 V. In the process of characterizing and testing the detector it was discovered that there was current leakage through the crystal when the voltage was set to the standard setting of +600 V. To avoid this problem the voltage was lowered to +300 V. At this setting, the leakage was not observed and the detector functioned properly, although lowering the bias voltage may have had an effect on the spatial resolution due to increasing the amount of charge cloud spreading.

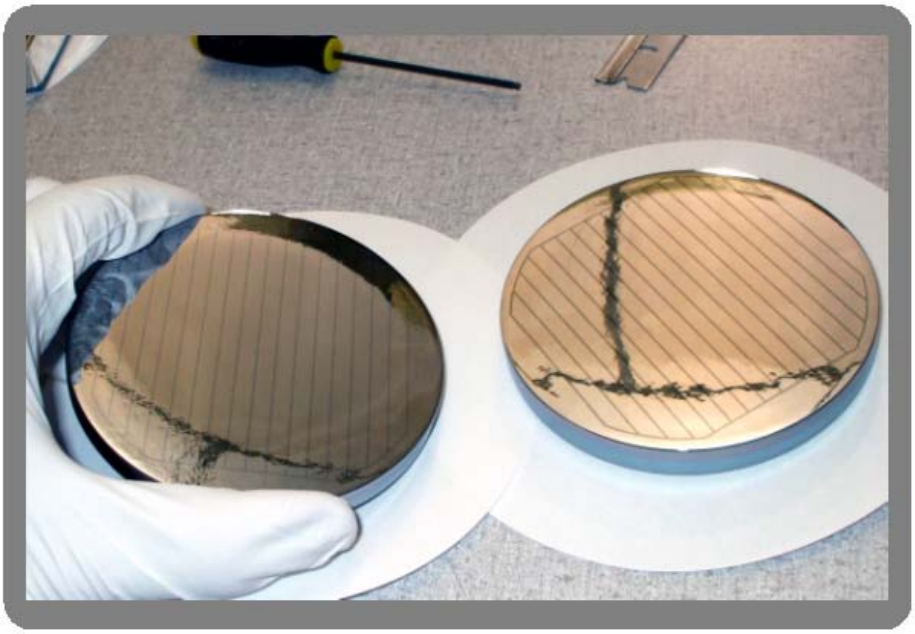

Figure 2.1. Picture of DSSD crystals with charge collection strips visible [34]

This effect was observed and is discussed in the results (section 4.2.7).

In order to achieve full depletion of the germanium crystal, it is necessary to keep the crystal at a low temperature, below 150 K [35–37]. To maintain this low temperature, it is advantageous to insulate the crystal in a vacuum. Both the mechanisms for cooling the crystal and maintaining the vacuum around it are built into the DSSD unit. The vacuum is achieved with an ion pump which keeps the pressure in the crystal chamber at 10^{-9} torr. The DSSD crystal is cooled with a built-in mechanical cooler which maintains a temperature below 65 K.

2.1.2 Coaxial Detector

The detector used for Compton rescue was a coaxial HPGe "Pop-Top" detector manufactured by Ortec. The coaxial detector crystal is much thicker than the DSSD and can therefore collect photons more efficiently. The crystal is a cylinder with an 8.5 cm diameter and a length of 3.3 cm. In the center of the back end of the cylinder a

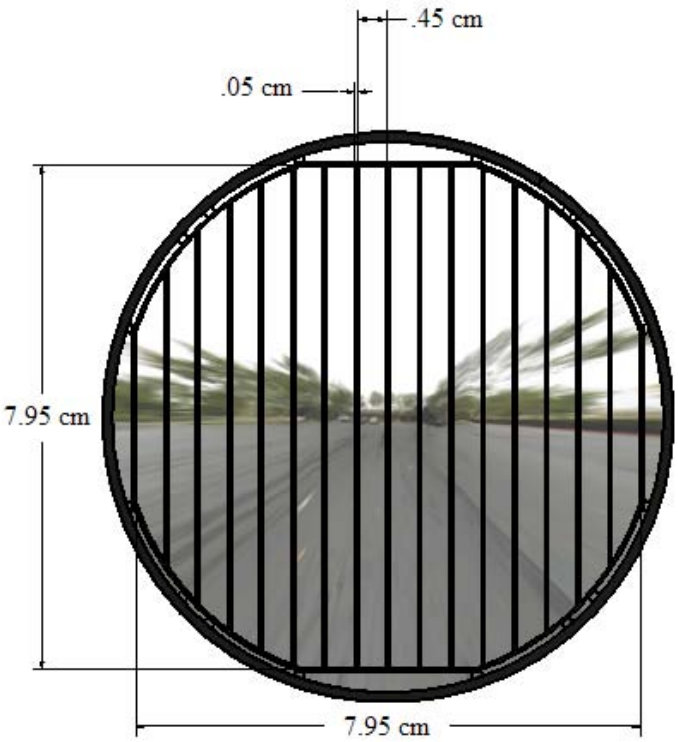

Figure 2.2. Diagram of DSSD crystal with one side of charge collection strips illustrated

hole is drilled 0.9 cm in diameter and 1.7 cm in depth (figure 2.3). The outer surface of the cylinder and the inner surface of the drilled hole provided the surface for the charge collection and depletion biasing contacts. The charge collection contacts are on the outside of the cylinder and the wall of the hole. To cool the crystal, a cryostat attached to a liquid nitrogen-filled dewar is used to achieve a crystal temperature of 107 K. Rather than using a vacuum to insulate the crystal, a thin layer of mylar surrounds the crystal. Since the crystal is much larger than the DSSD and the electric field is radial, the high-voltage bias required to fully deplete the semiconductor is also much larger. The coaxial detector was biased at +2500 V.

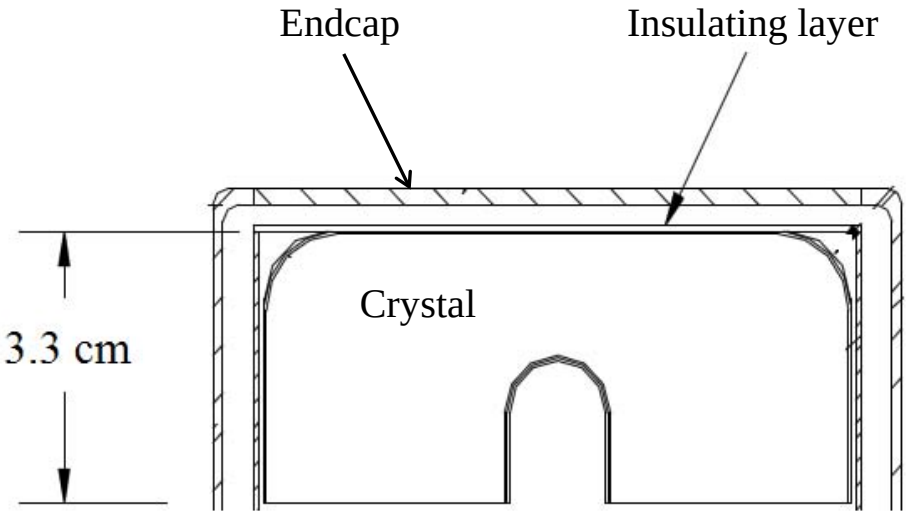

Figure 2.3. Diagram of coaxial detector crystal

2.1.3 Scintillation Detector

A sodium iodide (NaI) scintillation detector was used for annihilation coincidence measurements in the DBAR experiment portion of this research. Sodium iodide is hailed for its excellent scintillation qualities and high collection efficiency [7:234]. The detector was a 3x3 (3-inch diameter, 3 inch depth) thallium-doped sodium iodide crystal manufactured by the Saint-Gobain company (Serial number 60004-00026-I, figure 2.4). An Ortec 266 photomultiplier base (Serial number 09078222R) was used and the signal was amplified by an Ortec 113 preamplifier (Serial number 6511). Although the energy resolution of this detector is not good enough to contribute data to the DBAR spectrum, it was used to collect coincident photons from annihilation events and provide a flag for annihilation events in the experiment output data.

2.2 Electronics

The processing of the signals from the numerous inputs involved in collecting the position-sensitive rescue spectra require specialized electronics. A signal can be

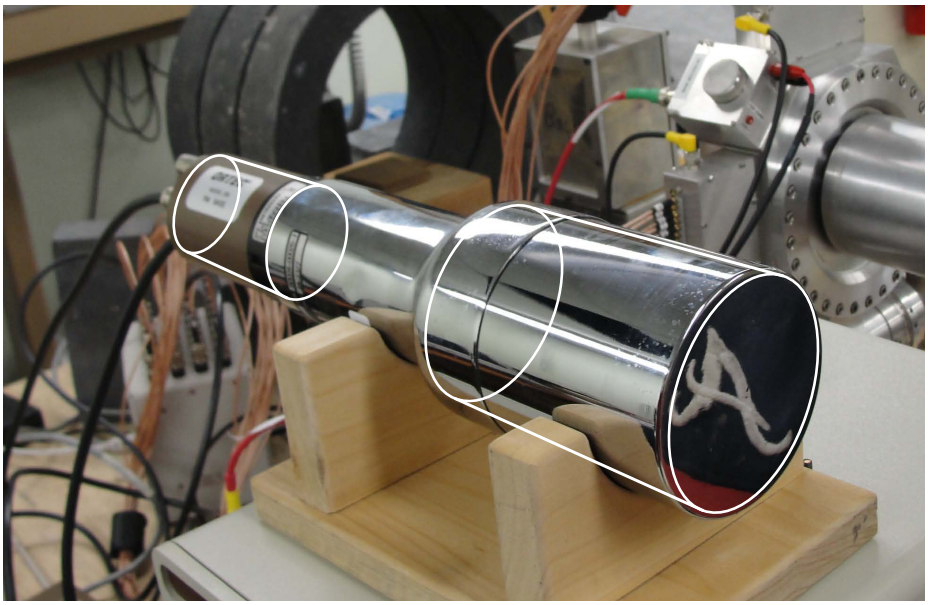

Figure 2.4. Picture of sodium iodide scintillator detector. Scintillator crystal and photomultiplier base are outlined in white cylinders.

associated with any or the thirty strips in the DSSD, the rescue detector, of the scintillator detector. To process the thirty-two data channels, an electronics system called Spect32, designed specifically for position-sensitive imaging, was employed. The Spect32 (figure 2.5) is a 32-channel, 50-MHz digitizer (clock cycle is 20 ns). Within the system are four independent electronic boards (called "daughter boards") that process eight channels apiece. The 32 channels were numbered 0-31. Each electronics board contains two 12-bit Analog-to-Digital Converters (ADCs) and two Alterra Cyclone field-programmable gate arrays (FPGAs). The preamplified waveforms from the thirty-two input channels are immediately digitized according to user-defined settings specified in the Spect32 software, Imager32. Some settings can be defined for each channel while others are applied to all channels on a daughter board [16:68-70]. A list of the specific settings used can be found in Appendix C. For this experiment, the FPGAs were programmed to record the energy deposited in each DSSD channel and a figure-of-merit (FOM) for the transient charge on the adjacent strips. Imager32 uses this data to collect spectrum data for each channel and event logs for coincident

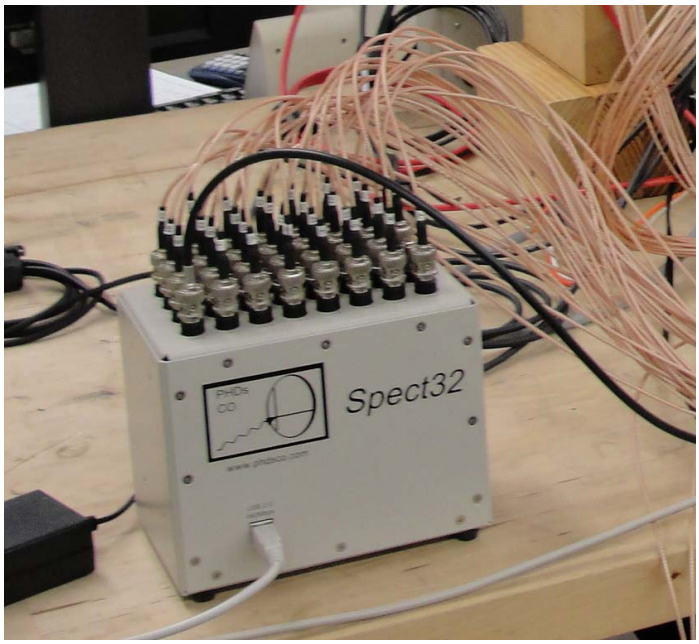

Figure 2.5. Picture of Spect32 digital electronics processing unit. Each of the cables plugged into the top of the unit carries a signal from either one of the DSSD channels or one of the other detectors.

signals. The charge collection strips were each associated with an output channel and were numbered 0-15 from top to bottom for horizontal (DC) strips and 16-31 from left to right for vertical strips (AC). For this experiment, each DSSD channel was connected to the Spect32 input of the same number, except for channels 0 and 15. Inputs 0 and 15 on the Spect32 were reserved for the rescue detector and the scintillator detector, respectively.

The Imager32 software populates a spectrum for each channel connected to the Spect32 according to the time integral of the signal pulses from the detector. These pulses are converted to energy values according to a calibration set by the user so that the result is an energy spectrum. In addition to creating energy spectra, the software can create output files that log raw coincident event data. The Spect32 records all signals collected on any channel within 256 clock cycles (5.12 μs) of a trigger signal as coincident. All signals within a coincidence event are logged in the output file. Data

logged for each signal include the order of arrival and number of clock cycles after the trigger, the calibrated energy, and the transient charge FOMs for the previous adjacent strip (or "predecessor") and succeeding adjacent strip (or "successor").

2.3 Sources

Several different radiation sources were used in the laboratory experiment. Each source had a specific application to the laboratory experiment. Data for each source is provided in appendix B.

2.3.1 ^{137}Cesium

^{137}Cesium is a standard source used for making resolution and efficiency characterization measurements for radiation detectors. The isotope has a half-life of 30.07 years which makes it an important source for many laboratories. The emitted γ-ray of 661.7 keV makes ^{137}Cesium a suitable high-energy source for detector characterization. The characterization of the HPGe detectors used in this research with the ^{137}Cesium source is summarized in appendices A.3 and A.5.

2.3.2 ^{85}Sr

^{85}Sr is a standard source with a characteristic γ-ray of 514 keV. Its half-life is 64.84 days The energy proximity to the 511 keV annihilation photons produced in positron annihilation makes it especially useful for characterizing detectors used for PAS applications. The characterization of the detectors with ^{85}Sr simulates the detector response to 511 keV photons without the effects of Doppler-broadening. These results are summarized in appendices A.4 and A.6.

2.4 Samples

Four material samples were used for the DBAR portion of the experiment. A sample of unannealed and annealed single-crystal nickel were used for samples with two different crystallographic orientations, (100) and (111). Samples of 99.999% pure single-crystal Ni for both orientations were acquired from Goodfellow Cambridge Ltd. The (100) samples were cut to 5×5 mm^2 squares of 0.2 mm thickness. The (111) samples were 10×10 mm^2 sqaures of 0.5 mm thickness. A sample of each crystal was annealed at 950^{o}C for one hour in argon gas, per procedures in [38]. The intent of having an unannealed and annealed sample of each crystal was to observe a qualitative difference in the DBAR spectra. The results of this experiment are discussed in section 4.2.8.

2.5 Shielding

Shielding procedures were exercised in the lab both for radiation safety purposes and for background shielding. Lead bricks were readily available in the laboratory for shielding purposes. Shielding was used to protect the coaxial detector during characterization to prevent background interference and interference from other sources in the lab. Because of the size of the crystal in the rescue detector, it was expected to be very sensitive to background radiation. The use of the ^{85}Sr source was hazardous due to its high level of activity (appendix B), and shielding was constructed to protect lab workers. Shielding was also used in the DBAR portion of the research for protecting the scintillator detector from background radiation. Annular lead rings of two-inch thickness were set up around the scintillator detector and the opening behind was covered with lead bricks. Shielding was used to prevent interference with the measurements and minimize sources of noise in the data.

2.6 Collimator

To qualify the spatial precision of the DSSD, a collimator was used to produce a narrow beam of radiation. Spatial resolution was assumed to be the same as measured in [16:83]. The spatial resolution of the detector is defined as the error associated with spatial data. The fabrication of this collimator is discussed in [ibid:73]. The collimator is made out of AIM 70 ^{TM}, an alloy composed of bismuth (50%), lead (27%), tin (13%), and cadmium (10%). The collimator was fabricated with a thickness of 3 inches, calculated to attenuate 99% of 514 keV photons outside of the desired beam width. The hole diameter is estimated to be 0.15 $\pm$.05 mm.

2.7 Equipment Layout

The DSSD was set 29 cm above the surface of the bench due to the structure of the unit. The coaxial detector was elevated to the level of the DSSD so that the crystals could be positioned in the desired orientation. For most characterization spectra, the sources were elevated to a height such that the source was approximately at the level of the center of the DSSD. For measurements using the finely collimated beam of photons, more location precision was necessary and a vertical translation adjustable platform was employed. All wires were attached in such a way that would minimize their interference with the experiment. The basic setup for a characterization of the Compton rescue system is shown in figure 2.6.

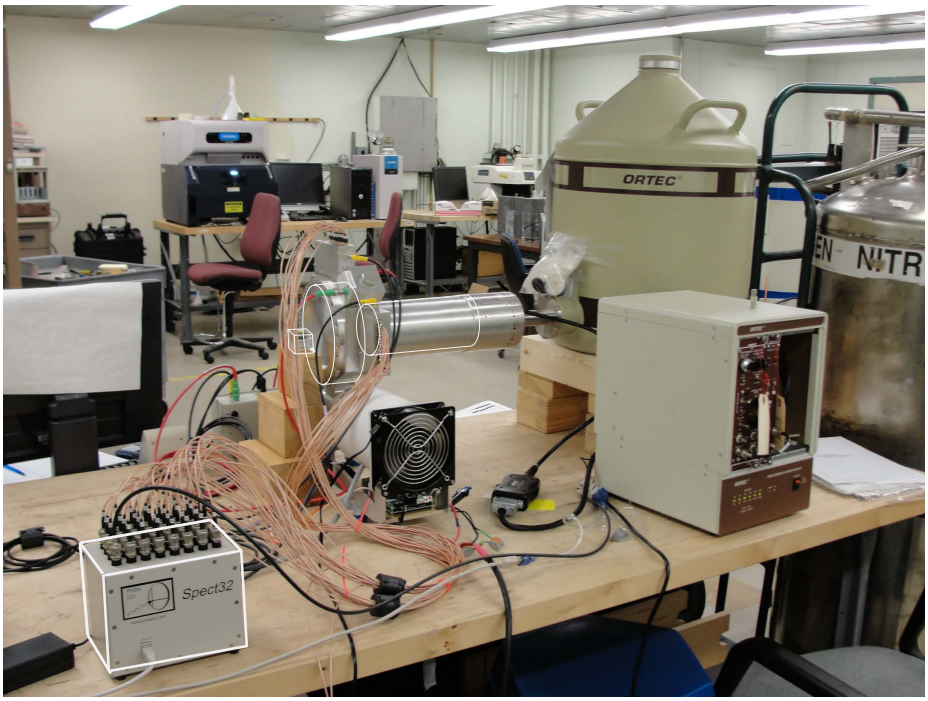

Figure 2.6. Photograph of setup for Compton rescue characterization (small source offset to primary). The approximate location of the DSSD and coaxial detectors are outlined as cylinders and the source is outlined as a cube. The Spect32 is also highlighted.

III. Procedures

3.1 Simulation

Before testing the Compton rescue technique directly in the laboratory, a Monte-Carlo computer simulation was used to predict the feasibility of the experiment. The use of Monte-Carlo methods to simulate detector response is standard practice in detector research [31, 39–41]. The geometry of the laboratory experiment was reproduced in a virtual environment and the interactions of source photons with the detector layout were simulated with computer software. Simulated photon histories were analyzed and tabulated as Compton rescues and full energy events according to the sequences of their interactions with the virtual detectors. The ratio of photons that underwent Compton rescue to those that underwent PE absorption in the primary was used as a measure of the efficiency improvement for the experiment.

3.1.1 MCNP5 Software and Implementation

The software used for the simulation was the Monte-Carlo n-particle transport code (MCNP) developed by Los Alamos National Laboratory. The code is open to modification and has seen continuous development since the initial release in 1977. The version used for this research is Version 5 [42].

The simulation was carried out by building an MCNP input deck composed of many different *cards* (simulation input specifications) that specify different aspects of the simulation. The input deck was used by the software as a basis for simulating a large number of photons. The photons were tracked by the software and a history of interactions was created for each photon from the source to its termination. Each history consisted of a line of data describing the photon's state at every point at which it underwent an interaction. These histories were collected and logged in an output file to be parsed and analyzed. By parsing and analyzing each history in the output

file, tallies were created to quantify the impact of Compton rescue. The following subsections provide details explaining the considerations for various aspects of the simulation and the implementation of those considerations.

3.1.2 Simulation Procedure and Design

3.1.2.1 Scene Geometry

The geometry input was designed to reflect the critical components of the detectors in the laboratory setup as accurately as possible without computing the effects from components of negligible contribution. The only components that photons of interest (Compton rescue and direct absorption photons) would interact with were the detector crystals and housing components in the path from the source to the detectors. The dimensions of the detector components were taken from documents provided from the manufacturers [43, 44]. For the DSSD, this includes the faces of the vacuum chamber and the faces of the outer housing of the detector. These components (yellow volumes in figure 3.1) are composed primarily of aluminum. The DSSD was designed such that there are no other components such as electronics boards in the path of incoming or outgoing photons through the detector faces. For the coaxial detector, a window component was simulated in front of the crystal composed of carbon fiber (green volume in figure 3.1). The mylar insulation layer was also included (indicated by the purple surface on front face of coaxial detector crystal in figure 3.1). The geometry code was created by defining a set of surfaces in Cartesian space and using logical operations to combine the surfaces into cell volumes. The rules for the MCNP syntax can be found in [42:2-5] and the geometry input cards used in the simulation are in appendix D.

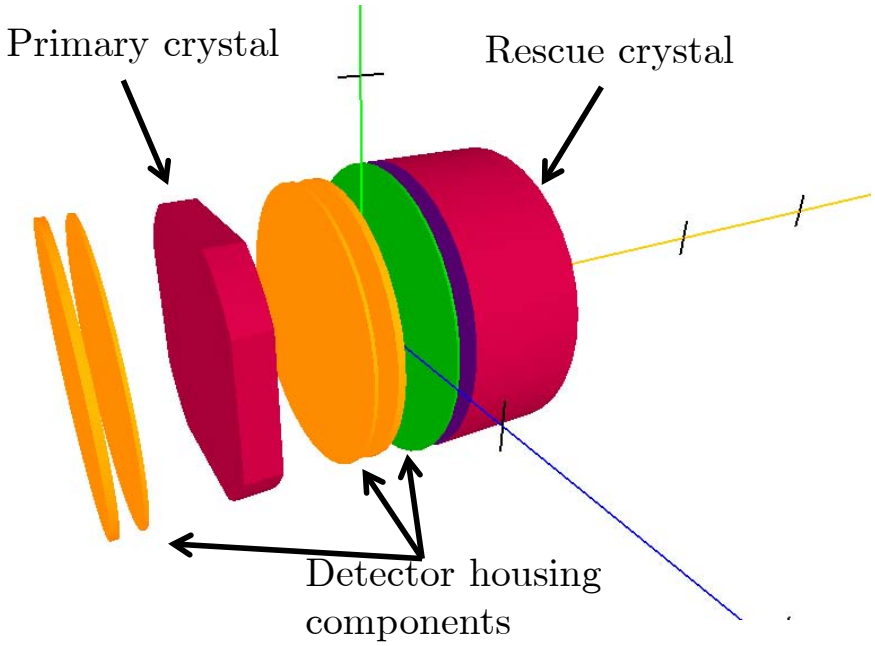

Figure 3.1. 3D rendering of MCNP geometry. The detector HPGe crystals are represented by the red shapes. In the scene represented by this image, the photon source would be to the left of the scene, collinear with the line running through the center of the shapes.

3.1.2.2 Materials Cards

One of the major advantages of using MCNP is the extensive library of material properties which are the foundation of particle interaction simulations. The materials libraries contain interaction cross-section data for many different types of particles with an impressively large number of material substances. These cross-section data are used by the software to make probabilistic calculations ("rolling the dice") for interactions of the simulated particles with material volumes. For this simulation, only a few substances were necessary to be defined. A material card is created for each substance in a simulation and is defined by the proportions of basic materials found in the libraries. The cell volume cards (section 3.1.2.1) each must reference a material card and define the density for that material. The materials used for the simulation are summarized in table 3.1.

Table 3.1. Summary of materials used in simulation

Material	Use	Composition	Density ($\frac{g}{cm^3}$)
HPGe	DSSD and Coaxial detector crystals	Ge (100%)	5.323
Air	Volume surrounding detectors	N (78.44%) O (21.08%) Ar (0.47%) C (0.02%)	.001275
Mylar	Thin surface of coaxial detector	C (45.46%) H (36.36%) O (18.18%)	1.38
Aluminum	DSSD housing	Al (100%)	2.70

3.1.2.3 Photon Source

A photon source was added to the scene to simulate the sourcing of the photons as they would be in the laboratory experiment. All photons from the source were monoenergetic 511 keV photons (no Doppler broadening) and the source location was uniformly distributed over a 2 cm radius flat disc, offset a specified distance from the face of the primary detector. The objective of the simulation was not to make predictions about changes in the absolute efficiency from the use of Compton rescue, rather the intrinsic efficiency. For this reason, the initial direction of the source particles was restricted to a cone such that all particles passed through the face of the primary detector (see figure 3.2). The directional distribution over this cone was also uniform. For various reasons, a number of source particles would not meet the criteria for tracking (discussed in section 3.1.2.4). The number of particles sourced was normalized such that the number of particle histories written to the output was $1 \times 10^6 \pm 10^2$. The code for the photon source can be found in appendix D.4.

3.1.2.4 Particle Tracking

MCNP simulates every particle from source to termination, including secondary particles. The series of events from source to termination was logged as a particle

history and written to an output file by using the *PTRAC* card in MCNP. Filters were applied to eliminate insignificant particle histories from being written to the output. Not all event types were included in the ptrac output. The event types were selected from the list in table 3.2. For every event in a history, there are two data lines (See appendix E for PTRAC data sample). On the first line are several data specific to the event type. On the second line are data concerning the state of the particle. These data include the 3-dimensional coordinate position of the particle, 3-axis directional cosines, particle energy, particle weight and time ($t = 0$ at source). These data were collected with a parsing algorithm for simulation analysis.

Table 3.2. PTRAC event types

Event types	Description
Source	The state of the particle "at birth"
Surface	The state of the particle as it crosses the border between volume cells
Collision	The state of the particle immediately after an interaction with matter, and the type of interaction
Bank	Events for which secondary particles are created
Termination	The state of the particle as it terminates and the type of interaction which results in termination

3.1.2.5 Output Processing

The output data files produced by the PTRAC card consist of header data followed by a long series of photon histories. Each history can be evaluated on the basis of defined criteria and counted to a significant tally such as Compton rescue, direct absorption, or some other classification. A parsing algorithm (detailed in appendix G) was developed in MATLAB®code to process the PTRAC output and produce photon

history analysis. Figure 3.2 provides a visual illustration of the most significant types of photon histories encountered in the PTRAC output for this research effort. Before applying the parsing algorithm, a few filtering criteria were applied within the

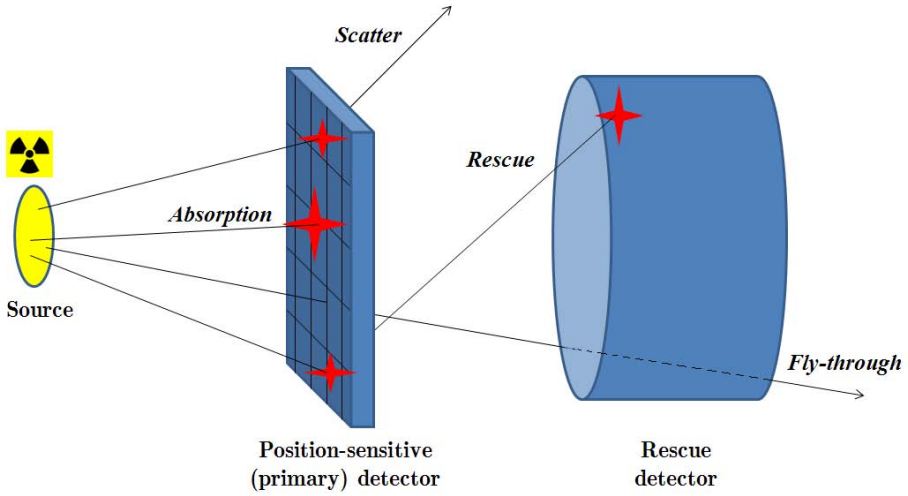

Figure 3.2. Visualization of different types of particle histories encountered in ptrac output. This figure does not include some rare types of histories, such as "bounce-back" (in which a particle is detected in the primary after being backscattered from the rescue) or any events including coherent scattering in the primary.

MCNP input to reduce the file size and eliminate unnecessary histories from the data. Histories can be filtered on the PTRAC card according to cells entered or surfaces crossed. The histories were filtered according to the criteria that the photon could not be written to the output if it did not, at any point in its history, enter the cell corresponding to the primary detector. Additionally, the PTRAC card allows certain events to be filtered from the output file. Two event filtering criteria were defined. One criterion restricted the events written to the PTRAC file to those events that took place inside an arbitrary volume surrounding the source and the detectors. The second criterion filtered events for photons that had experienced no interactions. This eliminated all histories in which no photon interactions occurred ("fly-through") and reduced the number of events for the parsing algorithm to sort through. By applying these filtering options, the size of the PTRAC files was significantly reduced by over

50%. The total number of events was cut approximately in half and the total number of histories was reduced by about 20%.

The qualifying criteria for defining a history as a Compton rescue are based on the physics of Compton rescue. By definition, the history for a Compton rescue event must begin with a source photon being Compton scattered in the primary detector and every successive interaction until absorption must take place in the rescue detector. If multiple scattering events occur in the primary detector, or if any collision events occur in a region outside of the active detector volume, the history cannot be a Compton rescue by definition. Multiple scatters within the primary detector could be counted as Compton rescues, however, since the electronics of the laboratory experiment do not have sufficient time resolution, these photons were discounted in the simulation. If a photon does not terminate in the rescue detector then the event cannot be tallied as a Compton rescue. As a check, the energy lost by the photon for each event in the history must sum to the energy of the photon emitted at the source (511 keV for all photons this simulation). In the laboratory experiment, the energy sum would have to equal the full energy to within a set window, ΔE, but in the simulation, all energy should be accounted for because perfect charge creation and collection was presumed.

The criteria for a direct absorption were defined in a similar manner. For direct absorption, only one collision should take place, and it should take place in the primary detector. The collision should be immediately followed by a termination at the same location. Because of the way MCNP simulates absorption, the termination of a photon consists of a collision event followed by a termination event, even though in physics this phenomenon is generally considered to be a single event [45:221].

The algorithm was realized into code by logically tallying significant histories into tallies. The code is provided in appendix G along with the pseudocode translation for easier understanding.

3.1.3 Important Metrics

The simulation data are expected to be consistent with the theory that the proposed detector scheme can improve the efficiency of position-sensitive measurements. Given that a thin planar detector is expected to capture only a fraction of photons incident on the crystal, a scheme to increase the efficiency of the detector should reflect an increase in this percent. An important metric for this effect is the Rescue-to-Capture ratio (R2C). This ratio expresses the proportion of photons that undergo Compton rescue to those that are directly captured by the primary detector by PE. The R2C can be defined as

$$R2C = \frac{\text{number of rescues}}{\text{number of captures}} \tag{3.1}$$

where the number of rescues and the number of captures are the tallies associated with the criteria for Compton rescue and direct absorption detailed in section 3.1.2.5. Because the R2C is independent of the absolute efficiency of the detector, any changes to the R2C due to changing the position of the source must be attributed to the changing geometry of the scattering angles covered by the rescue detector. At high energies most photons will be scattered in the forward direction [7:51]. If the source is located very near the face of the primary detector, the forward-scattered photons scattered near the edge of the primary detector will not enter the rescue detector. The R2C is therefore expected to be small for small source offset distances. Conversely, if the source is located far from the primary detector almost all forward scattered photons will be incident on the rescue detector, and the R2C is expected to be higher. The principle is illustrated in figure 3.3. This effect can be used to test the accuracy of the simulation, by running the simulation with the source set at different distances from the primary detector and observing the the change in the R2C. While the R2C should be higher at a large offset distance, the absolute efficiency will suffer due to

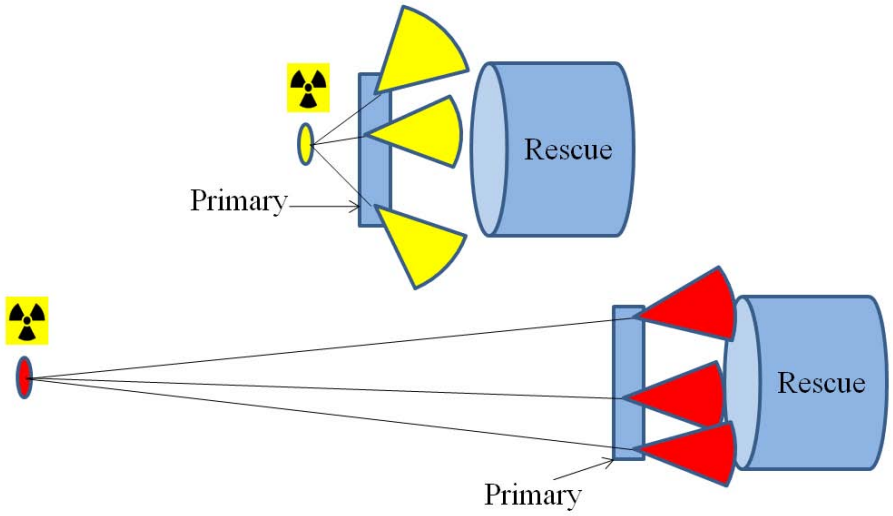

Figure 3.3. Illustration of the offset distance effect. Blue colored shapes represent detectors. Yellow and red colored sectors represent forward-scattering regions.

the smaller solid angle from the source to the primary detector.

Scattering information may also be inferred from the simulation data by examining the distribution of scattering energies from photons scattered in the primary detector. The mechanics of Compton scattering dictate that certain features will appear on the energy distribution of scattered photons. A peak known as the *Compton Edge* should appear at an energy defined in [7:310] by the relation

$$E_{ComptonEdge} = \gamma \frac{\frac{2\gamma}{m_0 c^2}}{1 + \frac{2\gamma}{m_0 c^2}} \tag{3.2}$$

where $E_{ComptonEdge}$ is the energy deposited by a photon in an event scattered directly back towards the source, γ is the energy of the incident photon, and $m_0 c^2$ is the electron rest mass energy. For the 511 keV gammas used in the simulation, $E_{ComptonEdge} = 340.7keV$ [46:861]. The appearance of this feature in the simulation results is expected for simulation verification.

These metrics will all be used to test the validity of the simulation. The simulation results are given in Chapter IV.

3.2 Experimental

The experiment was conducted in the nuclear engineering laboratory at AFIT. Several experiments were conducted to characterize the detector sensitivity and test the utility of Compton rescue as a means to increase efficiency. Data from the experiments were collected and analyzed with parsing algorithms to determine results.

3.2.1 Calibration and Characterization

3.2.1.1 Calibration

The detectors were calibrated using the sources discussed in section 2.3. The detectors were setup as shown in figure 2.6 and spectra were taken with the source in front of the bare detectors. The calibration was conducted first with ^{137}Cs sources 3 cm from the face of the DSSD for a one-point calibration at 662 keV. When each DSSD strip was calibrated, peak data was analyzed for resolution and efficiency. The detectors were characterized for efficiency and resolution at this energy and then recalibrated with the ^{85}Sr source to 514 keV. A one-point 514 keV calibration was used for all DBAR measurements.

3.2.1.2 Resolution Characterization

To characterize the resolution, the full-width half-maximum (FWHM) was taken of the full energy peak for each input channel on the Spect32. The FWHM for a peak on an energy distribution spectrum is a measure of the difference in energy between the points right and left of a FEP for which the number of counts is half that of the maximum value [7:115]. The FWHM was used to characterize the resolution of each detector channel. A small FWHM is considered "sharp" and achieving the smallest possible FWHM is desirable. By examining figure 3.4 it is apparent that the resolutions for each DSSD strip can vary widely. The resolution data for the

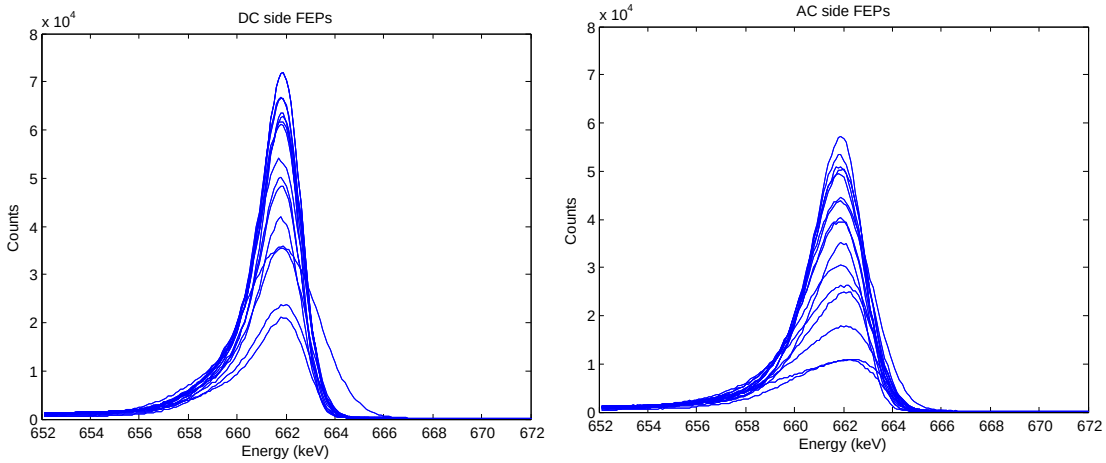

(a) Average FWHM=2.21 ±.06 (b) Average FWHM=3.09 ±.45

Figure 3.4. FEP plots for all 32 DSSD channels. AC and DC strips are separated for comparison. Note that the AC strips are less efficient and less well resolved. This is because the AC side of the crystal is biased negative and collects the positive "hole" charge. The free hole mobility in germanium is lower than the free electron mobility resulting in slightly worse charge collection efficiency.

detectors used in this research is provided in appendix A. The DC side strips (channels 0-15) have a resolution of 2.21 ± 0.06 keV while the AC side strips (channels 16-31) have a slightly higher resolution of 3.09 ± 0.45 keV. This is due to the difference in charge collection efficiency between positive free charge and negative free charge. A similar figure is the full-width tenth-maximum (FWTM), a measure of the energy difference between the points one-tenth of the maximum peak value on either side. The FWTM was used to determine the energy window for counting an event in the post processing algorithm. For the DC side, the FWTM was 5.50 ± 0.15 keV and for the AC side, 6.59 ± 0.95 keV. The full resolution characterization data for 662 keV is provided in appendix A.3 This data was taken for DSSD characterization, not for use in the Compton rescue setup.

3.2.1.3 Efficiency Characterization

To characterize the efficiency of the detectors, the number of counts in the FEP from the spectra collected of the calibrated sources was compared to the number of counts expected based on their calculated activity (see appendix A.1 for calculation method). As discussed in section 1.10, the solid angle was calculated using equation 1.12 [33:164]. This method assumes isotropic illumination from the source. The offset distances were recorded from each characterization spectrum and used to determine efficiency characteristics for each detector. The results of the efficiency characterization for the Cs and Sr sources can be found in appendices A.5 and A.6. As expected, the rescue detector was found to be three to four times as efficient as the DSSD for the FEP of a given characterization spectrum (this is not the efficiency increase from Compton rescue, rather, it is the efficiency ratio of the rescue detector and the DSSD). It may be noted that the AC side strips were slightly less efficient than the DC side strips. This is due to the fact that the AC side was the negative bias side and thus collected the free positive charge (or "holes"). Holes have a slightly lower mobility than electrons in germanium [23:51], thus are more prone to trapping and charge loss.

3.2.2 Data Processing

The data output from the Spect32 come in two forms. The energy spectrum is a histogram of all the energy deposition events recorded by the detectors. These data are used to characterize efficiency and resolution as discussed in sections 3.2.1.3 and 3.2.1.2. The other type of output is the coincidence event data. A coincidence event is written to an output file whenever two or more interactions (or "hits") are measured within 256 clock cycles of the Spect32 (5.12 μs). Each output file is a list of coincidence events comprised of an ordered list of the coincident hits that make up the event. Each hit is written sequentially to the output file as a row with entries in

each of seven data columns (table 3.3). For an example of an event from an output data set, see appendix F.

Table 3.3. Ordered list of data types included in a Spect32 hit

Data column	Data type
1	Sequential number of hit within event
2	Total number of hits in event
3	Number of clock cycles since trigger (first hit)
4	Channel number of hit
5	Calibrated energy deposition
6	Predecessor FOM
7	Successor FOM

Using this format, a data processing algorithm was written in MATLAB®to process the data files. Similarly to the processing of the simulation data, each event was individually analyzed according to qualification criteria (see appendix H). Qualifying events were saved and tabulated with all their data to be analyzed for the experiment results.

To qualify as a Compton rescue, an event must have a hit on the rescue detector (channel 0 on the Spect32 was reserved for this) and the sum of the energy collected by the rescue detector must sum with the energy deposited in the DSSD to a value within a set window of the full energy (the FWTM, as discussed in section 3.2.1.2). Since the charge collection for the AC strips was not as efficient as that of the DC side (see appendix A), the criteria were written such that the full energy need only be collected with the rescue detector and the DC strip. If the full energy was collected by both the DC and the AC side, the two were averaged to log the energy of the event. The criteria for direct absorption events were similar, the difference being the absence of a hit from the rescue detector.

The inclusion of charge sharing events in the results of an experimental spectrum was decided on the basis of analysis of charge sharing data. A spectrum was taken of four pixels exposed to the ^{85}Sr source and all charge sharing events were extracted.

The FOMs for these sharing events were analyzed the same way as for non-charge-shared events (equation 1.8). For charge-shared events to be counted, the distribution of the fine correction should fall mostly within the edgemost subpixels. If the distribution did not behave this way, the data would indicate erratic behavior for the FOMs in charge-shared events and they would have to be discarded. Furthermore, the fine correction distribution should not peak at the extreme edge of the pixel or subpixel ambiguity would be implied. The data for the charge-sharing analysis proved that charge shared events could be counted. The analysis is discussed in the results chapter (chapter IV).

A special algorithm had to be developed for charge sharing events. If two hits were registered on either the AC side or the DC side, they must be on adjacent strips or the event was disqualified. Events for which more than two hits occurred per side were discarded. The event was tallied in the strip for which the most energy was measured, however, the energy of both strips were summed to meet the full energy criteria.

3.2.3 Important Metrics

The results of the experiment are expected to be an evaluation of the utility of Compton rescue. The Compton rescue technique is intended to capture more photons than a lone detector would by itself, however, the effects of adding rescue events to primary detector data must be considered. The energy distribution of rescue events should differ from the distribution of full energy events from the primary detector. This could decrease the quality of energy resolution for DBAR measurements. Additionally, the spatial response of the position-sensitive detector could be degraded by including rescue data, because transient charge FOMs may be too small to measure for small energy depositions in the DSSD, such as those from Compton scattering. This degraded spatial resolution may have a negative effect on the quality of ACAR

measurements. The effects of Compton rescue on energy and spatial resolution will need to be characterized to evaluate the utility of the technique.

The R2C will be evaluated as in the simulation, the ratio of rescue events to full-energy events in the primary. This ratio will characterize the gain in efficiency from using Compton rescue.

3.3 DBAR measurement

After collecting all the characterization data for the Compton rescue setup, a DBAR measurement was taken to test the usefulness of the technique for research applications. The measurement was done to examine the structure of single-crystal nickel. Four total samples were analyzed by DBAR, one annealed and one unannealed for two crystallographic orientations, (111) and (100). A sample from a crystal of each orientation was annealed at 950 ^{o}C for one hour in argon gas, according to procedures in [38].

In this research, the DBAR measurement was carried out by using the NaI scintillator detector discussed in section 2.1.3 for coincidence. The scintillator was mounted on a platform so that it was collinear with the center of the Compton rescue detectors. The material sample and a positron source were sealed in a miniature vacuum chamber to minimize the interaction of positrons with air. The vacuum chamber was pumped down to a pressure of 1.5 torr. The chamber was mounted on a vertical translating platform and positioned on the center line of the three detectors, equidistant from the face of the DSSD and the scintillator. A picture of this setup is presented in figure 3.5. A DBAR spectrum was taken for each of the four samples for 3 hours and 38 minutes.

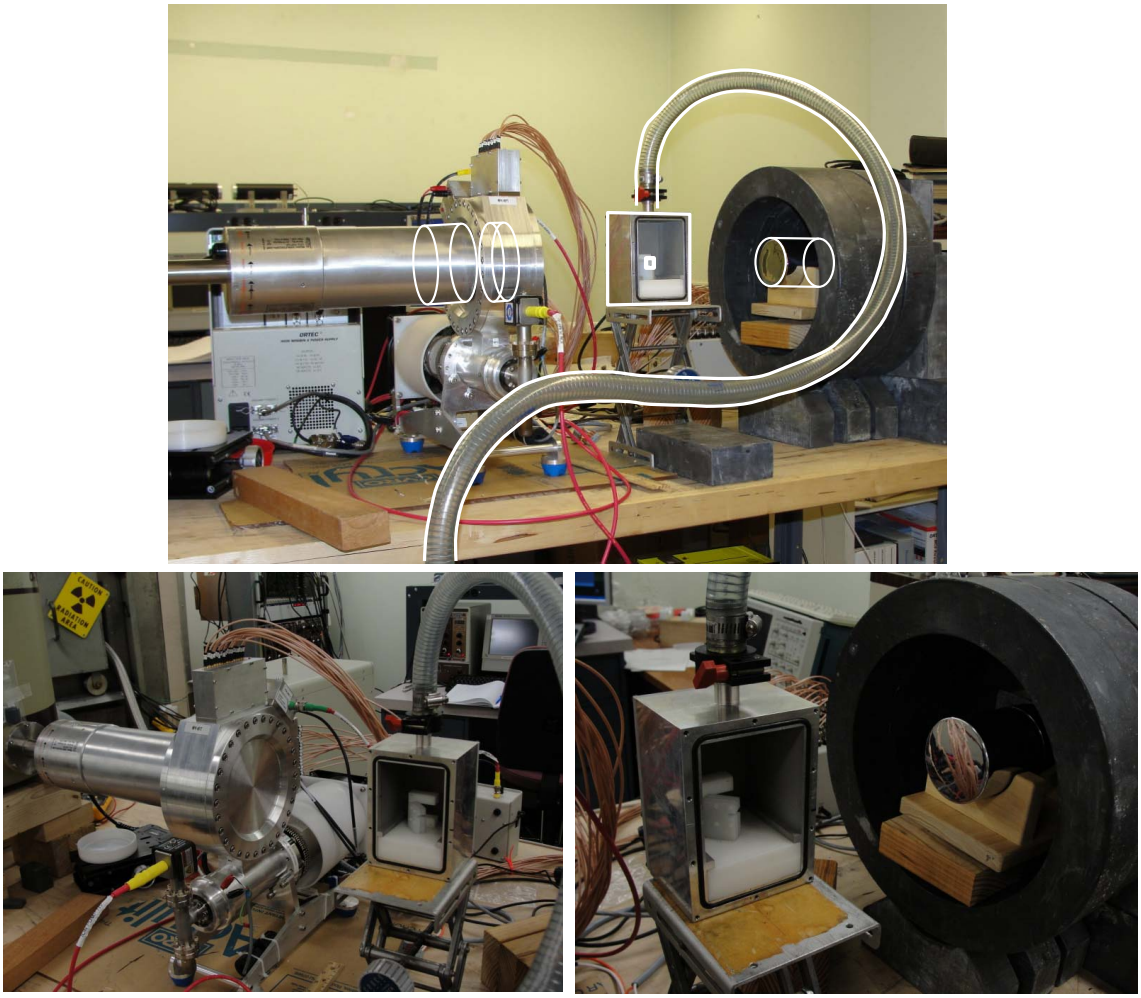

Figure 3.5. Picture of DBAR laboratory bench setup. In the top picture, the three detectors (DSSD, rescue, and scintillator) are outlined by cylinders, the vacuum chamber is outlined with a square with the location of the Ni sample indicated inside, and the vacuum hose is shown leading from the chamber to the vacuum. The two bottom pictures show the relative location of the sample bracket within the vacuum chamber to the Compton rescue system and the scintillator detector

IV. Results and Discussion

In this chapter the results of both the simulation and laboratory experiment are presented. Analysis of the results is discussed and conclusions are drawn in chapter V.

4.1 Simulation Results

The Compton rescue simulation was executed according to procedures described in section 3.1. 1.771×10^6 photons were sourced at a distance of 20 cm from the face of the primary crystal and their histories were filtered to include only those histories for which the photon was incident on the DSSD. Additionally, the events were filtered to exclude all photons that had experienced no interactions with either detector (virgin events). A visual rendering of the simulation is provided in figure 4.1. The source direction of the photons was constrained to a cone with an angle of 14.53 degrees. Of the total number of sourced photons, 1.000×10^6 histories were collected. These histories included collision and termination events and numbered 2.903×10^6 in total. This indicates an average of about three events per photon history. The R2C for this data was 1.030, that is, for every photon absorbed by PE in the primary detector, an average of 1.030 photons were Compton rescued. Said another way, this result indicates that Compton rescue more than doubles the efficiency of the detection system. Given that the simulation does not account for incomplete charge collection in the detector or other error factors introduced by the electronics of the detector system, this result was considered to be considered somewhat optimistic. The R2C of the experimental results is expected to be lower than this, however the simulation provides grounds for pursuing Compton rescue as a means to increase the number of photons collected by the system and improve detection efficiency.

The same simulation was run ten times varying the offset distance of the source

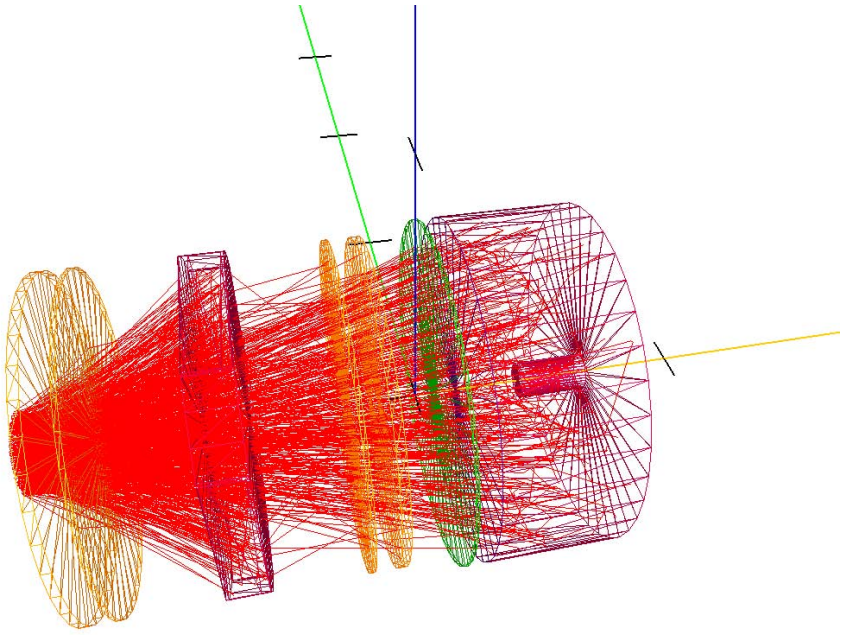

Figure 4.1. Visualization of MCNP simulation. Material volumes are the same as in figure 3.1, shown in wireframe.

from the DSSD from 10 cm to 100 cm in increments of 10 cm. This was done to test the simulation and determine if the measurement of Compton rescue effects could be trusted. The R2C was expected to vary with the source offset distance as discussed in section 3.1.3. For close offset, the R2C was expected to be small but increase towards a limit as the offset distance is increased. The data from these simulations is shown in figure 4.2. The fact that the data behave as predicted when the offset distance is varied can be taken as validation of the simulation model. This behavior indicates that the simulation photons are being scattered according to the expectations of the experiment and gives confidence to the simulation's prediction of increased photon collection. It is important to remember that the increasing R2C ratio does not indicate increasing efficiency, only an increase in the proportion of Compton rescued photons to direct absorption photons.

Additionally, the scattering spectrum from the simulation can be analyzed for

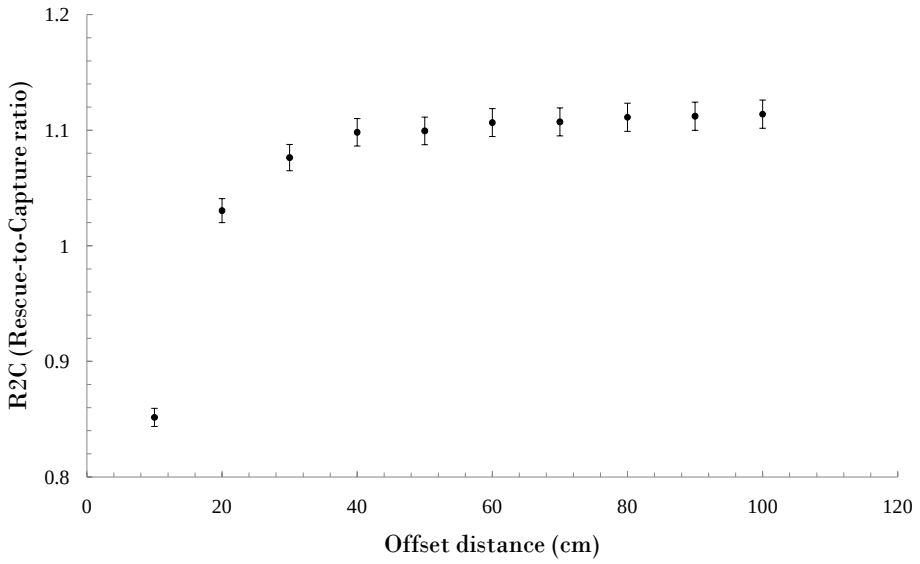

Figure 4.2. Variation of R2C with source offset distance

consistency with the physics of the experiment. By examining the spectrum of energy deposited in the DSSD by Compton scattered photons (figure 4.3) it can be seen that there is a distinct peak around 340 keV. This peak corresponds exactly with the backscatter peak predicted in equation 3.2 (section 3.1.3), further validating the simulation. A few other features are notable concerning the results of the simulation. Of the approximately one million photon histories that were written to the output, 25.5% underwent Compton scattering, more than 13 times the number that were directly absorbed by PE. This is consistent with the ratio of Compton scattering to photoelectric absorption at 511 keV, as can be seen in figure 1.18 (section 1.9). However, the number of rescues was only 7.84% of the total number of Compton scatters. The scattered photons not rescued were either not incident on or not fully absorbed by the rescue detector.

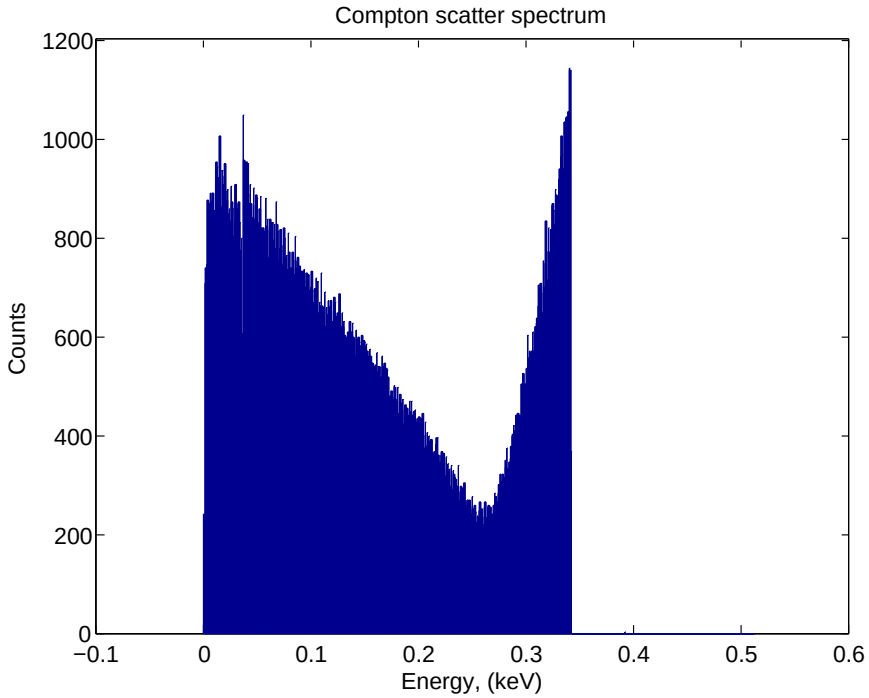

Figure 4.3. Simulation Compton scatter spectrum. Note the backscatter peak at 340 keV, consistent with equation 3.2

4.2 Experiment Results

4.2.1 ^{137}Cs Rescue Characterization

Several spectra were taken to characterize the detectors and determine how well the system could measure Compton rescues. Initially Cs-137 sources were used for characterization of the detectors (appendix A.3) although the 662 keV radiation produced by this source is higher than the annihilation photon energy. In analyzing the data, the energy window for counting an event was set based on the FWTM of the 661.7 keV peak in the DSSD characterization data. The channel with the largest FWTM on each side of the DSSD was used to set the full energy window. For the DC side, this was found to be 5.71 keV (channel 1) and for the AC side, 8.53 keV (channel 31). Collecting a spectrum from a source 20 cm from the face of the DSSD resulted in a R2C of 22.08±.28%. This meant that one photon was Compton rescued

for approximately every five PE events in the DSSD. As expected, this was significantly smaller than the R2C predicted by the simulation. This is most likely due to the error inherent with the detector system due to incomplete charge collection.

As in the simulation, the source offset distance was varied to see the effect of offset distance on the R2C. The same Cs-137 source was used for this test and spectra were taken at various distances from the DSSD ranging from 4 cm to 74 cm from the crystal. The data are presented in figure 4.4. The data show the same trend as was seen in the simulation (figure 4.2), albeit with lower R2C values.

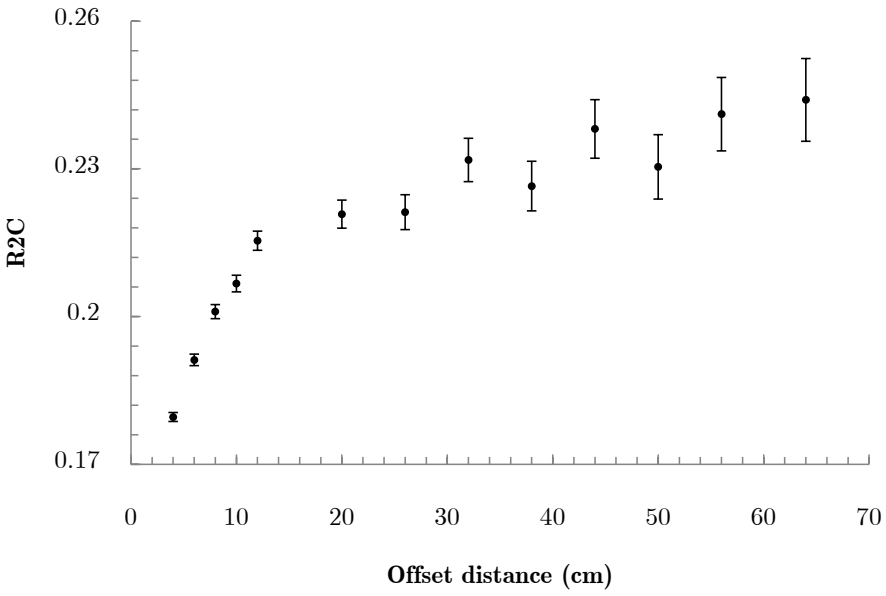

Figure 4.4. R2C as a function of offset distance of the source from the DSSD. Compare trend to figure 4.2

4.2.2 ^{85}Sr Spectrum

The Sr-85 source was then used to characterize the detector response for 514 keV photons, very close to the 511 keV annihilation photon energy. Based on this data, the energy window was set to 5.95 keV for the DC side and 9.26 keV for the AC side. A 30 minute collection time with the source approximately 20 cm away yielded an R2C

of 15.03±.07%. The data were processed and each primary capture and Compton rescue event was tallied into an array corresponding to subpixels on the DSSD. Since the functional subpixel resolution used was ±0.2 cm, each strip was divided into 5 substrips, resulting in 25 subpixels in each pixel. This results in two dimensional data important to ACAR measurements (figure 4.5). Since this measurement was only the bare detector exposed to the isotropic illumination of the Sr-85 source, there was no position-sensitivity in the measurement. However, the 2D data revealed important characteristics about the continuity of the subpixel data.

Visual inspection of the data shows that fewer counts were placed in the subpixels close to the edges of the strips. Since the source illuminated the face of the detector isotropically, this indicates that there is some error in the method used to make the fine correction to the position-sensitive data. Furthermore, it should be noted that the effect is much more pronounced in the Compton rescue data than in the direct absorption data. The energy deposited in the DSSD for Compton rescued photons is less than the amount deposited for PE. This suggests that the transient charge FOMs may be dependent on the energy deposited in the primary strip of the DSSD. This would in turn affect the fine correction and could lead to the observed non-uniformity in the subpixel tallying. This non-uniformity in subpixel data has important implications to the accuracy of position-sensitive measurements, such as ACAR.

4.2.3 Fine Correction Energy Dependence

The effect of energy on the transient charge was investigated by analyzing the energy-dependence of the fine correction data. It was hypothesized that for small energy depositions in the DSSD, the average fine correction would be a small number, that is, closer to the center substrip. The fine correction was set up as a FOM between -1 and 1, measuring relative distance on either side from the center of the primary

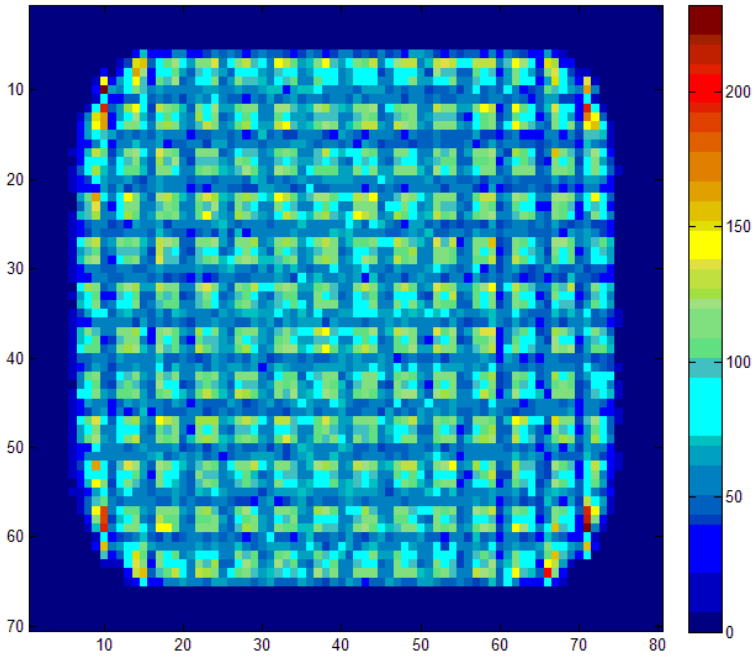

(a) Direct absorption

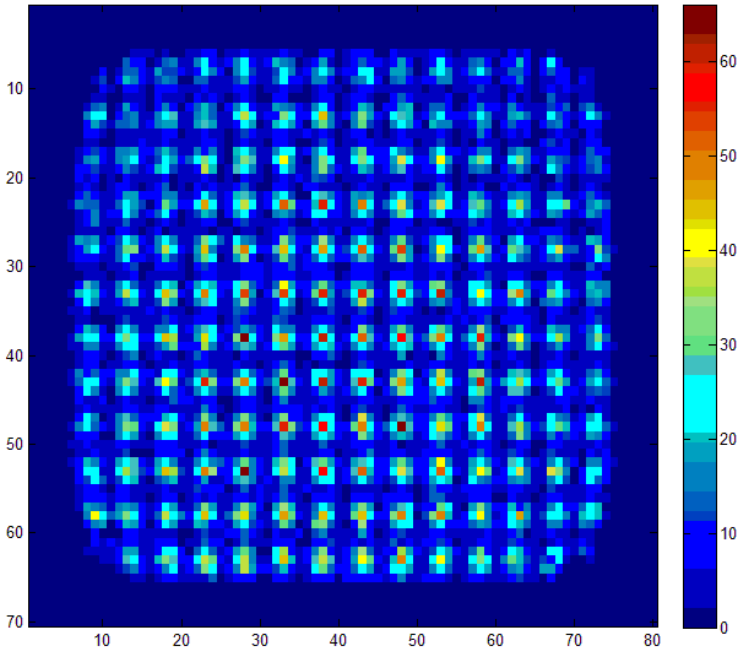

(b) Compton rescue

Figure 4.5. DSSD position-sensitive data from ^{85}Sr spectrum organized into 2D sub-pixel array

strip to the edge as discussed in section 1.8.1. A Compton rescue data set from the strontium experiment was analyzed by plotting the average fine correction value against the energy deposition. The absolute value of the fine correction was used so that it was a measure of the absolute distance from the center of the strip to improve statistics. The results are shown in figure 4.6a. If the fine correction were accurately representing the isotropic illumination of the detector, the average fine correction would be expected to be halfway between the edge and the center of the strip. The midpoint between the center and the edge of the incident strip is shown by the reference line in figure 4.6. For ideal detector response, the average FC would always fall on this line because the photons interactions were expected to be uniformly distributed throughout the strips. These data show a number of surprising features which are not intuitive, but apparently present. It is important to keep in mind that this data was subject to filtering according to the criteria in the parsing algorithm (section 3.2.2). Raw events were then similarly analyzed without being filtered for full energy deposition and the results are displayed in figure 4.6b. The disparity between the energy dependence of the fine correction between the filtered and unfiltered data suggests that some of the criteria used in the filtering algorithm may be skewing the subpixel position-sensitive data in an unpredicted manner. Investigation of this problem is beyond the scope of this research.

While the specific features of the data may require future investigation, these data reveal an important effect that will be inherent to Compton rescue using the DSSD. The average fine correction at all energies stays well below the value of 0.5. This seems to indicate that DSSD data on the substrip location of interactions will be "squeezed" towards the center substrip within a strip, and towards the center subpixel within a pixel. These data also suggest that this effect is amplified for interactions which deposit smaller amounts of energy in the DSSD (namely Compton scattering). In order to accurately gain position sensitive data from this detector system, this

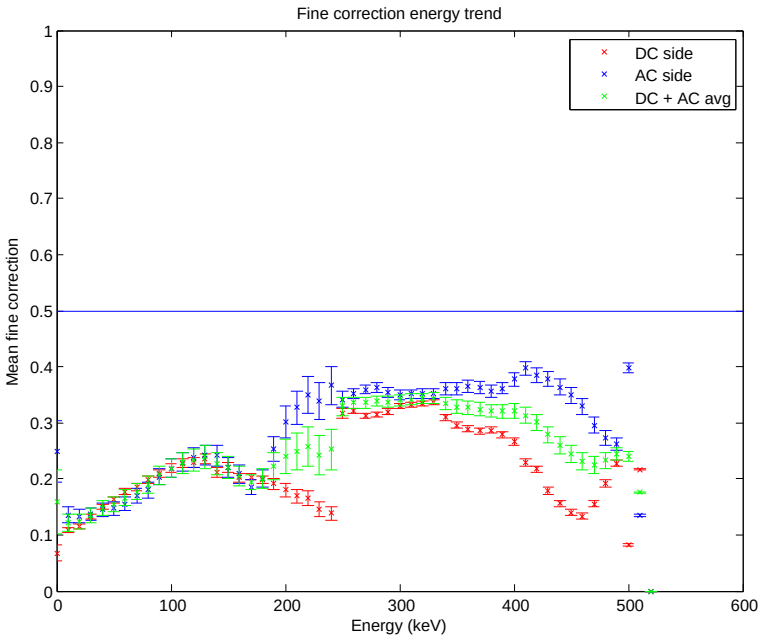

(a) Filtered data

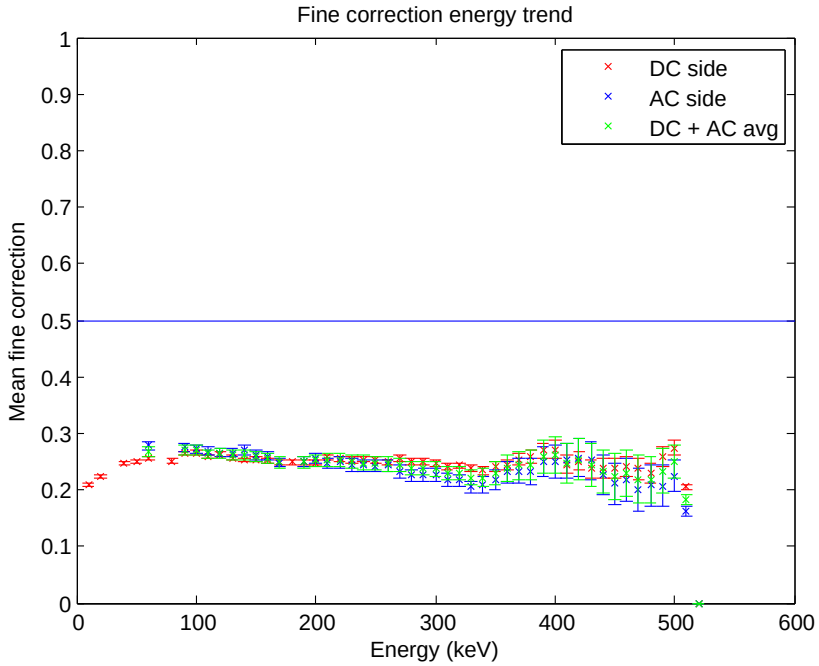

(b) Unfiltered data

Figure 4.6. Average absolute fine correction as a function of energy. The brackets represent standard deviation for counting statistics. Reference line at 0.5 provided to indicate ideal detector response to isotropic illumination of strips.

squeezing effect must be accounted for.

A possible source of the squeezing effect may be found by performing a simple error analysis on the FC equation. Based on equation 1.8, the associated error in the FC is

$$\delta FC = FC \cdot \sqrt{\left(\frac{\delta FOM_{pred}}{FOM_{pred}}\right)^2 + \left(\frac{\delta\left(FOM_{pred} + FOM_{succ}\right)}{FOM_{pred} + FOM_{succ}}\right)^2}. \tag{4.1}$$

The FOMs are generated by the electronics in the Spect32 and the method by which they are generated is proprietary. However, the FOMs are known to be a measure related to the integral of the transient charge seen in the strips adjacent to a primary charge collection strip. Intuitively, this means that the magnitude of the FOMs are directly correlated to the amount of free charge created by an ionization and in turn, the energy of the photon deposition in the crystal. This can be expressed as

$$FOM(E) \propto E \tag{4.2}$$

where E is the deposition energy in the primary strip. The nature of this relation is not defined and may be linear, exponential, or related in a more complex way. In general, however, the relationship must be direct in that as E increases, the FOM should increase. The average FC error may then be expressed as

$$\langle \delta FC \rangle = FC \cdot K(E) \tag{4.3}$$

where K is a function analogous to the expression under the square root in equation 4.1 and inversely proportional to the average FOM generated by a deposition of energy, E. This is expressed as

$$K \propto \frac{1}{\langle FOM(E) \rangle} \tag{4.4}$$

or, analogously

$$K \propto \frac{1}{E}. \tag{4.5}$$

The average ratio of the FC to its associated error may then be expressed as a function of energy and thought of as a signal-to-noise ratio such that

$$\frac{FC}{\langle \delta FC \rangle} = \frac{\cancel{FC}}{\cancel{FC} \cdot K(E)} \propto E. \tag{4.6}$$

This relation reveals a possible source of the observed squeezing effect in subpixel spatial data. For small energy depositions, the FC will not be as significant in comparison to its associated error. This will result in smaller energy depositions being placed in locations nearer to the "zero" location, the center subpixel. In other words, they will be "squeezed" to the middle.

4.2.4 Spatial Resolution Analysis

The ^{85}Sr source was collimated using the collimator described in section 2.6. The collimated source was aimed at a single pixel so that spatial resolution data could be collected. The pixel used for this experiment was the intersection of strip 8 on the DC side and strip 27 on the AC side. The width of the collimator aperture was 0.15 mm, smaller than the pitch of the subpixels. The data collected provides a qualitative measure of the effect of Compton rescue on spatial resolution. A truly quantitative measure could not be determined because the subpixel efficiency for each pixel was beyond the scope of this research. Nevertheless, examining the collimated data provides information about the spatial resolution of the Compton rescue data. The direct absorption and Compton rescue data from the collimated source are presented in figures 4.7 and 4.8. These data do not indicate that the spatial resolution of the system suffers by adding Compton rescue data. A qualitative comparison of the spread of the two dimensional spread of the beam indicates that the Compton rescue data is

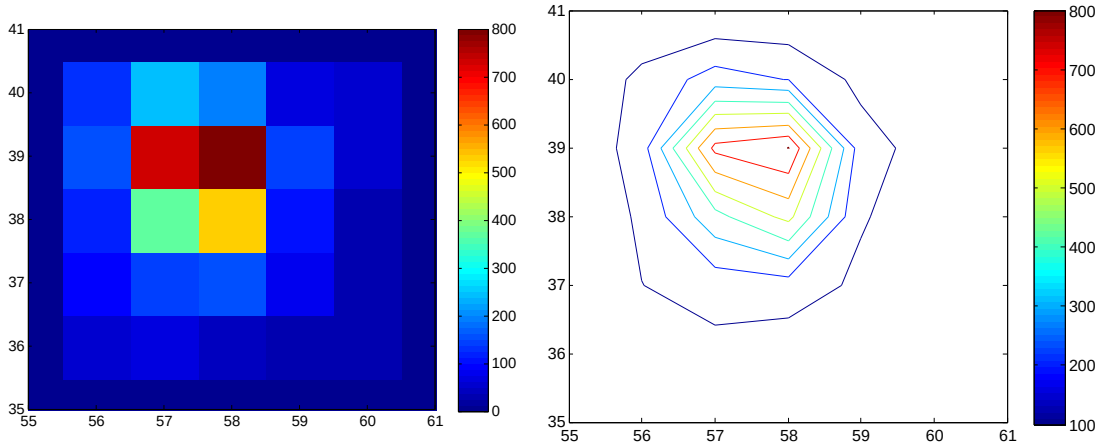

(a) Single pixel collimated beam data (b) Single pixel collimated beam contour plot

Figure 4.7. Direct absorption data from the collimated ^{85}Sr source aimed at the center of a single DSSD pixel. Each square is a subpixel 1 mm^2 in area.

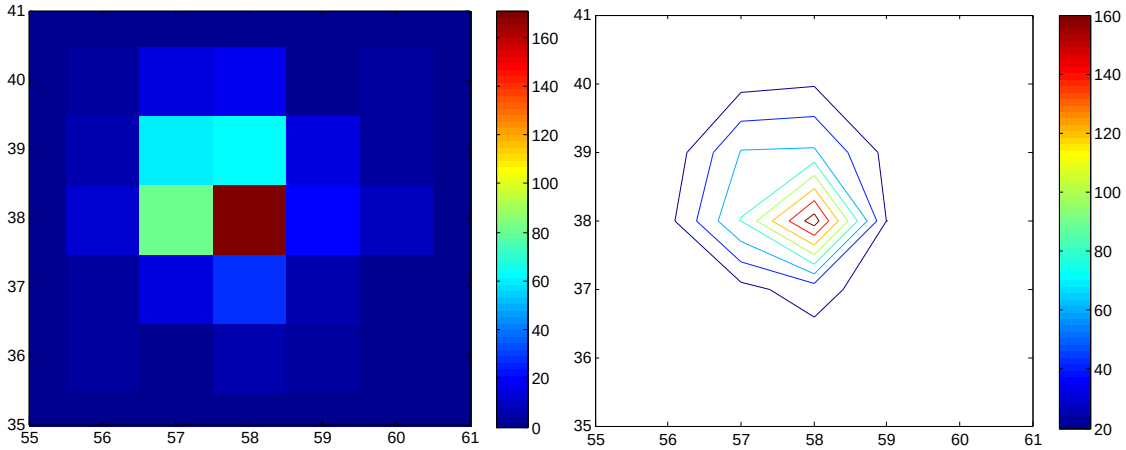

(a) Single pixel collimated beam data (b) Single pixel collimated beam contour plot

Figure 4.8. Compton rescue data from the collimated ^{85}Sr source aimed at the center of a single DSSD pixel. Each square is a subpixel 1 mm^2 in area.

in fact more closely grouped than the direct absorption. However, this qualitative assessment may be misleading. The collimated beam was not focused exactly on the center of the DSSD pixel as can be seen from the direct absorption data. However, the Compton rescue data appear to be grouped around the center subpixel, similar to what is seen in figure 4.5. This is consistent with the squeezing effect described in

section 4.2.3. Compton rescue data seem to be more susceptible to the squeezing than the direct absorption data, apparently because the scattering events in the DSSD are at generally lower energies than the PE events in direct absorption. To quantify the squeezing effect, the data from the collimated source was analyzed to determine the subpixel centroid location. This method used the same data shown in figures 4.7 and 4.8, however, it was reanalyzed with 21 substrips in the parsing algorithm. By parsing the data this way, the data has improved spatial resolution, although the associated error is also increased. While this degree of spatial resolution is much finer than permitted according to the spatial characterization in [16:83], it allowed the centroid location of the data to be more precisely characterized. The collimated source was aimed slightly off the center of the incident pixel. For the PE events in the primary detector, the centroid of the data was located 0.91±0.23 mm away from the center subpixel. For the Compton rescue events, the centroid was 0.35±0.23 mm from the center. These two figures are shown graphically in figure 4.9. The centroid for the PE events was taken for pixels with a threshold of 30 counts, and 5 counts for the Compton rescue events. The fact that the centroid of the Compton rescue data is much closer to the center subpixel than the centroid of the direct absorption data is consistent with the theory that the subpixel spatial resolution is poorer at lower energies than for full energy depositions. This is likely because the transient charge FOMs are not as large for smaller energy deposition events.

4.2.5 Energy Resolution Analysis

The Compton rescue data were analyzed to determine how using the technique would affect the energy resolution of the system. The Compton rescue data were separated from the direct absorption data and the FEP data were analyzed to determine if the rescued events displayed any deterioration in energy resolution. This would have implications on the collection of DBAR spectra. The Compton rescue and

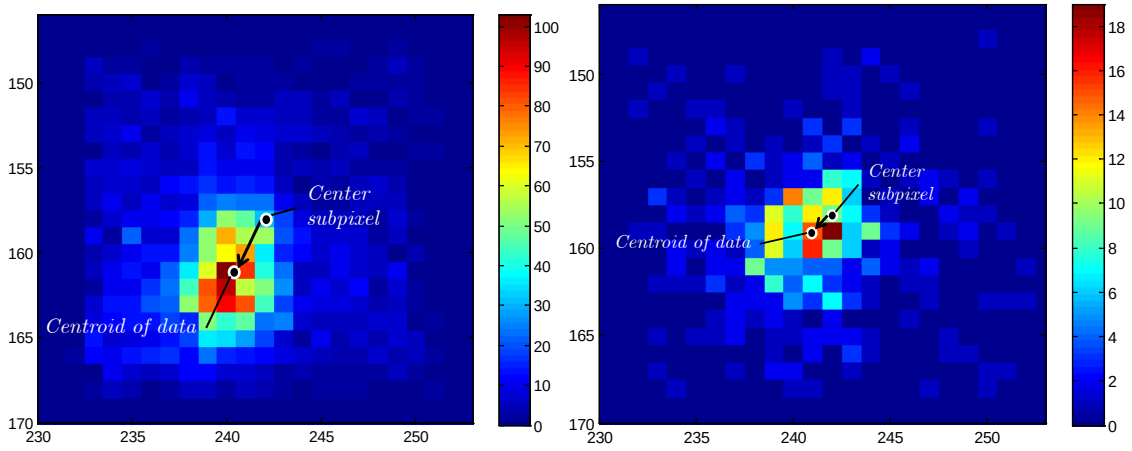

(a) Direct absorption; centroid distance from center: 0.91±0.23 mm

(b) Compton rescue; centroid distance from center: 0.35±0.23 mm

Figure 4.9. Data from a collimated source aimed on a single subpixel. The centroid location of the data with relation to the center subpixel is shown. Each square is a subpixel 0.23 mm^2 in area.

direct absorption peak energy distributions are displayed in figure 4.10, from which it can be seen that Compton rescue has little effect on the energy resolution. The FWHM of the Compton rescue FEP is 4.2±0.2 keV and 2.4±0.2 keV for the direct absorption peak. The reason for the degradation in the energy resolution is possibly explained by the fact that in Compton rescue, the photon is detected twice, once in the DSSD and again in the coaxial detector, as opposed to once in direct absorption, introducing another source of error into the the detection.

4.2.6 Charge Sharing analysis

In the course of developing the parsing algorithm for analyzing the experimental data, the question arose of whether or not the charge sharing events in the DSSD were being counted to the correct subpixels. As discussed in section 1.7.4, an event in which the charge was shared and collected by two adjacent strips was counted to whichever strip had the higher energy collected. The energy of both strips would be summed for the energy collected by that side of the DSSD. However, it was postulated that

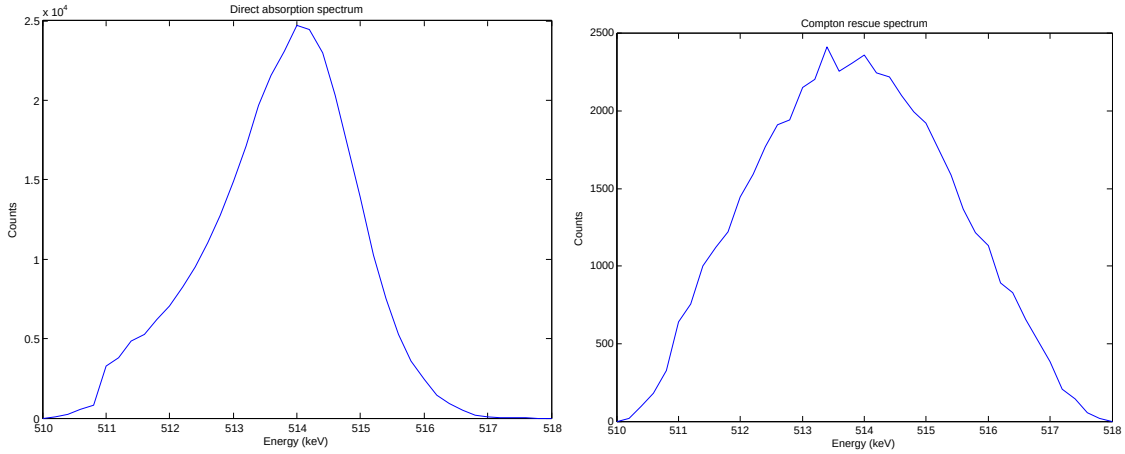

(a) Direct absorption full energy peak, FWHM=2.2 ± 0.2 keV

(b) Compton rescue full energy peak, FWHM=4.0 ± 0.2 keV

Figure 4.10. Full energy peak data for ^{85}Sr source

the charge being collected on both strips might interfere with the transient charge inducing more error in the fine correction and possibly skewing the subpixel location of the interaction. To determine the validity of including charge sharing in the parsing algorithm, the charge shared events were extracted from the rest of the data and analyzed separately to observe the distribution of the fine correction data. The data for this test was taken from a measurement in which only eight strips were connected to the Spect32 (DC: 6-9, AC: 22-25) so that a 2×2 grid was formed in the central four pixels (the outer strips were connected to provide the transient charge data). The distribution of the fine correction for the shared events is shown in figure 4.11. The data indicated that the fine corrections for charge sharing events generally locate the interactions near the boundary between the two strips, however, as the boundary itself is approached the distribution approaches zero. This would seem to accurately represent the charge sharing events because of the small gap that exists between the two strips. The fact that the fine correction figures are grouped very close to the edge indicates that for most charge sharing events, the interaction will be placed in the edgemost subpixel, as expected. Based on this analysis it was determined that charge sharing events can be confidently included in the experimental data from the

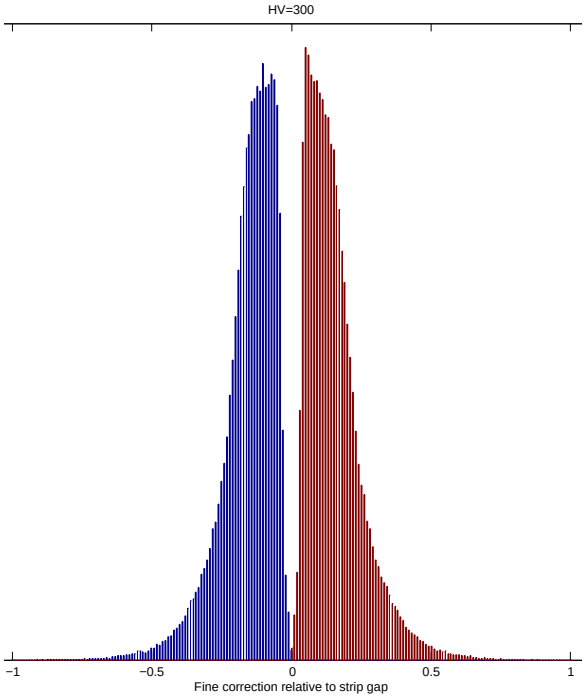

(a) 300 V high voltage bias, FWHM=0.09±.005 cm (both peaks)

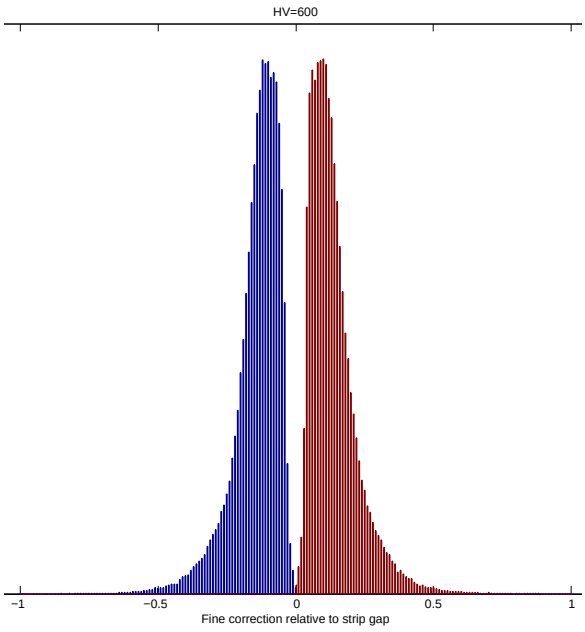

(b) 600 V high voltage bias, FWHM=0.07±.005 cm (both peaks)

Figure 4.11. Distribution of fine correction data for charge sharing events between two DSSD strips. The fine correction is adjusted to be relative to the center of the gap between the strips (0 is in the strip gap, -1 and 1 are the opposite edges of the preceding and succeeding strip , respectively). The FWHM figures are calculated based on a strip width of 0.5 cm.

DSSD.

4.2.7 Charge Cloud Spreading

An additional effect was noted from conducting the charge sharing experiment at two different bias voltages. The experiment was done twice, once with the high voltage set at 300 V and once at 600 V to determine if the the effect of changing voltage on charge spreading could be observed (see section 1.7.4). Increasing the high voltage across the DSSD crystal would be expected to reduce the amount of spreading of the free charge cloud in the semiconductor. In figure 4.11, the spread of fine correction data is noticeably narrower for the 600 V experiment compared to the 300 V experiment. For the 300 V data, the FWHM of both left and right peaks was 0.09±0.005 cm and for the 600 V data, 0.07±0.005 cm. This would seem to be consistent with the theory pertaining to charge cloud spreading as a function of applied bias as discussed in [25].

4.2.8 DBAR Results

The results of the DBAR experiment (section 3.3) were analyzed with respect to the effect of implementing Compton rescue on the quality of the data. While the technique may be seen to improve the efficiency of the measurement by rescuing counts that would otherwise have been lost, it is important to qualify any degradation of the results induced by the technique. The best figure for this analysis is the ratio plot (see section 1.6.2) of the annihilation peak data including rescue events to the peak data excluding rescue events. Ideally, this ratio would not vary with energy, indicating that Compton rescue was evenly amplifying the data across the whole annihilation peak. However, the analysis does not reveal this to be the case. The results are displayed visually in figure 4.12. These data indicate that Compton rescue amplification is greater for energies higher than the 511 keV annihilation peak than below. This may

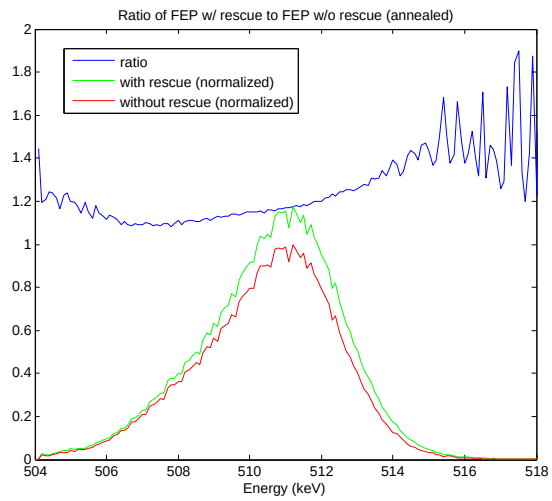

(a) Ni(100) annealed:R2C=17.25%

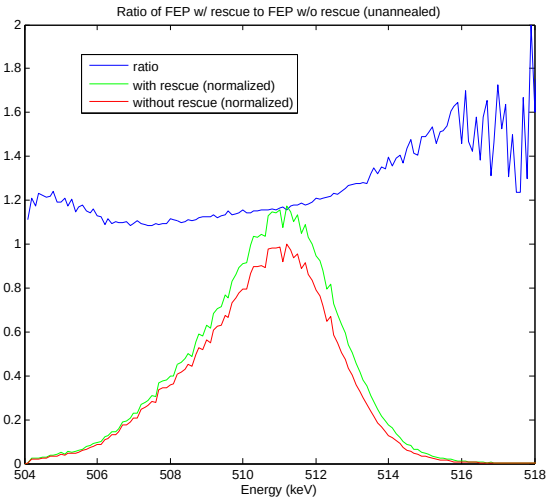

(b) Ni(100) unannealed:R2C=17.07%

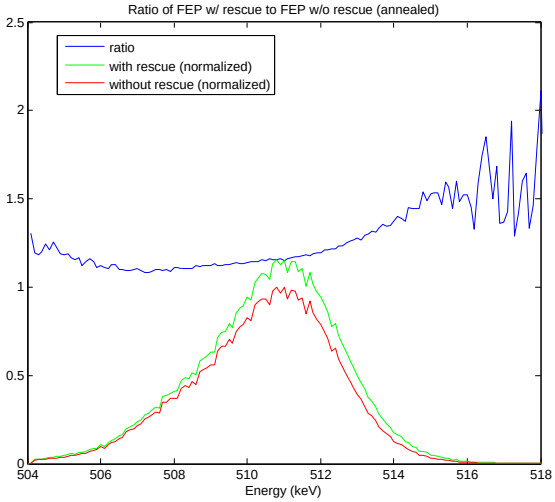

(c) Ni(111) annealed:R2C=17.01%

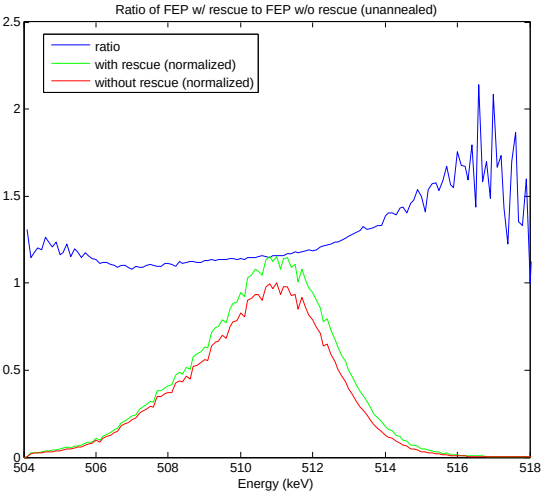

(d) Ni(111) annealed:R2C=17.01%

Figure 4.12. Ratio of annihilation peak data including rescue to data excluding rescue. The normalized peak plots are provided for visual aid.

be due in part to the extended tail of the peak which may be an artifact of the signal processing electronics. The R2C figures for these data sets indicate that Compton rescue added approximately 17% more counts to the annihilation spectrum.

The DBAR experiment did not yield any conclusive results about the difference between the annealed and unannealed nickel samples. The ratio of the unannealed sample to the annealed sample did not deviate above the noise level. This inconclusive result may be attributed to both samples being mostly defect-free even without annealing. The samples had not been irradiated or subjected to any stress which might have caused defects to appear, thus it is unlikely that any PAS technique would noticeably reveal different characteristics about them.

V. Conclusions and Future Work

5.1 Conclusions

The research presented in this thesis investigated the feasibility of improving the efficiency of thin planar HPGe detectors by collecting scattered photons with a secondary detector with the intent of enhancing data collection techniques for positron annihilation spectroscopy (PAS). The Compton rescue process was simulated and predicted to be feasible with regard to the physical mechanisms underlying it. The process was then tested in a laboratory experiment using a position-sensitive detector as the primary and a large volume coaxial detector for rescue. The experiment was then extended by adding a scintillator detector for coincidence and conducting an experiment to detect the Doppler-broadening of positron annihilation radiation. Compton rescue was determined to be a possible method to improve PAS measurements, although more research is required to properly quantify the degradation in the quality of the data from using the technique.

In the simulation portion of the research, photons were simulated to interact with detectors based on known energy- and material-dependent interaction characteristics (equation 1.11 [32]). The simulation was designed to determine whether or not the number of photons that would go through the Compton rescue series of interactions would be significant compared to the number absorbed directly by PE in the primary detector. The simulation predicted that for a given number of photons incident on the detector system, the portion that Compton scattered once in the primary detector and then are fully absorbed in the rescue detector would at least be comparable to the number detected conventionally by PE in the primary detector. The simulation data were validated by testing for consistency with known physical phenomena such as interaction ratios (figure 1.18), geometry variation sensitivity (figure 4.2), and scattering spectrum features (figure 3.2). While the simulation could not make

predictions concerning the efficient electronic conversion of photon interactions into experimental data points, it revealed at least that the physics and geometry of photon interactions could potentially make Compton rescue very effective in improving detection efficiency.

In the experimental portion of the research, a dual-sided strip detector (DSSD) was used as the primary detector. The planar semiconductor crystal of the DSSD is very thin and therefore relatively inefficient in detecting high-energy photons at full energy. Its position-sensitive capabilities make it especially useful for PAS research, but the inefficiency of the detector means that spectra must be collected over a long time interval. The rescue detector was a coaxial HPGe detector with a large active detection volume that is more sensitive to photons in the range of 100 keV and above. The rescue detector was positioned immediately behind the back face of the DSSD and known radioactive sources were used to illuminate the detectors. Coincidence data was generated from the detector system and Compton rescue and primary detector PE events were parsed from the data according to interaction criteria. From these data, Compton rescue was found to be less significant relative to PE in the primary detector than predicted by the simulation. Compton rescue was found to add 10-25% to the number of photons collected by the DSSD. As predicted by theory and simulation, the relative improvement in efficiency from using Compton rescue decreased as the source was moved closer to the primary detector

The energy resolution of the rescue events was found to be somewhat degraded from the primary detector PE data. The FWHM value of the Compton rescue FEP was roughly twice that of the primary detector FEP. Intuitively, this would seem explainable by the fact that Compton rescue photons deposit their energy in two interactions, first by Compton scatter then by PE, as opposed to only once by PE for direct absorption. The degraded energy resolution may have implications on the usefulness of Compton rescue since the ability to distinguish minute features of energy

spectra is important for PAS experiments.

The position sensitivity of the DSSD was also analyzed in order to qualify the degradation of spatial resolution induced by Compton rescue. The position-sensitivity of the DSSD is enhanced by its ability to leverage the phenomenon of transient charge to resolve the location of interactions to an area smaller than the intersection area of two charge collection strips. The data from this research suggest that this resolution ability may be energy dependent, and that lower energy photons may not induce transient charge FOMs high enough above noise to produce good subpixel location data. This was suggested by an observed "squeezing" effect in which the subpixel locations of lower energy depositions were biased towards the center subpixel. This squeezing effect may cause the spatial resolution for Compton rescue events to be degraded since the Compton scattered energy deposition in the position-sensitive detector will generally be much lower than the full energy. The quantification of this degradation and techniques to compensate for it may be useful topics for future work.

5.2 Future Work

The results presented suggest several possibilities for future research. While the results of the research show some promise for Compton rescue to be developed into a useful tool for radiation detection applications, the techniques used while conducting this research were limited. The disparity in the predictions from the simulation and the results from the experiment suggest that the experimental techniques used in this research did not fully harness the potential efficiency improvement of Compton rescue. The simulation suggested that Compton rescue could potentially more than double the number of counts in the output data, however, in the laboratory experiment the number of counts was only increased by about 20%. Future work may contribute to resolving this disparity.

Some of the disparity between the simulation and experiment is likely due to

incomplete charge collection in the HPGe detectors. The predictions from the Monte-Carlo simulation were based solely on the physical interaction of photons with matter and did not take into account the production and collection of free charge in the semiconductor. The loss of charge carriers may be a significant factor in the efficiency improvement from Compton rescue and also in the degradation of energy and spatial resolution. Work done by Amman and Luke has investigated the loss of charge carriers between charge collection strips [26]. Research into other sources of charge loss in DSSDs and in large volume semiconductor detectors may explain some of the discrepancy between the simulation and experiment results of this research and suggest methods of improving the implementation of Compton rescue.

The development of a method of compensation for the subpixel squeezing effect is another possible direction for future research. In order for Compton rescue to be used effectively for applications involving position-sensitive detectors, such as ACAR experiments, spatial resolution must be fairly consistent over a wide range of energy deposition. Since Compton rescue inherently involves the deposition of energy at levels significantly lower than the full energy of the photon, methods to compensate for spatial resolution at lower energies must be developed to make the technique feasible. For DSSDs, this may involve improvements to the method of generating transient charge FOMs in the detection system electronics. Alternatively, or in compliment, the implementation of a spreading function in the data processing algorithm to reverse the squeezing effect may be possible. This method would require the characterization of the subpixel spatial response to a very high degree of accuracy, involving very precise measurements using a finely collimated high-energy source.

This research demonstrates the potential of Compton rescue to be applied to technical applications with further development. For the equipment used in this research, both the energy and spatial resolution of the Compton rescue data were significantly degraded. For the implementation of Compton rescue to applications of technical

interest, the technique has been shown to add a significant amount of efficiency, but for a given detection system, the energy and spatial resolution must be shown to meet operational requirements. While the position-sensitive detection system used in this research was a thin planar HPGe detector, the Compton rescue technique could be applied to other position-sensitive systems. PAS Applications of interest to the Air Force, such as the noninvasive testing of components, can potentially benefit by implementing the Compton rescue technique to decrease the time necessary for measurements.

5.3 The Final Word

This research has investigated Compton rescue to improve the detection efficiency of thin planar detectors. The results of the procedures and techniques used in this research have yielded data with questionably acceptable improvements in efficiency and significant degradation of quality. Nevertheless, the physical processes that form the basis for the technique have been demonstrated and future work to realize the potential efficiency improvements and reduce the data degradation may make the technique a valuable tool for many types of radiation detection experiments, such as PAS. The improvement of efficiency of these measurements without degrading data quality will accelerate the pace of research in these areas.

Appendix A. Detector Characterization Data

A.1 Efficiency Calculation Equation

For this calculation, the source and detector faces must be circular, in order to use equation 1.12, reproduced here:

$$\Omega_{disc}(c,d) = \frac{4\pi}{c^2}[(1+c^2)^{\frac{1}{2}} + (1+d^2)^{\frac{1}{2}} - 1 - (1+c^2+d^2)^{\frac{1}{2}}], \tag{A.1}$$

where c and d are the radii of a disc source and detector (both oriented on-axis), divided by D, the offset distance between them. The detector is approximated as a disc the size of the cylindrical face. This equation gives the solid angle of radiation from the source covered by the detector. The solid angle is necessary to calculate the intrinsic efficiency of the detector (see section 1.10). In order to calculate the efficiency of a spectrum, several pieces of information are needed about the source and detector:

-activity of the source (A)

-date the source activity was calibrated (T_i)

-date of spectrum measurement (T_f)

-source isotope(s)

-half-life(t_{12}) and decay constant($\lambda = \frac{t_{12}}{ln2}$)

-spectrum sampling time (t)

-number of counts in full energy peak(N)

With all this information, the intrinsic efficiency is calculated by equation A.2.

$$\epsilon_{int} = \frac{A \cdot e^{-\lambda(T_f - T_i)} \cdot t}{N} \cdot \frac{4\pi}{\Omega_{disc}} \tag{A.2}$$

A.2 Initial Detector Characterization

Table A.4. Cs-137 calibration

	Efficiency	Resolution
Position-sensitive (DSSD)	1.04%	DC side average: 2.21 keV (.33%) AC side average: 3.16 keV (.48%)
Rescue (Coaxial)	4.00%	3.00 keV (.45%)

Table A.5. Co-60 calibration

	Efficiency	Resolution
Coaxial detector, 1172 keV	5.46%	3.79 keV (.32%)
Coaxial detector, 1333 keV	4.71%	3.78 keV (.28%)

Table A.6. Sr-85 calibration

	Efficiency	Resolution
Position-sensitive (DSSD)	1.51%	DC side average: 2.26 keV (.44%) AC side average: 2.76 keV (.54%)
Rescue (Coaxial)	8.31%	3.16 keV (.61%)

A.3 ^{137}Cs Resolution Characterization

4 November 2010 characterization data, Source: Cs-137 (664-69)			
Resolution data:			
channel	FWHM (keV)	FWTM (keV)	Gross Area (cts)
0 (rescue)	3	6.71	48306561
1	2.33	5.84	1380000
2	2.2	5.71	1722000
3	2.22	5.64	2011000
4	2.18	5.53	2267000
5	2.24	5.48	2443000
6	2.21	5.41	2549000
7	2.25	5.44	2589000
8	2.3	5.51	2577000
9	2.22	5.35	2554000
10	2.2	5.32	2462000
11	2.23	5.54	2271000
12	2.25	5.55	1996000
13	2.12	5.34	1718000
14	2.11	5.41	1373000
16	4.11	8.47	737000
17	3.44	7.44	1183000
18	3.1	6.74	1570000
19	2.89	6.22	1893000
20	3.3	6.74	2152000
21	2.83	5.91	2334000
22	2.91	5.92	2412000
23	2.93	5.98	2420000
24	2.67	5.43	2367000
25	2.74	5.65	2293000
26	2.82	5.82	2173000
27	2.79	5.89	1934000
28	3.55	7.42	1654000
29	3.03	6.42	1365000
30	3.31	6.82	994000
31	4.13	8.53	595000

A.4 ^{85}Sr Resolution Characterization

10 December 2010 DBAR characterization data, Source: T-142 (Sr-85)			
Resolution data:			
channel	FWHM	FWTM	Gross Area
0 (rescue)	3.16	7.14	598480
1	2.29	5.95	7521
2	2.48	5.69	8916
3	2.08	5.79	10206
4	2.22	5.58	10823
5	2.82	6.02	11335
6	2.36	5.54	11469
7	2.31	5.78	11680
8	2.29	5.62	11500
9	2.09	5.22	11984
10	2.13	5.73	12063
11	2.22	6.18	11545
12	2.13	5.39	10489
13	2.15	5.06	9758
14	2.03	5.7	8433
15 (coincidence)	42.59	78.48	3488138
16	3.57	8.91	4316
17	2.64	8.71	6492
18	2.6	8.3	8167
19	2.73	6.15	9579
20	3.16	6.58	10021
21	2.52	6.06	10756
22	3.3	6.81	11030
23	2.59	5.55	10883
24	2.4	4.96	10863
25	2.72	5.47	10749
26	2.71	6.19	10761
27	2.65	6.32	10043
28	2.61	5.79	9183
29	2.75	6.26	7984
30	2.39	7.18	6251
31	3.02	9.26	4044

A.5 ^{137}Cs Efficiency Characterization

Parameter	DSSD	Coaxial detector
Activity (μCi)	10	10
Source date	1 Sept 2000	1 Sept 2000
Spectrum date	3 Nov 2010	3 Nov 2010
Half-life (days)	10961.2	10961.2
Decay constant ($1/days$)	6.32367E-05	6.32367E-05
Sampling time (s)	66157	66157
Counts	29912000	48306561
Detector radius (cm)	4	4.25
Source radius (cm)	.5	.5
Offset distance (cm)	3	6
Intrinsic Efficiency	.784%	2.716%

A.6 ^{85}Sr Efficiency Characterization

Parameter	DSSD	Coaxial detector	Scintillator detector
Activity (μCi)	90.91	90.91	90.91
Source date	1 Dec 2010	1 Dec 2010	1 Dec 2010
Spectrum date	10 Dec 2010	10 Dec 2010	10 Dec 2010
Half-life (days)	64.849	64.849	64.849
Decay constant ($1/days$)	0.0107	0.0107	0.0107
Sampling time (s)	456	456	456
Counts	147722	598480	3488138
Detector radius (cm)	4	4.25	1.5
Source radius (cm)	.5	.5	.5
Offset distance (cm)	22	27	22
Intrinsic Efficiency	1.314%	7.066%	34.12

Appendix B. List of Radioactive sources

Source Designator Number	Isotope	Activity (μCi)	Reference date	Half life
664-69	^{137}Cs	10	1 Sep 2000	30.07 yr
T-083	^{137}Cs	8.829	15 Jul 1998	30.07 yr
T-084	^{137}Cs	10.14	15 Jul 1998	30.07 yr
T-142	^{85}Sr	90.91	1 Dec 2010	64.84 dy
T-111	^{22}Na	53.96	1 Jan 2005	2.604 yr

Appendix C. Spect32 channel settings

Instrument properties:				
Channel(s)	0 (rescue)	15 (scintillator)	1-14, 16-31 (DSSD)	
Gap	40	12	50	
Peaking time	131	200	200	
Shift by	0	2	2	
P/Z correction	31	30	30	
Energy threshold	0	152	152	
Board parameters:				
Board	0	1	2	3
Pulse threshold	9	9	9	9
Signal polarity	positive	positive	negative	negative

Appendix D. MCNP Input Deck

This is the simulation input file for the simulation with 15 cm offset, and 10,000 photons simulated. Descriptions of the sections follow. Lines are numbered for convenience. Lines that begin with a c are commented out and not read into the program.

1- 12 October shot 02

2- c cell cards

3- 1 1 -5.323 1 -2 -3 4 -5 6 -7 imp:p 1 $Primary

4- c 1 2 -0.001205 1 -2 -3 4 -5 6 -7 imp:p 1 $Primary

5- 2 1 -5.323 10 -11 -12 #(14 -13) imp:p 1 $rescue

6- c 2 2 -0.001205 10 -11 -12 #(14 -13) imp:p 1 $rescue

7- 3 3 -1.38 15 -10 -12 imp:p 1 $rescue Mylar layer

8- c 3 2 -0.001205 15 -10 -12 imp:p 1 $rescue Mylar layer

9- 4 4 -2.00 18 -17 -12 imp:p 1 $rescue Carbon window

10- c 4 2 -0.001205 18 -17 -12 imp:p 1 $rescue Carbon window

11- 10 5 -2.70 -30 31 -7 imp:p 1 $primary front inner

12- 11 5 -2.70 -32 33 -7 imp:p 1 $primary front outer

13- 12 5 -2.70 34 -35 -7 imp:p 1 $primary back inner

14- 13 5 -2.70 36 -37 -7 imp:p 1 $primary back outer

15- c 10 2 -0.001205 -30 31 -7 imp:p 1 $primary front inner

16- c 11 2 -0.001205 -32 33 -7 imp:p 1 $primary front outer

17- c 12 2 -0.001205 34 -35 -7 imp:p 1 $primary back inner

18- c 13 2 -0.001205 36 -37 -7 imp:p 1 $primary back outer

19- 100 2 -0.001205 #1 #2 #3 #4 #10 #11 #12 #13 -1000 imp:p 1

20- 1000 0 1000 imp:p 0

21-

22- c surface cards

23- 1 px -5 $primary detector front face

24- 2 px -4 $primary detector back face

25- 3 py 1.5 $primary detector left

26- 4 py -1.5 $primary detector right

27- 5 pz 1.5 $primary detector top

28- 6 pz -1.5 $primary detector bottom

29- 7 cx 4 $primary detector cylinder

30- 10 px 1 $rescue front face

31- 11 px 4.28 $rescue back

32- 12 cx 4.25 $rescue cylinder

33- 13 cx .435 $rescue hole

34- 14 px 2.63 $rescue hole stop

35- 15 px .9994 $Mylar insulator (face)

36- 16 px .99999 $Mylar insulator (back)

37- 17 px .4994 $Endcap (back)

```
38- 18 px .4234 $Endcap (front)
39- 30 px -7.24 $
40- 31 px -7.34 $
41- 32 px -7.89 $
42- 33 px -8.10 $
43- 34 px -1.76 $
44- 35 px -1.66 $
45- 36 px -1.11 $
46- 37 px -0.90 $
47- 50 px -20 $Source plane
48- 1000 so 30 $The world
49-
50- c data cards
51- mode p
52- c Material cards
53- m1 32000 1.0 $ Elemental Germanium
54- m2 6000 0.000151 7000 0.784437 8000 0.210750 18000 0.004670 $ This is air
55- m3 1000 0.363632 6000 0.454552 8000 0.181816 $Mylar
56- m4 6000 1.000000 $Plain ol' Carbon
57- m5 13000 1.0000000 $Aluminium
58- c Source cards
59- sdef sur=50 pos=-20 0 0 rad=d2 par=2 erg=.511 vec=1 0 0
60- dir=d1
61- si1 -1 .94 1
62- sp1 0 0 1
63- sb1 0 0 1
64- si2 0 1
65- sp2 -21 1
66- c Number of Particles
67- nps 1e4
68- c The famous PTRAC card
69- ptrac write=all event=src,col,ter file=asc max=100000000
70- filter=-21,5,x -10,10,y -10,10,z 1,50,ncp
71- cell=1
```

D.1 Cell Cards

Lines 1-20 are cell cards. Cells are volumes in 3D space composed of surfaces defined by surface cards (counterintuitively, the surface cards are defined after the cell cards). By using geometrical constructs of union, intersection, and compliment, volumes may be specified. Each volume is assigned a number (1-99), a material number (from materials

Table D.7. Cell descriptions

Cell number	Line number	Volume description
1	3	DSSD crystal
2	5	Coaxial detector crystal
3	7	Coaxial mylar insulator layer
4	9	Coaxial carbon fiber window
10	11	DSSD vacuum seal front face
11	12	DSSD front face
12	13	DSSD vacuum seal back face
13	14	DSSD back face
100	19	"The world"-air volume surrounding detectors
1000	20	"The universe"-region outside of world (photons exiting world are killed)

cards specified elsewhere), a density (in $\frac{g}{cm^3}$), component surfaces, and an importance number (for this example all photon importances are set to 1). Table D.7 is a summary of what each defined cell in this input deck is.

D.2 Surface Cards

The only surface types used in this simulation are planes and cylinders. The surface cards can be found on lines 23-48. The dimesions of the detector components were taken from reference documents provided by the manufacturers [43, 44].

D.3 Material Cards

Five different materials are used in this simulation. These five materials are defined on lines 53-57. Each material is assigned a number preceded by an "m-." This number is referenced by the cell cards when assigning material properties to the cell volumes.

D.4 Source Cards

The source cards define the source location, the energy distribution of the photons source, the initial location distribution (for area and volume sources), and the initial direction distribution for the photons. This simulation uses a disc source centered at [-20 0 0] with the x-axis as its normal vector. The second number on line 61 is the directional cosine that defines the maximum angle for which a particle may deviate from the normal direction (in this case 19.9°). Line 65 dictates that the particles are sourced uniformly over the area of the disc. Specific rules for source definition can be found in chapter 3 of [42:53-79]

D.5 Ptrac Card

The Ptrac card is found on lines 69-71. The event variable is specified to include only source, collision, and termination events. A maximum number of 100 million events is defined, although the number of particles the simulation tracks is set on the NPS card (line 67). The filter variable restricts the events logged to those that occur with in a box such that $-21 < x < 5, -10 < y < 10, -10 < z < 10$. This box contains all the components described in the cell and surface cards. The filter also removes events for which the collision value is not between 1 and 50, i.e., eliminates particles that have not interacted. The cell variable filters out particles that are not inciden on cell 1 (the DSSD). Rules for the Ptrac card are defined in chapter 3 of [42:152-5]

Appendix E. PTRAC Sample Data

A sample of the output from the ptrac card in MCNP is provided here (figure E.1). The structure of the ptrac output has four main components: the header, input variables, event line references, and histories. Details of all four components and the indexes for the event line references can be found in chapter one of [42:1-17].

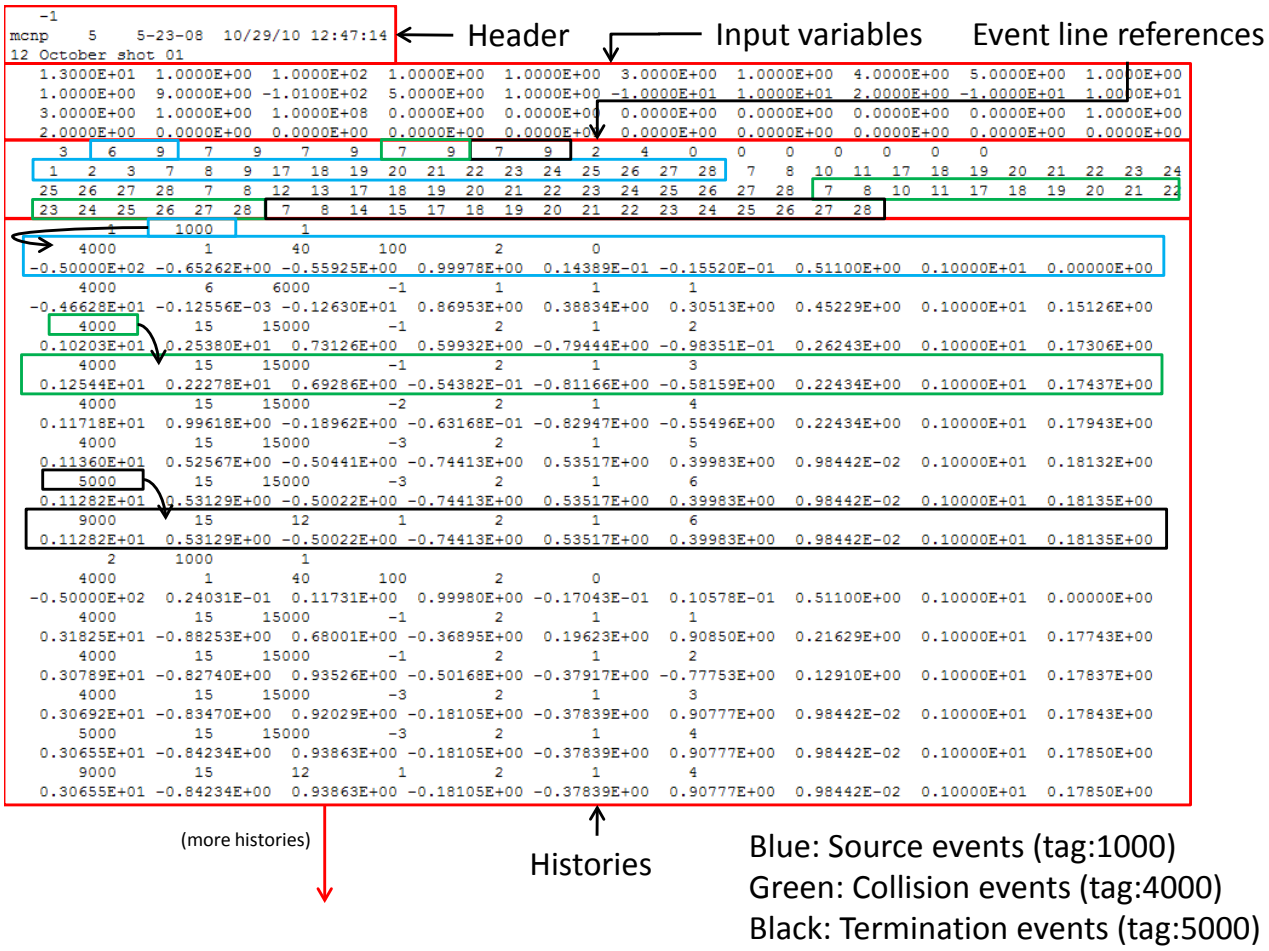

Figure E.1. Sample Ptrac output

The header gives information about the simulation run and a date/time stamp

The input variables list the user-selected options from the ptrac card on the input deck. Reference chapter 3 of [42:153] for description of input options.

The event line references list index numbers that refer back to table I-4 in [42:I-4]. The first line of the references section gives the number of variables on the particle ID, source, bank, surface, collision, and termination lines, respectively. There are two lines for all events and one line for the particle ID. In the sample provided, there are 6 variables on the first line of a source event (blue) and 7 for the first line of collision (green) and termination (black)

Table E.8. PTRAC event line descriptions

Event type	1st variable	2nd variable	3rd variable	4th variable	5th variable	6th variable	7th variable
Source	next event	node	source type	cell	material	collision count	
Collision	next event	node	cross-section data	interaction type	cell	material	collision count
Termination	next event (9000 if last event)	node	termination type	branch number	cell	material	collision count

events. The nine variables on the second line for all events are the same and list (in order): x-position, y-position, z-position, x-velocity, y-velocity, z-velocity, energy, weight, and time.

Each history begins with a NPS line which gives the number of the photon simulated, the type of the first event in the history as well as any filtering variables defined by the user. Each event type is determined by the event tag given in the first line of the previous event. The variable for the first line of each event are listed in table E.8.

Appendix F. Experimental Sample Data

Table F.9 is a sample of an event taken from a data set from the Spect32 raw coincidence output. The event shown represents a Compton rescue event in which the charge collected on the AC side was shared between two strips.

Table F.9. Sample DSSD coincidence event

Event #	Event cnt	Time	Channel	Slow	Fast Pred	Fast Succ
1	4	0	26	16.92	1.59	14.27
2	4	2	27	22.14	8.68	4.37
3	4	5	9	41.17	4.70	0.53
4	4	11	0	201.84	0.00	1.44

In this event, there are 4 hits (ref. the "Event #" and "Event cnt" columns). The first two hits come two clock cycles apart on channels 26 and 27, contiguous AC side strips (ref. "Time" and "Channel" columns). The two hits sum to 39.06 keV (ref. "Slow" column, the column that counts the energy calibration of the charge collected on the strip in the "Channel" column). On the DC side, a hit came 5 clock cycles after the trigger hit with an energy of 41.17 keV. At 11 clock cycles, the rescue detector registered an event with an energy of 201.84 keV. The predecessor and successor FOMs ("Fast Pred" and "Fast Succ") can be used according to eqn. 1.8 to determine the subpixel location within strips 9 and 27. This event represents a Compton rescue event where the photon interacted with the DSSD at the intersection of strip 9 on the DC side and strip 27 on the AC side, very close to strip 26. The full energy of this event would be counted as $\frac{(16.92+22.14)+41.17}{2} + 201.84 = 241.96keV$.

Appendix G. Simulation Parsing Algorithm

G.1 Simuation Parsing:Matlab Code

This is the code used to parse the ptrac files from the simulation. This is the raw MATLAB®code used. The pseudocode has been provided for easier understanding in section G.2. Line number references are included in the pseudocode for comparison to the MATLAB®code.

Listing G.1.

```
clear all; close all; clc;

ptrac=fopen('/Users/Stevenson/Documents/MATLAB/30octp10');
fscanf(ptrac,'%c',124);                 %header strip (there are ...
    125 characters
                                        %in the header

m=str2double(fscanf(ptrac,'%s',1));
n=zeros(m,20);
for i=1:m
    n(i,1)=str2double(fscanf(ptrac,'%s',1));
    if n(i,1)~=0
        for j=2:(n(i,1)+1)
            n(i,j)=str2double(fscanf(ptrac,'%s',1));
        end
    end
end
                                        %These numbers are based ...
                                           on
                                        %variables set on the ...
                                           PTRAC card in
                                        %MCNP...

remainder=40-(14+sum(n(:,1)));
str2double(fscanf(ptrac,'%s',remainder));
                                        %...but the last few are ...
                                           usually
                                        %zeros.


histnum=1000328;                         %This is the max number ...
    of histories this script will parse.
                                        %It will not give an error...
                                            if there
                                        %are fewer entries in the ...
                                           ptrac
                                        %file.

N=zeros(20,1);
for i=1:20
    N(i,1)=str2double(fscanf(ptrac,'%s',1));
end
```

```
                                        %N series (from MCNP ...
                                           manual vol II,
                                        %appendix I):
                                        %N(1): #vars on NPS line
                                        %N(2,3): # vars on src ...
                                           event lines
                                        %N(4,5): # vars on bnk ...
                                           event lines
                                        %N(6,7): # vars on sur ...
                                           event lines
                                        %N(8,9): # vars on col ...
                                           event lines
                                        %N(10,11):#vars on ter ...
                                           event lines
                                        %N(12):IPT for transport ...
                                           (2=photon)
                                        %N(13): not important
                                        %N(14:20): nothing (zeros)
totvars=sum(N(1:11));
r=zeros(totvars,1);
for i=1:totvars
    r(i)=str2double(fscanf(ptrac,'%s',1));
end
                                        %These are just variable ...
                                           references
                                        %from the manual

rescues=0;                              %Let's count our rescues...
   ...
pcaptures=0;                            %primary captures...
cscatters=0;                            %single Compton scatters...
   ...
endcheck=str2double(fscanf(ptrac,'%s',1)); %If this is empty we'll...
    know we're at the end of the file...
hist=1;
collision=zeros(10,4,histnum);          %PREALLOCATION!  This one ...
   line improved speed 30%
NPS=zeros(histnum,1);                     %also preallocation
rescue=zeros(histnum,5);                %also preallocation
pcapture=zeros(histnum,4);
cscatter=zeros(histnum,2);
while hist<=histnum
    %%  This section picks apart each history.  Currently it only ...
       deals
    %  with the collision events, but could be customized to pull ...
       out
    %  source, bank, surface and termination events too.  See MCNP
    %  documentation

    NPS(hist)=endcheck;
    currentevent=str2double(fscanf(ptrac,'%s',1));
    if n(2,1)~=0                        %get rid of the cell ...
       filter number
        str2double(fscanf(ptrac,'%s',1));
```

```
    end
    if n(9,1)~=0                          %get rid of the surf ...
       filter number
        str2double(fscanf(ptrac,'%s',1));
    end
    numevents=1;                          %The src event counts as ...
       one
    numcollisions=0;
    pe=0;                                 %Termination flag
    while currentevent~=9000
        if currentevent==1000             %we don't care about src ...
           events
            nextevent=str2double(fscanf(ptrac,'%s',1));
            fscanf(ptrac,'%s',(N(2)+N(3)-1));
        end
        if currentevent==2000             %we don't care about bnk ...
           events
            nextevent=str2double(fscanf(ptrac,'%s',1));
            fscanf(ptrac,'%s',(N(4)+N(5)-1));
        end
        if currentevent==3000             %we don't care about sur ...
           events
            nextevent=str2double(fscanf(ptrac,'%s',1));
            fscanf(ptrac,'%s',(N(6)+N(7)-1));
        end
        if currentevent==4000             %we DO care about col ...
           events
            numcollisions=numcollisions+1;
            nextevent=str2double(fscanf(ptrac,'%s',1));
            fscanf(ptrac,'%s',2);  %don't care about node or x-...
               section
            collision(numcollisions,2,hist)=str2double(fscanf(...
               ptrac,'%s',1)); %rxn type
            collision(numcollisions,3,hist)=str2double(fscanf(...
               ptrac,'%s',1)); %cell #
            fscanf(ptrac,'%s',1);  %don't care about material
            collision(numcollisions,1,hist)=str2double(fscanf(...
               ptrac,'%s',1)); %collision #
            fscanf(ptrac,'%s',6);  %don't care about location or ...
               direction
            collision(numcollisions,4,hist)=str2double(fscanf(...
               ptrac,'%s',1)); %energy
            fscanf(ptrac,'%s',2);  %don't care about weight or ...
               time
        end
        if currentevent==5000
            numcollisions=numcollisions+1;
            term=1;
            nextevent=str2double(fscanf(ptrac,'%s',1));
            fscanf(ptrac,'%s',1);  %don't care about node
            collision(numcollisions,2,hist)=str2double(fscanf(...
               ptrac,'%s',1)); %term type
            fscanf(ptrac,'%s',1);  %don't care about branch number
            collision(numcollisions,3,hist)=str2double(fscanf(...
```

```
            ptrac,'%s',1)); %cell#
        fscanf(ptrac,'%s',1);  %don't care about material
116     collision(numcollisions,1,hist)=str2double(fscanf(...
            ptrac,'%s',1)); %collision #
        fscanf(ptrac,'%s',6);  %don't care about location or ...
            direction
        collision(numcollisions,4,hist)=str2double(fscanf(...
            ptrac,'%s',1)); %energy
        fscanf(ptrac,'%s',2);  %don't care about weight or ...
            time
    end
121
    numevents=numevents+1;
    currentevent=nextevent;                 %if this is 9000, then...
        we are at the end of the history
end
if numcollisions==0                         %if there are no ...
    collisions we still need to keep track
126  collision(1,:,hist)=zeros(1,4);
else
    if collision(numcollisions,2,hist)==12
        pe=1;               %trip the flag if the term type was...
            a PE
    end
131 end
%%  This section does the analysis of the history.  I want ...
    this section
%  to count the number of Compton rescue events that happen.
err=0;              %Innocent until proven guilty
if collision(1,3,hist)==1 && collision(1,2,hist)==-1    %if ...
    the first collision is CS in cell 1
136  for i=2:numcollisions
        %do any other collision events happen outside of cell ...
            2?
        if collision(i,3,hist)~=2
            %a collision outside of cell 2 is an "error" (or
            %"guilty")
141             err=1;
        end
    end
    if pe==0
        %Can't count if there was never a PE
146     err=1;
    end
    %If still innocent, then we have a rescue!
    if err~=1
        if collision(numcollisions,3,hist)==2   %Just in case ...
            there was only one collision
151             rescues=rescues+1;          %Increment rescue ...
                counter
            rescue(rescues,1)=hist;         %log the NPS number
            rescue(rescues,2)=0;            %energy in primary ...
                detector
            rescue(rescues,3)=0;            %energy in rescue ...
```

```
                    detector

                %The amount deposited in the
                %first collision (had to be in
                %the primary detector and) is
                %.511 minus whatever was in the
                %energy log of the event
                rescue(rescues,2)=.511-collision(1,4,hist);
                for i=2:numcollisions-1
                    %If the next event was in the
                    %primary, then add the energy
                    %difference of the previous
                    %event and this one to the
                    %rescue entry (col 1: primary,
                    %col 2: rescue).
                    if collision(i,3,hist)==1
                        rescue(rescues,2)=rescue(rescues,2)+(...
                            collision(i-1,4,hist)-collision(i,4,...
                            hist));
                    elseif collision(i,3,hist)==2
                        rescue(rescues,3)=rescue(rescues,3)+(...
                            collision(i-1,4,hist)-collision(i,4,...
                            hist));
                    end
                    %The last energy deposited will
                    %just be whatever is in the
                    %energy log for this event
                    %because that's just how ptrac
                    %does it.
                end
                rescue(rescues,3)=rescue(rescues,3)+collision(...
                    numcollisions,4,hist);
                %This is just to make sure that it
                %all adds up to .511 MeV.
                rescue(rescues,4)=rescue(rescues,2)+rescue(rescues...
                    ,3);
                rescue(rescues,5)=pe;   %We might want to know ...
                    this eventually
            end
        end
    end

    %%  This section does the analysis of the history.  I want ...
        this section to
    %  compare the number of photons that compton scatter once to ...
        the
    %  number of photons that are absorbed directly in the primary
    %  detector (cell 1).
    err=0;          %Testing for any cell 1 interactions after the...
         1st one
    for i=2:numcollisions
        if collision(i,3,hist)==1
            err=1;
        end
```

```
    end
                    %If the 1st collision is a CS in cell 1...
    if collision(1,3,hist)==1 && collision(1,2,hist)==-1
                    %... and if it is not guilty...
        if err==0
                    %...count it!  Single Compton scatters.
            cscatters=cscatters+1;
            cscatter(cscatters,1)=hist;                 %log the ...
               NPS
            cscatter(cscatters,2)=collision(1,4,hist);  %log the ...
               energy deposited
        end
    else
        err=0;      %innocent until proven guilty
        cs=0;       %Keep track of Compton scatters
        rs=0;       %Keep track of Rutherfor scatters
        fl=0;       %Keep track of flourescences
        for i=1:numcollisions   %do any collisions happen outside ...
           of cell 1?
            if collision(i,3,hist)~=1
                err=1;          %a collision outside of cell 1 ...
                   means guilty
            end
            if collision(i,2,hist)==-1
                    %Compton scatter
                cs=cs+1;
            end
            if collision(i,2,hist)==-2
                    %Rutherford scatter
                rs=rs+1;
            end
            if collision(i,2,hist)==-3
                    %Flourescence
                fl=fl+1;
            end
        end
                    %no PEs = guilty!
        if pe==0
            err=1;
        end
                    %If we've made it this far without an error, ...
                       then we at
                    %least know it was fully absorbed in the ...
                       primary
        if err~=1
            pcaptures=pcaptures+1;
            pcapture(pcaptures,1)=hist;
                    %I want to keep track of Compton and ...
                       Rutherford
                    %scatters because I'm not sure I can count it ...
                       as a
                    %primary detection if it bounced around before...
                        being
                    %absorbed.
```

```
            pcapture(pcaptures,2)=cs;
            pcapture(pcaptures,3)=rs;
            pcapture(pcaptures,4)=fl;
        end

    end
    %%  This part is mainly just here so that  we don't get an ...
       error every
    %  time we get to the end of the file.  It's just a style ...
       thing.
    endcheck=str2double(fscanf(ptrac,'%s',1));
    if isnan(mode(endcheck))==1          %Matlab will give you a ...
       warning about this.  Don't worry about it.
        maxnps=hist;
        hist=histnum;
    end
    hist=hist+1;
end

                    %So we don't have a bunch of empty cells in ...
                       our
                    %matrices...
cscatter(cscatters+1:histnum,:)=[];
pcapture(pcaptures+1:histnum,:)=[];
rescue(rescues+1:histnum,:)=[];
collision(:,:,maxnps+1:histnum)=[];

                    %This is because you can't really count a ...
                       primary
                    %capture if it bounced in the crystal before ...
                       being
                    %absorbed.
realpcaptures=0;
for i=1:pcaptures
    if pcapture(i,2)==0 && pcapture(i,3)==0
        realpcaptures=realpcaptures+1;
    end
end

rescues
cscatters
pcaptures
realpcaptures
particles_tracked=maxnps
rescue_percent=rescues/maxnps
cscatter_percent=cscatters/maxnps
primary_capture_percent=realpcaptures/maxnps
scatter_to_capture_ratio=cscatters/realpcaptures
rescue_to_capture_ratio=rescues/realpcaptures
rescue_to_scatter_ratio=rescues/cscatters
```

G.2 Simuation Parsing:Pseudocode

This is the pseudocode that summarizes the above MATLAB®script. Line references to the above script have been provided where appropriate.

Listing G.2.

```
Clear environment, open ptrac file, strip off header data (lines ...
   1-6)

Read in input variable data, store for later use (lines 7-26)

Read in event line reference.  This data will be used to count the...
    number of variables on each event line (lines 32-51).

Declare variables, preallocate for speed.  Variables keep tallies ...
   of significant histories, and preallocation matrices log the ...
   data from each significant history (lines 55-64).

while number of histories parsed < max number of histories
        use event line data to pull the collision events out of a ...
           single history and load into a ''currentevent'' matrix ...
           (lines 66-131)

        analyze current history to determine if it is compton ...
           rescue (lines 134-87)

        if first event is Compton scatter in cell 1 (DSSD)
                if all proceeding collisions occur in cell 2 (...
                   rescue)
                        if event ends with PE absorption
                                increment compton rescue tally, ...
                                   log the photon number, log the ...
                                   energy deposited in primary and...
                                    rescue detectors, log the ...
                                   number of collisions
                        end
                end
        end
        analyze current history to determine if it was directly ...
           absorbed by the primary detector (lines 189-248)
        if All collisions in current event take place in cell 1 (...
           DSSD)
                if final collision is PE absorption
                        Increment primary absorption tally, count ...
                           number of Compton scatters, Rutherford ...
                           scatters, and flourescences.
                end
        end
end
Make a separate tally for primary absorptions where there are no ...
   scattering or flourescence events (REAL primary absorptions), ...
   lines 269-74.
```

```
print results (lines 276-86)
```

Appendix H. Experiment Data Parsing Algorithm

H.1 Experiment Data Parsing:Matlab Code

Listing H.1.

```
clear all; close all; clc;
%close all; clc;

tic

filename='06Dec10_Sr_85_coll6strip_Events002.phd';
rawdata=dlmread(filename,'',1,0);
D=size(rawdata);
maxrow=D(1);

numevents=1500000;
fullenergy=514;                          %This is the photon energy ...
   we are looking to rescue

substrips=13;                              %best if this is odd
face=zeros(14*substrips,16*substrips);                  %This will...
    map out the rescue counts
oldface=zeros(14*substrips,16*substrips);               %This will...
    map out the non-rescue counts

correction=1.0;

eventlog=zeros(6,7,numevents);
coordinates=zeros(numevents,13);          %dcstrip acstrip ...
   dcsubstrip acsubstrip totalenergy dcenergy dcmax dcpred dcsucc ...
   acenergy acmax acpred acsucc
rescue=zeros(numevents,2);
capture=zeros(numevents,2);
event=1;
datarow=1;
rescues=0;
captures=0;
significants=0;
%%
while datarow<maxrow
                                %This section resets all variables...
                                    for each
                                %new event:
    current=zeros(6,7);                    %This is a matrix of all ...
       hits in the current event
    rescuehit=0;                           %This is a flag for a hit ...
       in the rescue
    dchit=0;                               %flag for hit on dc side
    achit=0;                               %flag for hit on ac side
    rescueind=zeros(3,1);                  %These three indicies will...
        keep
```

```
    dcind=zeros(4,1);                       %track of which hits in ...
       the event
    acind=zeros(4,1);                       %are for which component (...
       rescue, dc side, ac side)
40  rescenergy=0;                           %This is the energy ...
       deposited in rescue
    dcenergy=0;                             %Energy collected on dc ...
       side
    acenergy=0;                             %Energy collected on ac ...
       side
    dcsum=0;                                %Sum of dcenergy and ...
       rescenergy
    acsum=0;                                %Sum of acenergy and ...
       rescenergy
45  dcyes=0;                                %Flag for criteria being ...
       met on the dc side
    acyes=0;                                %'' ...
                              ''on the ac side
    dccentroid=0;                           %This is the average of ...
       the dc strip numbers
    accentroid=0;                           %''                 ''of ...
       the ac strip numbers
    dcstrip=0;                              %This is where we are ...
       counting the dc hit, and...
50  dcstripind=0;                           %This keeps track of which...
        hit in the current event corresponds to dcstrip
    acstrip=0;                              %'' ...
                                ''the ac hit, and...
    acstripind=0;                           %'' ...
                                ''to acstrip
    dcmax=0;                                %The max energy deposited ...
       on a dc strip
    acmax=0;                                %'' ...
                              ''an ac strip
55  dcpred=0;                               %Transient charge on ...
       predecessor dc strip (dcstrip-1)
    dcsucc=0;                               %Transient charge on ...
       successor dc strip (dcstrip+1)
    dctran=0;                               %Sum of dcpred and dcsucc
    dcfine=0;                               %substrip coordinate ...
       within dcstrip
    dcsubstrip=0;                           %substrip coordinate on ...
       face of detector
60  acpred=0;                               %
    acsucc=0;                               %
    actran=0;                               %Same as previous 5 ...
       variables, for ac side
    acfine=0;                               %
    acsubstrip=0;                           %
65  dcedge=0;                               %Flag for a hit on ...
       edgemost strip on dc side
    acedge=0;                               %Flag for a hit on ...
       edgemost strip on ac side
```

```
                                        %The "current" matrix ...
                                           grabs all the
                                        %lines (hits) for the ...
                                           current
                                        %event.
70      current(1,:)=rawdata(datarow,:);
        datarow=datarow+1;
                                        %The second entry on the ...
                                           first row
                                        %of the event tells how ...
                                           many hits
                                        %are in the event.
75      hits=current(1,2);
                                        %This part reads ...
                                           information about
                                        %the first hit...
                                        %If the channel is zero, ...
                                           then it's
                                        %a rescue hit
80      if current(1,4)==0
            rescuehit=1;            %count the rescue
            rescueind(1)=1;         %log the first rescue hit as being on ...
               the first line
                                        %If the channel is between...
                                            1 and 14 inclusive,
                                        %then it's a dc hit
85      elseif current(1,4)>=1 && current(1,4)<=14
            dchit=1;                %count the dc hit
            dcind(1)=1;             %log the first dc hit as being on the ...
               first line
                                        %If the channel is between...
                                            16 and
                                        %31 inclusive, then it's ...
                                           an ac hit
90      elseif current(1,4)>=16 && current(1,4)<=31
            achit=1;                %count the ac hit
            acind(1)=1;             %log the first ac hit as being on the ...
               first line
        end
                                        %This part does the same ...
                                           thing as
95                                      %the previous 'if' did for...
                                            the rest
                                        %of the hits in the event.
        for i=2:hits
                                %add another hit to current
            current(i,:)=rawdata(datarow,:);
100                             %so we don't lose count of what row we...
                                    are
                                %on...
            datarow=datarow+1;
                                %Same as before, but for each ...
                                   successive hit
            if current(i,4)==0
```

```
            rescuehit=rescuehit+1;
            rescueind(rescuehit)=i;
        elseif current(i,4)>=1 && current(i,4)<=14
            dchit=dchit+1;
            dcind(dchit)=i;
        elseif current(i,4)>=16 && current(i,4)<=31
            achit=achit+1;
            acind(achit)=i;
        end
    end
    %%
    %We have the all the hits in the event.
    %Now we need to figure out if it's worth
    %anything...

    %%%%
    %This is the rescue section
    if dchit>=1 && achit>=1
        if rescuehit==1     %Is the rescue flag up?
            rescenergy=current(rescueind(1),5);

            %%
                                    %dc centroid is the ...
                                       average of all
                                    %the strip numbers.  This ...
                                       is so we
                                    %can figure out if there ...
                                       are too
                                    %many hits on one side.  ...
                                       You'll see
            for i=1:dchit
                                    %Sum energy from dc side
                dcenergy=dcenergy+current(dcind(i),5);
                                    %sum all the strip numbers...
                                       ...
                dccentroid=dccentroid+current(dcind(i),4);
            end
                                    %...and divide them by the...
                                        number
                                    %of dc hits.  Gives us the
                                    %"average" strip (could be
                                    %"between" strips).
            dccentroid=dccentroid/dchit;
            dcsum=rescenergy+dcenergy;  %this is what we'll use to...
                see if the event is in the barn
                                    %it's in the barn if it ...
                                       falls
                                    %within 1.6% of the full ...
                                       energy
                                    %(determined empirically ...
                                       from FWHM)
            if dcsum>=fullenergy*(1-.006) && dcsum<=fullenergy...
               *(1+.006)
                dcyes=1;        %yes flag for being in the barn
```

```
        end
                        %this for loop checks to see if ...
                           any hits
150                     %fall on strips outside 6/10 of a ...
                           strip
                        %away from the centroid.  If they ...
                           do, then
                        %there are more than 3 hits on the...
                            dc side
                        %and we don't count this event.
        for i=1:dchit
155         if current(dcind(i),4)<dccentroid-.6 || current(...
               dcind(i),4)>dccentroid+.6
                dcyes=0;    %lower the yes flag
                acyes=0;
            end
                        %This finds which strip the max ...
                           energy was
160                     %on, and finds where it is in the ...
                           hit index
            if current(dcind(i),5)>dcmax
                dcstrip=current(dcind(i),4);
                dcstripind=i;
                dcmax=current(dcind(i),5);
165         end
                        %This part gets rid of events for ...
                           which
                        %there is a hit where transient ...
                           charge
                        %didn't register
            if current(dcind(i),6)==0 || current(dcind(i),7)...
               ==0
170             dcyes=0;
            end
        end
                        %This is a flag for a hit on the ...
                           edgemost
                        %strips.  We will need it later.
175     if dcstrip==1 || dcstrip==14
            dcedge=1;
        end
                            %At this point:
                                %-dcyes says whether or ...
                                   not the hit
180                             %on the dc side is in the ...
                                   barn
                                %-dcsum is the size of the...
                                    hit on
                                %the dc side
                                %-dcstrip tells us which ...
                                   pixel it
                                %is on the dc side (but we...
                                    don't
185                             %know the substrip yet!)
```

```
                                    %-dcstripind is the index ...
                                        number
                                    %for dcstrip

                                    %This section determines ...
                                        the
190                                 %subpixel bin.
            dcpred=current(dcind(dcstripind),6);
            dcsucc=current(dcind(dcstripind),7);
            dctran=dcpred+dcsucc;
            if dcpred~=0 && dcsucc~=0
195                                 %This will be a number ...
                                        between 0
                                    %and 1, for how far left ...
                                        or right
                                    %the subpixel is from ...
                                        center.
                dcfine=((dcsucc/dctran)-.5)*2;
                                %I included this part to try and
200                             %correct for subpixel efficiency, ...
                                    but I
                                %don't know that it works very ...
                                    well.  You
                                %may be best off leaving '...
                                    correction' (at
                                %the top) set to 1.
                if dcfine > 0
205                 dcfine=round(dcfine^(1/correction)*(substrips)...
                        /2);
                elseif dcfine < 0
                    dcfine=round((-dcfine)^(1/correction)*(...
                        substrips)/2);
                    dcfine=-dcfine;
                end
210         else
                dcfine=0;
            end
                                %This translates the strip number ...
                                    and the
                                %fine correction to a substrip ...
                                    number for
215                             %the face array.
            dcsubstrip=(dcstrip*substrips-(substrips-1)/2)+dcfine;
            %%
                                    %All the same logic as ...
                                        above is
                                    %repeated here for the ac ...
                                        side
220         for i=1:achit
                acenergy=acenergy+current(acind(i),5);
                accentroid=accentroid+current(acind(i),4);
            end
            accentroid=accentroid/achit;
225         acsum=rescenergy+acenergy;
```

```
        if acsum>=fullenergy*(1-.009) && acsum<=fullenergy...
           *(1+.009)
            acyes=1;
        end

        for i=1:achit
            if current(acind(i),4)<accentroid-.6 || current(...
               acind(i),4)>accentroid+.6
                dcyes=0;
                acyes=0;
            end
            if current(acind(i),5)>acmax
                acstrip=current(acind(i),4)-15;
                acstripind=i;
                acmax=current(acind(i),5);
            end
            if current(acind(i),6)==0 || current(acind(i),7)...
               ==0
                acyes=0;
                dcyes=0;
            end
        end

        if acstrip==1 || acstrip==16
            acedge=1;
        end
                                %At this point:
                                    %-acyes says whether or ...
                                       not the hit
                                    %on the ac side is in the ...
                                       barn
                                    %-acsum is the size of the...
                                        hit on
                                    %the ac side
                                    %-acstrip tells us which ...
                                       pixel it
                                    %is on the ac side (but we...
                                        don't
                                    %know the substrip yet!)

        acpred=current(acind(acstripind),6);
        acsucc=current(acind(acstripind),7);
        actran=acpred+acsucc;
        if acpred~=0 && acsucc~=0
            acfine=((acsucc/actran)-.5)*2;
            if acfine > 0
                acfine=round(acfine^(1/correction)*(substrips)...
                   /2);
            elseif acfine < 0
                acfine=round((-acfine)^(1/correction)*(...
                   substrips)/2);
                acfine=-acfine;
            end
        else
```

```
270                 acfine=0;
                end
                acsubstrip=(acstrip*substrips-(substrips-1)/2)+acfine;
                    %We will add the counts to the tallies if at least
                    %the dc side is in the barn.  The ac side
275                 %doesn't have to be because it's not as
                    %efficient at collecting charge.
                    if dcyes==1  && acyes==1
                        %significants is the tally of
                        %absorptions+rescues
280                     significants=significants+1;
                        rescues=rescues+1;
                        %If both dc and ac were in the barn, total is
                        %the average of the two
                        totalenergy=(dcsum+acsum)/2;
285                     rescue(rescues,1)=event;
                        rescue(rescues,2)=significants;
                        %We'll want to keep track of a few things...
                        coordinates(significants,:)=[dcstrip acstrip ...
                           dcsubstrip acsubstrip totalenergy dcenergy ...
                           dcmax dcpred dcsucc acenergy acmax acpred ...
                           acsucc];
                        eventlog(:,:,significants)=current;
290                     %I don't add edge hits to theface array ...
                           because
                        %they can't see transient charge on one side.
                        if dcedge~=1 && acedge~=1
                            face(dcsubstrip,acsubstrip)=face(...
                               dcsubstrip,acsubstrip)+1;
                        end
295
                    elseif dcyes==1
                        significants=significants+1;
                        rescues=rescues+1;
                        totalenergy=dcsum;
300                     rescue(rescues,1)=event;
                        rescue(rescues,2)=significants;
                        coordinates(significants,:)=[dcstrip acstrip ...
                           dcsubstrip acsubstrip totalenergy dcenergy ...
                           dcmax dcpred dcsucc acenergy acmax acpred ...
                           acsucc];
                        eventlog(:,:,significants)=current;
                        if dcedge~=1 && acedge~=1
305                         face(dcsubstrip,acsubstrip)=face(...
                               dcsubstrip,acsubstrip)+1;
                        end
                    end


310         elseif rescuehit==0                                    %This ...
               is the capture section

                    for i=1:dchit
                        dcenergy=dcenergy+current(dcind(i),5);
```

```
            dccentroid=dccentroid+current(dcind(i),4);
        end
        dccentroid=dccentroid/dchit;    %this is the "mean ...
           strip" for the dc side
        dcsum=dcenergy;
        if dcsum>=fullenergy*(1-.006) && dcsum<=fullenergy...
           *(1+.006)
            dcyes=1;
        end

        for i=1:dchit
            if current(dcind(i),4)<dccentroid-.6 || current(...
               dcind(i),4)>dccentroid+.6
                dcyes=0;
                acyes=0;
            end
            if current(dcind(i),5)>dcmax
                dcstrip=current(dcind(i),4);
                dcstripind=i;
                dcmax=current(dcind(i),5);
            end
            if current(dcind(i),6)==0 || current(dcind(i),7)...
               ==0
                dcyes=0;
            end
        end

        if dcstrip==1 || dcstrip==14
            dcedge=1;
        end

        dcpred=current(dcind(dcstripind),6);
        dcsucc=current(dcind(dcstripind),7);
        dctran=dcpred+dcsucc;
        if dcpred~=0 && dcsucc~=0
            dcfine=((dcsucc/dctran)-.5)*2;
            if dcfine > 0
                dcfine=round(dcfine^(1/correction)*(substrips)...
                   /2);
            elseif dcfine < 0
                dcfine=round((-dcfine)^(1/correction)*(...
                   substrips)/2);
                dcfine=-dcfine;
            end
        else
            dcfine=0;
        end
        dcsubstrip=(dcstrip*substrips-(substrips-1)/2)+dcfine;

        for i=1:achit
            acenergy=acenergy+current(acind(i),5);
            accentroid=accentroid+current(acind(i),4);
        end
```

```
            accentroid=accentroid/achit;    %"mean strip" for the ...
               ac side
            acsum=acenergy;
            if acsum>=fullenergy*(1-.009) && acsum<=fullenergy...
               *(1+.009)
                acyes=1;
            end

            for i=1:achit
                if current(acind(i),4)<accentroid-.6 || current(...
                   acind(i),4)>accentroid+.6
                    dcyes=0;
                    acyes=0;
                end
                if current(acind(i),5)>acmax
                    acstrip=current(acind(i),4)-15;
                    acstripind=i;
                    acmax=current(acind(i),5);
                end
                if current(acind(i),6)==0 || current(acind(i),7)...
                   ==0
                    acyes=0;
                    dcyes=0;
                end
            end

            if acstrip==1 || acstrip==16
                acedge=1;
            end

            acpred=current(acind(acstripind),6);
            acsucc=current(acind(acstripind),7);
            actran=acpred+acsucc;
            if acpred~=0 && acsucc~=0
                acfine=((acsucc/actran)-.5)*2;
                if acfine > 0
                    acfine=round(acfine^(1/correction)*(substrips)...
                       /2);
                elseif acfine < 0
                    acfine=round((-acfine)^(1/correction)*(...
                       substrips)/2);
                    acfine=-acfine;
                end
            else
                acfine=0;
            end
            acsubstrip=(acstrip*substrips-(substrips-1)/2)+acfine;
                if dcyes==1 && acyes==1
                    significants=significants+1;
                    captures=captures+1;
                    totalenergy=(dcsum+acsum)/2;
                    capture(captures,1)=event;
                    capture(captures,2)=significants;
```

```
                    coordinates(significants,:)=[dcstrip acstrip ...
                        dcsubstrip acsubstrip totalenergy dcenergy ...
                        dcmax dcpred dcsucc acenergy acmax acpred ...
                        acsucc];
                    eventlog(:,:,significants)=current;
                    if dcedge~=1 && acedge~=1
                        oldface(dcsubstrip,acsubstrip)=oldface(...
                            dcsubstrip,acsubstrip)+1;
                    end

                elseif dcyes==1
                    significants=significants+1;
                    captures=captures+1;
                    totalenergy=dcsum;
                    capture(captures,1)=event;
                    capture(captures,2)=significants;
                    coordinates(significants,:)=[dcstrip acstrip ...
                        dcsubstrip acsubstrip totalenergy dcenergy ...
                        dcmax dcpred dcsucc acenergy acmax acpred ...
                        acsucc];
                    eventlog(:,:,significants)=current;
                    if dcedge~=1 && acedge~=1
                        oldface(dcsubstrip,acsubstrip)=oldface(...
                            dcsubstrip,acsubstrip)+1;
                    end
                end
            end
        end
        if datarow>=maxrow          %Matlab will give you a warning ...
            about this.  Don't worry about it.
            maxnps=event;
            %          event=numevents;
        else
            event=event+1;
        end
end

eventlog(:,:,significants+1:numevents)=[];
rescue(rescues+1:numevents,:)=[];
capture(captures+1:numevents,:)=[];
coordinates(significants+1:numevents,:)=[];

figure(1)
colormap(jet)
imagesc(face)

figure(2)
colormap(jet)
imagesc(oldface)

rescues_to_captures=rescues/captures
significant_percent=significants/maxnps

time=toc
```

H.2 Experiment Data Parsing:Pseudocode

This is the pseudocode that summarizes the above MATLAB®script. Line references to the above script have been provided where appropriate.

Listing H.2.

```
Clear workspace, load data (lines 4-12)

Declare variables, preallocate (lines 14-28): the full subpixel ...
   array of the DSSD is represented by the matrix ‘‘face’’ for the...
    rescue events and ‘‘oldface’’ for the direct absorption events...
   .  The variable ‘‘correction’’ was an early attempt to ...
   compensate for the squeezing effect (lines 223, 225, 282, 284)....
     It didn’t work very well, so it is best to leave it at 1, ...
   where it does not contribute to the subpixel distribution.

while the parser has not reached the ’end’ of the data matrix
        Declare variables: There are a lot of them and they all ...
           get reset after each event is analyzed.  They are each ...
           described in the comments of the script (lines 33-66).

        Load the next hit in the data set into a matrix called ‘‘...
           current’’:  The number in the second column of the ...
           first line of data is the number of hits in the event, ...
           thus the number of lines to put into current, ref ...
           appendix \ref{Chap:ExperimentalSampleData} (lines ...
           70-93).  Determine the type of hit (AC side, DC side, ...
           rescue), and keep track of what type of hit came first ...
           (the ‘‘-ind’’ matrices).

        Load the rest of the hits in the event, and index the ...
           order in which they occur.  The ‘‘-ind’’ matrices keep ...
           track of where each type of hit comes in the correct ...
           order for each event (line 97-114).

        if There is at least 1 hit on both the AC and DC side
                Analyze the event to determine if it is a rescue ...
                   event (lines 120-307)
                if There is a hit in the rescue detector (line ...
                   123)
                        Get the rescue detector energy (line 124)

                        Get the energy from the DC side, if ...
                           multiple DC hits, sum them (lines ...
                           131-136)

                        Find the average the the strip numbers (...
                           lines 135, 141).  This average number ...
                           (‘‘dccentroid’’) will be used to make ...
```

```
                sure that the two strips are contiguous...
                .  If either strip is .6 or more ...
                greater than or less than the average, ...
                then they are not contiguous and the ...
                event will not be counted as a rescue(...
                lines 154-8).

            Determine if the DC energy + the rescue ...
                energy falls within the $\Delta E$ of ...
                the full energy (lines 142-8).  For ...
                this example the window is set to $\pm...
                .6 \%$ of the full energy, but this can...
                 be changed.  If the DC energy does not...
                 fall in this window the event is not ...
                counted.

23          if there were multiple strips with hits
                    find which one had the highest ...
                        energy (lines 161-5)
            end

            If a hit had no transient charge
28                  throw the event away (lines ...
                        169-72)
            end

            If a hit occurred on one of the edgemost ...
                strips of the array
                    make a note not to add it to the ...
                        ``face'' array because it will ...
                        have not have an accurate ...
                        transient charge FOM on one ...
                        side and will have a wrong FC ...
                        figure (lines 175-7, 292-5).
33          end

            Calculate the FC, and determine the ...
                substrip number (lines 191-216).

            Repeat the same analysis of lines 131-216 ...
                for the AC side (lines 220-272).
38
            if the event has not been disqualified ...
                because of any of the criteria in lines...
                 131-272
                    then it is counted as a Compton ...
                        rescue (lines 277-307)

                    if both DC and AC side energy plus...
                         the rescue energy are within $...
                        \Delta E$ of the full energy (...
                        lines 277-95)
43                          The energy of the hit is ...
                                stored as the average ...
```

```
                                                of the DC and AC side ...
                                                energy plus the rescue ...
                                                energy
                                        elseif only the DC side energy is ...
                                           within $\Delta E$ of the full ...
                                           energy (lines 296-307)
                                                The energy of the hit is ...
                                                stored as the DC side ...
                                                energy plus the rescue ...
                                                energy
                                        end
                                end
48                      end
                        if there is no hit on the rescue detector
                                Do the same analysis as lines 123-307.  ...
                                   Events that meet the criteria are now ...
                                   counted as Direct absorptions (called ...
                                   ``captures'' in the code).  This ...
                                   section runs from lines 310-427.
                        end
                end
53  end
    Display results (lines 436-52)
```

Bibliography

[1] I. K. MacKenzie, J. A. Eady, and R. R. Gingerich, "The interaction between positrons and dislocations in copper and in an aluminum alloy," *Physics Letters*, vol. 33A, pp. 279–80, 1970.

[2] M. Wirtz *et al.*, "Non-destructive evaluation of plasticity and prediction of fatigue failure in industrial aluminium alloys with positrons," 2010.

[3] R. Zaleski and K. Zaleski, "Positron annihilation in steel burnished by vibratory shot peening," *Acta Physica Polonica*, vol. A 110, pp. 739–46, 2006.

[4] M. Cunningham *et al.*, "First-generation hybrid compact compton imager," in *IEEE Nuclear Science Symposium Conference Record*, 2005.

[5] R. A. Kroeger *et al.*, "Gamma ray polarimetry using a position sensitive germanium detector," 1999.

[6] T. E. Beveridge *et al.*, "High-purity germanium strip detectors possible applications to sr studies," in *IEEE Nuclear Science Symposium Conference Record*, pp. 4672–5, 2004.

[7] G. F. Knoll, *Radiation Detection and Measurement*. Wiley, 2000.

[8] H. J. Ache, "New developments in positron and positronium chemistry," in *Positron Annihilation*, Proceedings of the fifth international conference on positron annihilation, pp. 31–47, Japan Institute of Metals, 1979.

[9] P. A. M. Dirac, "The quantum theory of the electron," *Proceedings of the Royal Society of London. Series A, Containing Papers of a Mathematical and Physical Character*, vol. 117, pp. 610–24, 1928.

[10] C. D. Anderson, "The positive electron," 1933.

[11] M. Deutsch, "Evidence for the formation of positronium in gases," 1951.

[12] R. Krause-Rehberg and H. S. Leipner, *Positron Annihilation in Semiconductors*. Springer, 1999.

[13] R. Firestone, "Nuclear data sheets for a=22," tech. rep., Lawrence Berkeley National Laboratory, 2005.

[14] R. R. Hasiguti and K. Fujiwara, eds., *Positron Annihilation*, The Japan Institute of Metals, The Japan Institute of Metals, April 1979.

[15] A. Uedono *et al.*, "Vacancy-type defects in ultra-shallow junctions fabricated using plasma doping studied by positron annihilation," in *10th International Workshop on Junction Technology, IWJT-2010*, pp. 149–154, 2010.

[16] C. S. Williams, *Three-Dimensional Positron Annihilation Momentum Measurement Technique Applied to Measure Oxyget-atom Defects in 6H Silicon Carbide*. PhD thesis, Air Force Institute of Technology, 2010.

[17] R. Beringer and C. Montgomery, "The angular variation of positron annihilation radiation," *Physical Review*, vol. 61, pp. 222–24, 1942.

[18] A. Uedono, "Annealing properties of open volumes in strained sin films studied by monoenergetic positron beams," *Journal of Applied Physics*, vol. 102, 2007.

[19] M. Charlton and J. W. Humbertson, *Positron Physics*. Cambridge University Press, Cambridge, 2001.

[20] A. Baranowski *et al.*, "A two-detector spectrometer for measurements of doppler broadned positron annihilation spectra," *Nuc. Inst. Meth.*, vol. A526, pp. 420–431, 2004.

[21] P. Asoka-Kumar *et al.*, "Increased elemental specificity of positron annihilation spectra," *Phys. Rev. Lett.*, vol. 77, pp. 2097–2100, 1996.

[22] M. Haaks *et al.*, "Analyzing the high-momentum part of positron annihilation doppler spectra with a single germanium detector," 2006.

[23] S. M. Sze, *Semiconductor Devices: Physics and Technology*. Wiley, 2nd ed., 2002.

[24] A. L. Kuhn, *Advanced Pulse-Shape Analysis and Implementation of Gamma-Ray Tracking in a Position-Sensitive Coaxial HPGe Detector*. PhD thesis, University of California, Berkeley, 2002.

[25] R. A. Kroeger *et al.*, "Charge spreading and position sensitivity in a segmented planar germanium detector," *Nuc. Inst. Meth*, vol. A 422, pp. 206–210, 1999.

[26] M. Amman and P. N. Luke, "Three-dimensional position sensing and field shaping in orthogonal-strip germanium gamma-ray detectors," *Nuc. Inst. Meth.*, vol. A 452, pp. 155–166, 2000.

[27] E. L. Hull and et al, "A germanium orthogonal strip detector system for gamma-ray imaging," *Proc. SPIE*, vol. 4507, pp. 132–140, 2001.

[28] R. M. Keyser and T. W. Raudorf, "Germanium radiation detector manufacturing: process and advances," *Nuc. Inst. Meth*, vol. A 286, p. 357, 1990.

[29] J. H. Hubbell and S. M. Seltzer, "Tables of x-ray mass attenuation coefficients and mass energy-absorption coefficients from 1 kev to 20 mev for elements z = 1 to 92 and 48 additional substances of dosimetric interest," tech. rep., 1996.

[30] Z. Kis *et al.*, "Comparison of efficiency functions of ge gamma-ray detectors in a wide energy range," *Nuc. Inst. Meth.*, vol. A 418, pp. 374–386, 1998.

[31] D. J. Decman and M. N. Namboodiri, "Monte carlo study of a high-sensitivity gamma-ray detection system," tech. rep., Lawrence Livermore National Laboratory, 1995.

[32] O. Klein and T. Nishina, *The Oscar Klein Memorial Lectures*, vol. 2, pp. 113–129. World Scientific Publishing, 1994.

[33] R. A. Rizk, A. M. Hathout, and A.-R. Z. Hussein, "On solid angle calculations," *Nuc. Inst. Meth.*, vol. A245, pp. 162–166, 1986.

[34] PHDs Co. http://phdsco.com/, January 2011.

[35] R. H. Pehl, E. E. Haller, and R. C. Cordi, "Operational characteristics of germanium detectors at higher temperatures," *IEEE Trans. Nuc. Sci.*, vol. NS-20, p. 494, 1973.

[36] G. H. Nakano, D. A. Simpson, and W. L. Imhof, "Characteristics of large intrinsic germanium detectors operated at elevated temperatures," *IEEE Trans. Nuc. Sci.*, vol. NS-24, p. 68, 1977.

[37] G. A. Armantrout, "High operating temperature limitations for germanium detectors," *IEEE Trans. Nuc. Sci.*, vol. NS-19, p. 289, 1972.

[38] R. Vaidyanathan, "A doppler broadening positron annihilation spectroscopy study of magnetcially induced recovery in nickel," *J. Phys.: Condens. Matter*, vol. 5, pp. 4563–4572, 1993.

[39] S. Kamboj and B. Kahn, "Evaluation of monte carlo simulation of photon counting efficiency for germanium detectors," *Health Physics*, 1996.

[40] A. Owens *et al.*, "Monte-carlo calculations of ge detector escape-peak efficiencies," *IEEE Trans. Nuc. Sci.*, vol. 38, no. 2, pp. 221–225, 1991.

[41] L. K. Herold and R. T. Kouzes, "Intrinsic germanium detector efficiency calculations," *IEEE Trans. Nuc. Sci.*, vol. 38, no. 2, pp. 231–238, 1991.

[42] Los Alamos National Laboratory, *MCNP5 Manual, February 2008 revision*, 2008.

[43] PHDs Co., "Afit-np4 detector crystal and housing drawing." Email correspondence with Ethan Hull, PHDs Co., 2010. Proprietary information.

[44] Ortec Co., "Germanium detector diagram, serial number 49-tp50645a." Email correspondence with Amy Kennedy, Ortec Co., 2010. Proprietary information.

[45] K. S. Krane, *Introductory Nuclear Physics*. Wiley, 1988.

[46] C. S. Williams, "Toward simultaneous 2d acar and 2d dbar: Sub-pixel spatial characterization of a segmented hpge detector using transient charges," *IEEE Trans. Nuc. Sci.*, vol. 152, pp. 860–9, 2009.

REPORT DOCUMENTATION PAGE

Form Approved
OMB No. 0704–0188

1. REPORT DATE *(DD–MM–YYYY)*	2. REPORT TYPE	3. DATES COVERED *(From — To)*
24–03–2011	Master's Thesis	Aug 2009 — Mar 2011

4. TITLE AND SUBTITLE

Improving the Efficiency of Photon Collection By Compton Rescue

5a. CONTRACT NUMBER

5b. GRANT NUMBER

5c. PROGRAM ELEMENT NUMBER

6. AUTHOR(S)

Alexander W. Stevenson, 2nd Lt, USAF

5d. PROJECT NUMBER

5e. TASK NUMBER

5f. WORK UNIT NUMBER

7. PERFORMING ORGANIZATION NAME(S) AND ADDRESS(ES)

Air Force Institute of Technology
Graduate School of Engineering and Management (AFIT/EN)
2950 Hobson Way
WPAFB OH 45433-7765

8. PERFORMING ORGANIZATION REPORT NUMBER

AFIT/GAP/ENP/11-M10

9. SPONSORING / MONITORING AGENCY NAME(S) AND ADDRESS(ES)

Intentionally Left Blank

10. SPONSOR/MONITOR'S ACRONYM(S)

11. SPONSOR/MONITOR'S REPORT NUMBER(S)

12. DISTRIBUTION / AVAILABILITY STATEMENT

APPROVED FOR PUBLIC RELEASE; DISTRIBUTION UNLIMITED.

13. SUPPLEMENTARY NOTES

14. ABSTRACT

A method to improve the efficiency of photon collection in thin planar HPGe detectors was investigated. The method involved implementing a second HPGe detector to collect Compton scattered photons from the primary detector and incorporating coincident interactions in the two detectors that sum to the full energy event into the energy spectrum. This method is termed "Compton rescue" because the Compton scattered photons make a partial energy deposition in the primary detector and are added back to the spectrum after being detected by the second detector. This research has implications on improving the efficiency of positron annihilation spectroscopy (PAS) techniques including the use of the method in angular correlation of annihilation radiation (ACAR) and Doppler-broadening of annihilation radiation (DBAR) applications. The effect of using Compton rescue on the energy and spatial resolution on these two PAS techniques was investigated. The research was conducted in two phases: simulation, in which a Monte-Carlo program was used to predict the effectiveness of the Compton rescue method based on photon interaction simulations, and experiment, in which a position-sensitive HPGe detector and a large coaxial HPGe detector were used to implement Compton rescue. A two-detector DBAR experiment on single-crystal Ni was conducted using the Compton rescue setup to illustrate its utility.

15. SUBJECT TERMS

Compton Rescue, Positron Annihilation Spectroscopy, High-Purity Germanium, Semiconductor Detectors, DBAR, Compton Scattering

16. SECURITY CLASSIFICATION OF:			17. LIMITATION OF ABSTRACT	18. NUMBER OF PAGES	19a. NAME OF RESPONSIBLE PERSON
a. REPORT	b. ABSTRACT	c. THIS PAGE			Lt Col Christopher S. Williams, PhD, (ENP)
U	U	U	U	129	19b. TELEPHONE NUMBER *(include area code)* (937) 255-3636 x4689 ; cwilliam@afit.edu